Trace Elements in Deep-Sea Black (*Antipatharian*) Coral Skeletons

Harrison Stanley Martin Parr

A thesis submitted to Victoria University of Wellington

in partial fulfilment of requirements for the degree of

Master of Science in Geology

School of Geography, Environmental and Earth Sciences

Victoria University of Wellington

2022

Abstract

The proteinaceous skeletons of deep-sea *Antipatharian* 'black' corals are a new proxy archive that has shown promise for providing high resolution marine records in a wide range of waters. Although stable isotopes have been used successfully for palaeoceanographic reconstruction, there have been few studies of trace metals in these skeletons. In this thesis we study a suite of trace elements in black coral skeletons to assess their utility in paleoenvironmental reconstructions.

Fifty black corals were sampled from the NIWA Invertebrate Collection, broadly distributed around New Zealand from ~25˚S to 47 ˚S and 165˚E to 155˚E. Small powder samples were taken from the outer layers of the coral skeleton, dissolved in nitric acid and analysed by ICP-MS using a new methodology developed as part of this thesis. We critically evaluate this new method, quantifying the limits on accuracy and intrinsic reproducibility, and comparing this to the range of concentrations found in coral specimens.

A necessary step in evaluating the potential for trace elements to provide palaeoenvironmental information is to understand how trace elements become incorporated into the corals' skeletons. Questions include whether uptake is passive or active (i.e. biologically mediated); and whether trace elements derive from the coral's food (originating in the surface ocean) or from the ambient water in which the coral is growing.

In this thesis we explore these questions by studying spatial patterns of coral trace elements to determine if they show similarity to surface or intermediate-depth ocean trace element distributions. We investigate the influence of several variables on coral trace elements including proximity to the NZ mainland, the depth at which the corals grew, regional oceanography, and primary productivity. We examine the enrichment of skeletal trace elements compared with both coral tissue and particulate organic material (POM). Finally, we examine subsets of the coral samples that control for several environmental variables in an attempt to isolate the effect of coral size and taxonomy on trace element concentrations. Replicate samples from the same specimens and from different specimens at the same site (or within a 25Km radius) were used to assess differences in trace element content within and between coral specimens, respectively.

Our results indicate that black corals strongly enrich many trace elements (TE) in their skeletons and tissues (Br>Zn>Cd>Mo>V>U>Fe>Cu>Ni>I) at levels up to 10^8 times higher than seawater concentrations. A large intrinsic variability in TE content was found between and within all black coral specimens. This variability largely obscures any relationship that may indicate a water column origin and mechanism of uptake. Coral taxonomy at a genus level strongly influences most TE concentrations, contributing up to 80% of the variation in some elements. Although largely inconclusive, the data hints at a combination of active and passive uptake pathways from ambient or surface seawater sources for some elements which might warrant further investigation.

In order to advance this field of study further, we suggest that a better understanding is needed of the taxonomic control over trace element incorporation, including biomineralisation and biological utilisation of trace elements by black corals. We also note that there is a lack of data on trace element biogeochemical cycles in the waters around NZ, which would be important in order to better constrain the behaviour of the TEs in black corals and to better evaluate their paleoenvironmental utility.

Acknowledgements

Firstly, I would like to thank my supervisor – Dan Sinclair. Dan, I could not be more appreciative of your patience, insights, support, feedback, and supervision over the course of the master's research. I could not have asked for a kinder and more supportive supervisor.

I would like to extend a huge thanks to Di Tracey, Peter Marriott, Sadie Mills, Diana Macpherson and Grace Frontin-Rollet at NIWA for their support and insight during the initial specimen sampling at NIWA and throughout the project.

I would also like to extend a huge thanks to Bruce Charlier and Luisa Ashworth in the geochemistry Laboratory at VUW for their insights, feedback, assistance in developing the analytical protocol and introducing me to the world of micro-analytical chemistry.

Thank you, Nick Hitt and Ashley Davis, for your help and support during the initial stages of the project and friendly chats in Milk and Honey. It has been a privilege to work alongside such bright minds.

Funding for this project was provided by VUW and NIWA through both a Ministry of Business and Innovation (MBIE) "smart ideas grant" (no. 55794) awarded to Dan Sinclair, Di Tracey, Erik Behrens and Stewart Fallon.

Finally, I would like to extend a massive thanks to all the students in CO421, my family, friends, and flatmates for being such a supportive bunch – offering feedback, brains to bounce ideas off, ears to vent to, and a much need distraction in times of stress.

Table of Contents

List of Figures

List of Tables

Chapter 1 - Introduction

1.1 Primary Productivity: Climate and Fisheries

Planktonic primary producers are the foundation of life in the ocean. Forming the foundations of the ocean food web, they exert a first order-level control over ocean productivity, and sustain a $2bn (annual) fishing industry in New Zealand alone (Friedland et al., 2012). Primary producers comprise the basis of the biological pump (De La Rocha and Passow, 2014a; DeVries et al., 2012) through which they biologically fix carbon, ultimately regulating the drawdown of atmospheric carbon into the ocean (Arrigo et al., 1999; DeVries et al., 2012; Smetacek et al., 2012). Because of this, a better understanding of phytoplankton dynamics will be critical for managing our marine resources and forecasting anthropogenic-CO_2-driven climate change.

The (inter)relationships between primary productivity, climate and fisheries are complex. Changes to primary productivity in the ocean will undoubtedly impact New Zealand's environment and primary industries (Environment, 2019). One study suggests climate change may result in a decline in potential fish production by 30%-60% in the Eastern Indo-Pacific, the North Atlantic and the Central-Western Pacific (Blanchard et al., 2012). These changes are strongly coupled to changes in primary production; however, the response in New Zealand may not be straightforward. Projections (Chiswell and Sutton, 2020; Law et al., 2018) and observational data (Environment, 2019; Stats, 2019) suggest that primary productivity may increase in one area but decline in another. Unfortunately, the statistical significance of these projections/predictions is limited by the length of the datasets used, with most being limited to the satellite era (after the 1970s). Therefore, we need a way to generate *proxy records* that can extend observations of phytoplankton dynamics beyond our limited observation interval.

1.2 Proxy Records: Introducing Black Corals

Reconstructions of phytoplankton dynamics need to be long enough to usefully extend our records beyond instrumental times, yet high enough resolution that decadal dynamics can be resolved. Sediment cores are the primary tools traditionally used by palaeoceanographers to reconstruct past ocean changes. These cores offer the ability to reconstruct significant changes to ocean chemistry over broad timescales (Barnola et al., 1987; Petit et al., 1999; Schmiedl and Mackensen, 1997). However, sediment records are

often poorly resolved on short timescales (decades) due to bioturbation, compaction, diagenesis, erosion and slow sedimentation rates. Additionally, core retrieval expeditions can be costly and logistically challenging, especially when coring the deep ocean.

The carbonate skeletons of tropical corals (such as Porites corals) precipitate quickly and systematically accumulate trace elements in levels proportional to their concentration in the water column (Sinclair et al., 1998; Ehrlich, 2019) . This makes them excellent tracers for marine chemistry (Corrège, 2006; Fallon et al., 1999; Gothmann et al., 2019), able to provide reconstructions on (sub) annual timescales (Harriott, 1999; Lough and Barnes, 2000; Shen, 1986; Shen and Sanford, 1990). Unfortunately, these corals are confined to shallow tropical waters and thus cannot provide information about temperate or polar waters.

Antipatharian 'black' corals are a new proxy archive that has shown promise for providing marine records in a wide range of waters at resolutions higher than sediment cores can typically provide (Komugabe, 2015a; Komugabe et al., 2014; Raimundo et al., 2013; Williams, 2020; Williams and Grottoli, 2011). They are long-lived, widely distributed, colonial filter-feeding organisms of the Order *Antipatharia*. They inhabit deep-water environments in depths up to 8600m and can live for upwards of 4500 years (Hitt et al., 2020; Prouty et al., 2011; Roark et al., 2009a; Roark et al., 2006; Robinson et al., 2014; Sherwood and Edinger, 2009) .

The skeletons of black corals are composed of a proteinaceous organic material (Ehrlich, 2019; Goldberg, 1976; Goldberg et al., 1994) deposited in concentric growth rings similar to that of trees. Thus, their skeletons represent a simple progression of time, and chemical inclusions potentially capture a history of the corals' growing environment. The skeletons are thought to be built from particulate organic matter (POM) (the coral's food source) sinking from the upper water column (Roark et al., 2009b; Roark et al., 2006; Sherwood and Edinger, 2009; Sherwood et al., 2013). Black coral skeletons are, therefore, potential archives of *surface ocean* processes in parts of the ocean and, for periods of time unattainable from other palaeoceanographic proxies. As a bonus, black corals incorporate uranium in relatively high concentrations (5ppm-18ppm), allowing precise chronologies to be obtained by uranium-thorium disequilibria (Hitt et al., 2020; Komugabe et al., 2014).

To date, the main proxy records extracted from black corals are derived from stable isotopes of nitrogen and carbon ($\delta^{15}N$ and $\delta^{13}C$) (Schiff et al., 2014b; Sherwood et al., 2011), and radiocarbon (^{14}C) (Guilderson et al., 2013; Marchitto and Broecker, 2006; Sherwood et al., 2005) providing information on water-mass age (a proxy for ocean circulation), and phytoplankton productivity processes. However, recent work has also shown that *trace elements* are incorporated into black coral skeletons in a way that appears to be systematic (Raimundo et al., 2013; Williams and Grottoli, 2011), offering the potential for new marine proxy records. Although N and C show evidence of a surface ocean (POM) origin (Guilderson et al., 2013; Schiff et al., 2014a; Sherwood et al., 2011), the uptake of *trace elements* into the black coral skeleton may not be so straightforward. Recent research from Komugabe (2015a) posits multiple uptake pathways for trace elements in black coral skeletons, suggesting the corals may uptake trace elements either from POM or ambient seawater.

1.3 Trace Elements: Potential Records of Productivity

One way to study primary productivity and potentially reconstruct past dynamics would be to generate records of *nutrients*. Nutrient distributions dictate the growth of primary producers and the resultant strength of the biological pump (De La Rocha and Passow, 2014a; Rue and Bruland, 1995). Marine biota utilise the following elements in their tissues: C, H, O, N, P, Na, K, Cl, Ca, Mg, S & Si (Morel, 2013). Of these, C, N, P are termed the 'macro' nutrients as their availability fundamentally limits phytoplankton growth. Phytoplankton require these elements in a precisely defined ratio of 106 C atoms, to 16 N atoms to 1 P atom, which is known as the 'Redfield Ratio' (Redfield, 1958). When one of these elements are present in a lower ratio than this, phytoplankton can only grow until that element is used up, then growth ceases.

Reconstructing time histories of bioavailable C, N and P in the ocean from black corals would give information about phytoplankton uptake of, and control by, nutrients. Unfortunately, black corals utilise C, N and P as structural elements in their organic skeletons, and hence these elements are under heavy metabolic control (Adkins et al., 2003; Reinhard et al., 2017). This makes it impossible to directly reconstruct 'macro' nutrients from the skeletal C, N and P concentrations. However, there are a suite of

minor/trace elements, known as *micro*nutrients, that *also* function as nutrients (Bruland et al., 2013).

Micronutrients are essential nutrients for phytoplankton, having been shown to limit their growth in some major ocean basins (Boyd and Ellwood, 2010; de Baar et al., 1995; Martin and Fitzwater, 1988; Tagliabue et al., 2017). These elements include (but are not limited to) Fe, Mn, Zn, Co & Cd. They are typically present in low concentrations (parts per million – parts per trillion) in both seawater and phytoplankton tissues/tests (Bruland et al., 2013; Morel and Price, 2003). The biolimiting nature of micronutrient elements are recognised by the inclusion of Fe, Mn, Zn, Co & Cd in recent revisions of the Redfield Ratio (Morel and Price, 2003).

These micro-nutrient trace elements have oceanic distributions very similar to their macro counterparts (Figure 1.3a) (Bruland et al., 2013; Cullen, 2001; Lai et al., 2008; Marchitto and Broecker, 2006; Morel and Price, 2003; Sunda and Huntsman, 2000) and since they are not structural elements of coral skeletal organics, their skeletal concentrations may not be under strong metabolic control. If this is the case, trace elements in black coral skeletons may reflect the amounts in the corals' food source and/or the ambient seawater surrounding the corals and thus offer an alternative way of reconstructing surface and/or deeper ocean nutrient dynamics. This technique has been applied to other marine organisms, such as tropical corals from which cadmium and manganese (among other trace element micronutrients) have been used as palaeo upwelling indicators (Bruland et al., 1991; Cullen, 2001; Shen and Sanford, 1990; Sunda and Huntsman, 2000).

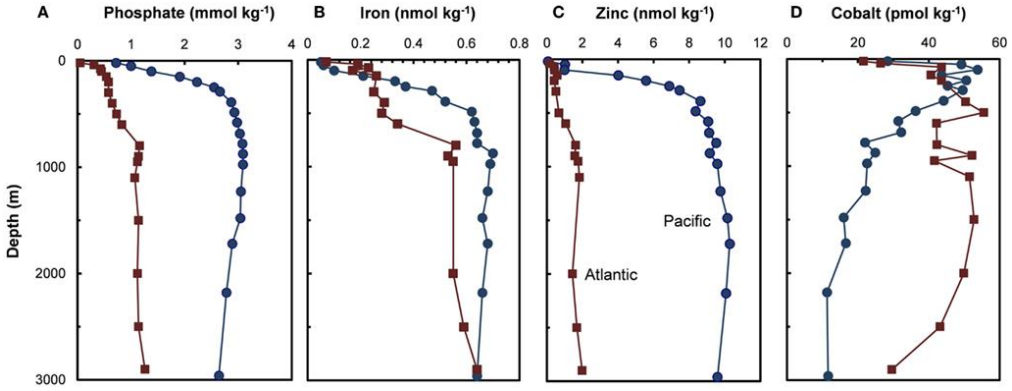

Figure 1.3a. Vertical depth profiles for (A) Phosphate and filtered concentrations of (B) Fe, (C) Zn and (D) Co in the Pacific and Atlantic Oceans (1987-1993). Taken from (W. Sunda, 2012). Squares = Atlantic profiles, circles = Pacific profiles.

1.4 Black Coral Trace Elements: Research Questions

Although the behaviour and dynamics of most major micronutrient metals in the ocean are *mostly* understood, much remains unknown about how these elements become incorporated into black coral skeletons. Micro-analyses of trace elements in black coral skeletons from Hitt (2020) (Figure 1.4a) and Electron Microprobe maps from Komugabe (2015a) shows that variations in trace element concentrations are consistent within growth rings. Although this does not prove that trace element concentrations reflect surface/ambient ocean concentrations, it suggests that the process modulating skeletal trace elements occurs systematically in skeletal material of the same age, which is a necessary first step in the use of these elements as environmental proxies.

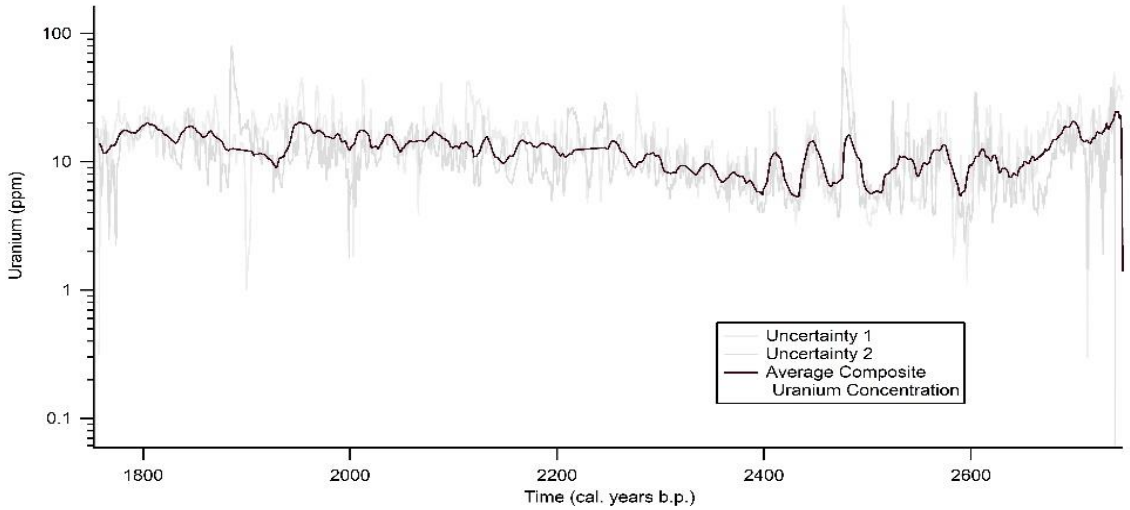

Figure 1.4a. Time series data for uranium in the skeleton of a black coral. Time presented in calibrated years before present. Uranium concentration representative of an averaged composite from four LA-ICP-MS transects on the same coral specimen.

However, some recent studies suggest that minor elements within black corals may be under metabolic control or have structural roles in the skeleton. For example, C, N, Na, and Mg have been observed to concentrate in the interior of skeletal cells (referred to as units of coral microstructure); Ca, Fe, K and I in the regions between successive layers of skeletal material (Nowak et al., 2009) and Br throughout the skeleton (Ehrlich, 2019; Juárez-de la Rosa et al., 2007). Unfortunately, there are no accompanying studies on micronutrient trace metals, so no information is available about whether they have a role in the skeletal formation.

Part of the problem is that very little is known about how trace elements are taken up by the corals and partitioned into their skeletons. For example, it is unknown whether trace elements are incorporated into the corals in some systematic relationship to the coral's environment or if internal biological processes affect their uptake. Similarly, if skeletal elements *do* reflect the environment, are they taken up from the sinking particulate matter that they eat (potentially reflecting surface waters as posited by Williams and Grottoli (2011))? Or from the ambient water (reflecting deep-water composition? See Komugabe (2015a))

1.5 This Research Project:

One way to test for a systematic relationship between coral trace elements and the ambient environment is to study coral skeleton compositions across known ocean trace element gradients. This requires access to coral specimens from a wide range of locations and depths. Fortunately, the National Institute of Water and Atmospheric Research (NIWA) holds a large collection of black corals from the waters around New Zealand at their National Invertebrate Collection (NIC). New Zealand is an ideal location for a study such as this as there are systematic variations in micronutrient trace elements with depth and across the major ocean fronts. These variations arise from New Zealand's unique oceanographic setting where cold macronutrient-rich, micronutrient-depleted waters from the south converge with warm macronutrient-depleted, micronutrient-rich waters from the north (Chiswell et al., 2015; Sutton, 2001). This setting creates an optimal chemical 'soup' for phytoplankton growth and sets up biogeochemically distinct gradients against which coral chemistry may be compared.

In this project, we analyse trace element concentrations in a suite of black corals to compare relative concentrations between corals living in biogeochemically distinct water masses (such as the Subtropical waters to the north of NZ and the Subpolar waters to the south). By comparing measured trace elements to known/expected dissolved nutrient and micro-nutrient concentrations, we hope to discern if there is a consistent relationship between black coral trace element uptake and regional oceanographic processes. This, in turn, may offer insight into the uptake behaviour (i.e. passive [abiotic] or active [biologically mediated]) and origin (i.e. surface [POM] or ambient seawater) of trace elements in black coral skeletons. This is an essential first

step for assessing the utility of trace elements in black coral skeletons as palaeogeographic proxies.

1.5.1 Hypotheses Being Tested

This research project is set up to examine the proposition that micronutrient trace elements are being incorporated into the coral skeleton via their food source, meaning their relative proportions of concentrated trace elements should reflect the distribution of surface nutrients and, ultimately, regional surface water masses. If we assume that:

1. Trace metals in the tissues of phytoplankton are proportional to the concentration in the surface waters, and
2. The trace element composition of the coral skeleton is proportional to the trace element composition of the corals' food,

then this leads to the following testable hypothesis:

"A spatial map of micronutrient trace elements in the skeletons of black corals will be correlated with the spatial distribution of those elements in the overlying *surface* ocean."

Falsification of this hypothesis (i.e. a lack of correlation between coral trace elements and those of the overlying water) could lead to multiple alternative conclusions depending upon patterns (or lack thereof) in the skeleton relative to other environmental parameters or processes. The wide range of coral specimens available also allows us to explore several other possible mechanisms affecting skeletal trace elements, such as distance from the New Zealand coast, the effect of coral size, depth and/or the influence of coral species/genera.

1.5.2 Project Design

Approximately 50 black corals were sampled from the NIWA Invertebrate Collection (NIC) between longitudes of 165˚E and -157˚W, and latitudes 23˚S to 48˚S, aiming for a broad distribution around the New Zealand subcontinent. This location range spans through the Tropical Front (TF) and the Sub Tropical Front (STF) of which incorporate Subtropical (STW) and the Sub-Antarctic (SAW) surface waters. Corals were selected and subsampled with care to allow for controlled comparisons of trace element chemistry with varying coral size, varying collection-depth, between coral species/genera and distance from the New Zealand coastline and Subtropical Front.

Small ~10mg powder samples were drilled from the outer portions of the coral skeletons, digested into solution, and analysed for trace elements on a high-resolution inductively-coupled plasma mass spectrometer (ICP-MS). The trace element data was then used to create spatial maps and regression plots of the elemental composition in the corals around New Zealand. These maps and trends were then compared with maps of surface ocean primary productivity (from MODIS satellite ocean colour) and trace element distributions generated as part of the GEOTRACES marine biogeochemistry programme. The GEOTRACES programme is an international study on the biogeochemical cycles of trace elements with available data, including full depth distributions of major trace elements, including Fe, Ni, Cu, Cd and Zn, along transects running from Tasmania to Antarctica (GIPY06), and from Sydney into the Southwestern Pacific (GP13). Details are presented in Sections 3.7 & 4.2.

1.5.3 Methodology Development

Very little work has been carried out on black coral trace element chemistry. As such, there are no suitable reference materials nor standard analytical protocols to follow. Therefore, an important initial component of this thesis has been the development and validation of an analytical protocol for measuring trace elements in organic black coral skeletons. Details of this method development are presented in Chapter 3. In brief, the method involved initial digestion of the organic material in concentrated nitric acid, followed by a 10,000x dilution. Solutions were run on a high-resolution ICP-MS to avoid isobaric interferences and calibrated against an in-house coral standard which was itself calibrated using Standard Additions.

1.5.4 Sections of this Thesis

Chapter 2 presents the background material and reading underpinning the project, introducing key concepts and ideas from which the result interpretations are based, and the discussion is drawn. **Chapter 3** presents the methodology followed throughout the project, including details of the specimen sampling, laboratory techniques, analytical method development, data processing steps, data evaluation, calculation of uncertainties. **Chapter 4** presents the results of the research. This includes spatial maps of trace elements in black corals along with numerous regression tests and additional studies exploring the behaviours and expression of trace element chemistry within and

between black corals of varying characteristics. **Chapter 5** summarises and combines the outcomes of the multiple environmental tests and associated spatial patterns presented in Chapter 4. Chapter 5 also presents interpretations for environmental origins, mechanisms of uptake and ultimately paleo-reconstructive utilities for Cd, Zn, Cu, Fe, Br, I, Ni, Mo, V and U concentrated in the skeletons of black corals. Finally, **Chapter 6** concludes and summarises the research, highlighting any findings of significance and identifying knowledge gaps and additional data that may help further consolidate any conclusions drawn.

Chapter 2 - Background

2.1 Black Corals

2.1.1 Biology and Ecology

Antipatharian (black) corals are among the least studied animals of the class Anthozoa. They represent a taxonomic order (*Antipatharians*) within the anthozoan subclass *Hexacorallia* which encompasses seven families, 43 genera and over 279 species (estimated 140 unknown species), 111 of which are endemic to New Zealand (Tracey and Hjorvarsdottir, 2019; Wagner et al., 2012). This study focuses on the *Leiopathidae, Antipathidae* and *Myripathidae* families which contain the *Antipathes*, *Leiopathes* and

Genus	References	Morphology	Size	Depth	Distribution around NZ
Antipathella spp	Grange, K.R. (1990), Opresko et al. (2014)	Bushy colonies, with thin branchlets arranged bi-latterally or irregularly on the main stem	up to 5m	1-514m (usually less than 200m)	Endemic to NZ. *A.fiordensis* species endemic to Fiordland. Other species may be found around the North Island
Antipathes spp.	Cairns et al. (2007), Opresko et al. (2014)	Bushy or flabellate. Variable branchlet and branching form.	up to several meters	10-1534m (usually less than 400m)	Common around the north of the North Island and around the Kermadec Arc.
Leiopathes spp.	Opresko et al. (2014) Opresko et al. (1998)	Small to large, bushy or fan shaped. Small branchlets are curved and end branchlets are short and thin. Thicker branches appear polsihed and smooth.	over 2m	256m to 1608m	Bay of Plenty, Kermadec Arc, Lord Howe Rise, Hikurangi Margin, Chatham Rise, Cape Reinga and N North Isalnd

Table 2.1a. Table of morphology, size, depth range and distribution of sampled black coral genera around New Zealand. Table made from research presented in Opresko et al. (2014), Opresko et al. (1998), Grange, K.R. (1990) and Cairns et al. (2007).

Antipathella genera, respectively. These corals tend to form the most robust main stems and large arborescent structures (Table 2.1a), unlike the unbranched whip-coral counterparts (*Cirrhipathes* and *Stichopathes*). These corals were also the most abundant at the NIWA Invertebrate Collection (NIC), offered the most extensive range of specimens identified to a genus/species level, and had multiple specimens that were large enough to reliably sample (main stem diameter >2cm).

In cross-section, these corals manifest concentric bands similar to growth rings in trees (Prouty et al., 2011; Roark et al., 2009b; Roark et al., 2006; Roark et al., 2005). Radial extension rates are in the order of microns per year but vary between species. Of the sampled coral genera, *Antipathes* corals show the fastest growth rates (90-140um/yr),

followed by *Antipathella* (~50um/yr) and *Leiopathes* (1-40um/yr) (Hitt et al., 2020; Roark et al., 2009b).

2.1.2 Morphology

Black corals are colonial, filter-feeding organisms that form a wide range of structures, from whip-like to tree-like. Colonies range from heights of a few centimetres to many metres (Wagner et al., 2012). All *Antipatharian* corals are ahermatypic and therefore do not build reefs (Tracey and Hjorvarsdottir, 2019; Wagner et al., 2012; Warner, 1981). Instead, they form dense thickets (Cairns, 2007). These corals, therefore, act as diverse habitats for deep-sea organisms such as polychaetes, barnacles, ophiuroids, copepods, crabs, shrimp, anemones, zoanthids, hydroids, crinoids, bryozoans, snails, bivalves, tunicates and fish (Wagner et al., 2012).

2.1.3 Distribution

Black corals are broadly distributed throughout the world's oceans, from tropical to sub-polar waters at depths down to 8600m (Cairns, 2007; Opresko et al., 2014; Wagner et al., 2012). 75% of recognized species are found below 50m (Cairns, 2007; Opresko et al., 2014; Tracey and Hjorvarsdottir, 2019). Black coral distribution is controlled by their preference for a solid substrate to attach to, low light conditions and exposure to strong and consistent deep-sea currents (Auscavitch et al., 2020; Tracey and Hjorvarsdottir, 2019; Wagner et al., 2012). Therefore, colonies are often found near bathymetric features that accelerate currents, such as seamounts, knolls and canyon edges (Auscavitch et al., 2020) and are considered azooxanthellate (Wagner et al., 2012). Black corals also avoid regions with high sedimentation rates due to the *Antipatharian* tissues having little resistance to abrasive forces (Wagner et al., 2012).

2.1.4 Feeding

Antipatharians are both suspension feeders, feeding passively off nutrients delivered by ocean currents and actively via filter-feeding, capturing food via interception filtration (Carlier et al., 2009; Lewis, 1978; Wagner et al., 2012). Zooplankton comprises a significant component of their diet; however, *Antipatharians* have also been observed to feed off copepods and amphipods from the photic zone (Carlier et al., 2009; Goldberg and Taylor, 1989). Research has shown that both the living tissue and outer skeletons contain bomb ^{14}C of surface origin, implying the corals source their carbon (food) from

surface ocean particulate organic matter (POM) (Hitt et al., 2020; Komugabe et al., 2014; Lewis, 1978; Marriott et al., 2020; Prouty et al., 2011; Roark et al., 2006; Robinson et al., 2014).

2.1.5 Black Coral Skeletons

2.1.5.1 Structure and Composition

Black coral skeletons are primarily composed of a combination of rigid chitinous material and a halogen-containing scleroprotein called antipathin, forming a laminated composite (Ehrlich, 2019; Nowak et al., 2009). Antipathin is more elastic and less rigid than other biomaterials such as wood, bone, calcite and insect cuticle (Ehrlich, 2019; Nowak et al., 2009). The skeletal structure is axial, with the laminates glued together with organic cement (Ehrlich, 2019; Juárez-de la Rosa et al., 2007; Nowak et al., 2009). There are no studies concerning the hypothetical role of antipathin in biomineralisation (Ehrlich, 2019) hence these pathways are poorly understood and minimally explored.

The bulk composition of *Antipatharian* corals is predominantly non-fibrillar protein (60%) and chitin fibrils (15%), with lipids, carbohydrates, sterols and phenols making up the remaining 25% (Ehrlich, 2019; Goldberg, 1976; Nowak et al., 2009). The amino acid composition of the protein fraction in these corals is comprised of glycine (35%), alanine (15%), histidine (13%), along with 4-6% serine, glutamine and leucine. Other amino acids comprise the remaining <4%. Bromine and iodine are present at up to 7wt% of the coral skeleton (Goldberg et al., 1994; Nowak et al., 2009). Minor elemental concentrations of antipathin have been found to vary between orders, within colonies and with changing seawater concentrations with depth (Williams and Grottoli, 2011).

2.1.5.2 Uptake Pathways and Trace Element Chemistry

There is a paucity of research on biomineralisation pathways for black coral skeletons. Most studies focus on marine organisms like bivalves that precipitate composites, comprising an organic matrix and micro- to nano-crystalline inorganic precipitates such as calcite or aragonite (Ehrlich, 2019). However, because black corals do not have an inorganic component to their skeletons little inference can be drawn from those studies.

One principle likely holds - that organisms gather many precursor elements essential to skeletal formation directly from their natural environment (Ehrlich, 2019), with most serving some biological purpose. Therefore, the key questions are whether skeletal elements are passively taken up (i.e. in proportion to their environmental concentration

or rate of supply) or actively taken up (which might imply that physiological processes exert a primary control on the skeletal concentration).

There are only a few studies on the trace element chemistry of black coral skeletons (see Komugabe (2015b), Raimundo et al. (2013) and Williams and Grottoli (2011)). As such, uptake pathways and methods of incorporation for most trace elements are particularly poorly understood. Trace element variations are usually moderately coherent around a growth ring, but concentrations vary from one ring to the next and between skeletal and glue layers (see EPMA maps from Komugabe (2015a) and Nowak et al. (2009)) (Figure 2.1a). This suggests that element variations are associated with conditions prevailing at the time the skeletal band was being deposited (Komugabe, 2015a; Nowak et al., 2009). This could be a varying environmental condition or a shift in the composition of the material deposited by the coral.

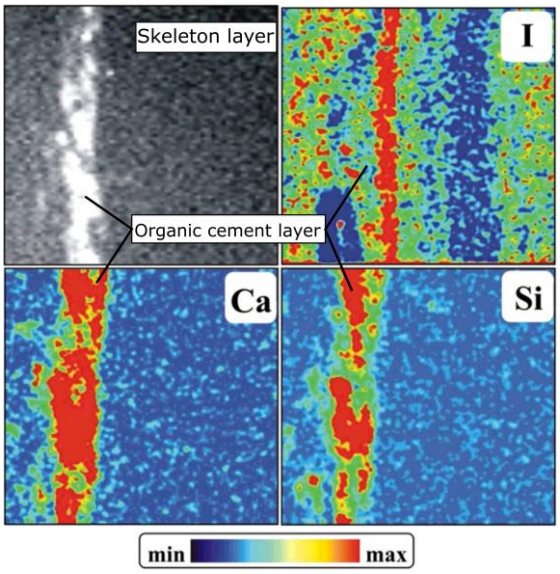

Figure 2.1a. EPMA chemical mappings of a black coral made by μ–PIXE method from Nowak et al., 2009. Scale - 250×250 μm. Note the distinct increase in I, Ca and Si in the cement layers.

As an example, electron microprobe (EPMA) results from Nowak et al. (2009) (Figure 2.1a) and Komugabe (2015a) show evidence for Ca and I concentrating at different levels between successive layers of coral skeleton, with larger concentrations generally being associated with the organic cement layers between major growth rings. Likewise, V exhibited some variation between successive layers (not pictured), although to a much lesser extent than with iodine. It is important to note, however, that the variation of elements between the matrix and gluing zones is not large enough to influence the overarching trace element signal of the whole coral (Komugabe, 2015a). While this provides evidence for the systematic uptake of trace elements by black corals (Komugabe, 2015a; Williams and Grottoli, 2011), the uptake pathways and biological roles for these elements, again, remain poorly understood.

The coral skeleton may incorporate trace elements through both a dissolved and particulate phase via multiple pathways as outlined in Komugabe (2015a) and presented in Figure 2.1b. *Particulate* trace elements may be ingested and incorporated into the living tissue, then metabolized and secreted into the coral skeleton (Figure 2.1b) (Komugabe, 2015a). *Dissolved* elements enter the skeleton via the coral tissue (ingestion or absorption) or directly into the skeleton by absorption or precipitation (Komugabe, 2015a). This implies that skeletal trace elements may be sourced from the coral's food source (particulate organic matter) and/or ambient seawater. Radiocarbon studies reveal that corals predominantly source their food from POM from the surface ocean (see Section 2.1.4), leading some researchers to infer that some/most trace metals are also sourced from POM (Williams and Grottoli (2011)). However, there is no clear evidence to confirm this.

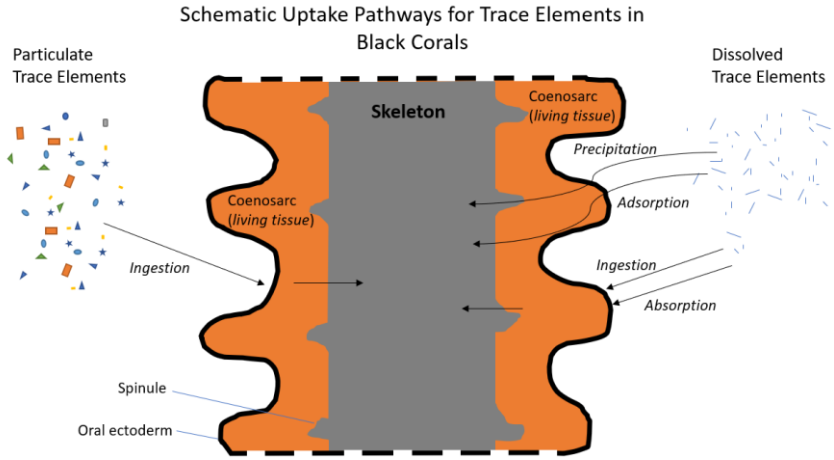

Figure 2.1b. Schematic diagram of suggested uptake pathways for trace elements into the coral skeleton adapted from Komugabe (2015b). Particulate phase trace elements are absorbed or ingested into the coral living tissue, then metabolized and secreted into the coral skeleton. Dissolved phase elements are thought to be absorbed or ingested into the coral living tissue then metabolised into the skeleton or directly precipitated onto the coral skeleton.

2.2 The Oceanography of New Zealand

The oceanography of a region acts as a significant control on deep sea corals. For example, strong currents act as nutrient sources, providing a continuous supply of particulate matter while also providing a dispersal mechanism for coral larvae (Miller and Hay, 1998; Tracey and Hjorvarsdottir, 2019). In addition, since corals must be sourcing their trace elements from either food or ambient water (Komugabe, 2015a; Williams and Grottoli, 2011) it is hoped their skeletal concentrations may reflect the

regional oceanography. In this section, therefore, we review the oceanography of the waters around New Zealand.

2.2.1 Bathymetry

Coral distribution is predominantly controlled by seafloor geology and proximity to deep-sea currents (Tracey and Hjorvarsdottir, 2019; Wagner et al., 2012). Bathymetric features such as seamounts and hydrothermal vents not only provide suitable substrates for corals to grow on (Bostock, 2019; Wagner et al., 2012) but may also act as significant sinks or sources for trace metals (Bruland et al., 2013; German et al., 1991; Ho et al., 2018). Therefore, understanding the bathymetry around New Zealand is essential for understanding the chemistry of black coral skeletons.

Much of the ocean around New Zealand sits upon a shallow continental shelf, no more than a few hundreds of meters deep along the Campbell Plateau, the Chatham Rise and most coast proximal areas of NZ (Mitchell et al., 2012) (Figure 2.2a). This shelf is cut by troughs and canyons (notably the Bounty Trough, the Hikurangi Trough and the Kaikoura Canyon) that extend to thousands of meters water depth (Mitchell et al., 2012; Mountjoy et al., 2018) (Figure 2.2a). These features are generally linked to riverine discharge off the continental shelf and tectonic activity (Mountjoy et al., 2018). These canyons act as transport channels for cold, dense polar base waters as well as delivery pathways for coastal sediments and nutrients to the deep ocean (Heezen et al., 1955; Mountjoy et al., 2018). This complex bathymetry exerts considerable control on the behaviour of ocean currents, and ultimately the distribution of macro/micronutrients and black coral colonies.

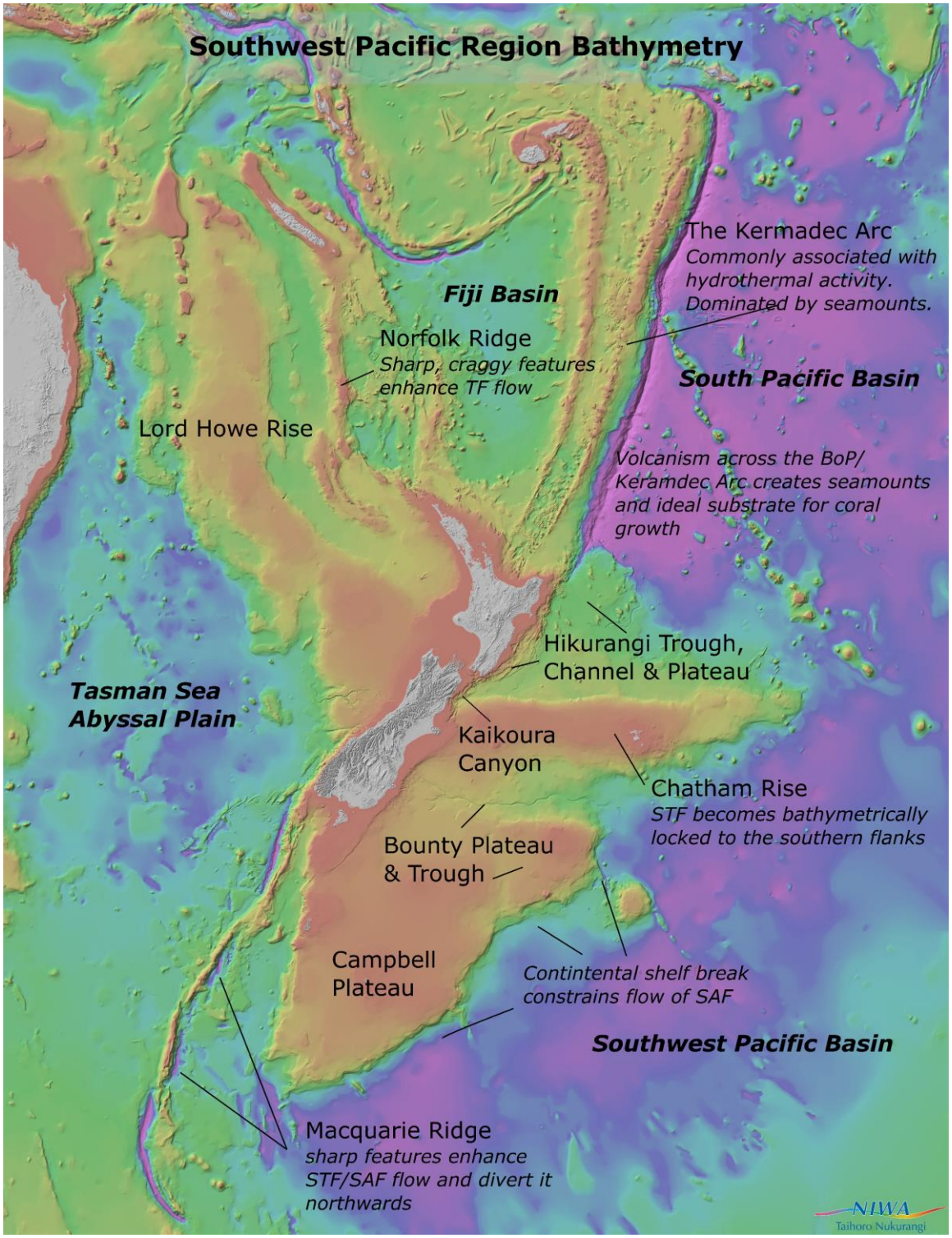

Figure 2.2a. Annotated 2016 Bathymetric map of the Southwestern Pacific. Map published by the National Institute of Water and Atmospheric Research Ltd. Data from Mitchell et al. (2012). TF – Tasman Front, SAF – Sub Antarctic Front, STF – Subtropical Front, BoP – Bay of Plenty

2.2.2 Surface Waters

2.2.2.1 Sub-Tropical Water (STW) & the East Australian Current (EAC)

The East Australian Current (EAC) defines the primary western boundary current of the South Pacific (Chiswell et al., 2015), transporting subtropical surface waters (STW) down Australia's East Coast, through the Coral Sea and into the Tasman Sea (Figure 2.2c). These STWs are amongst the warmest and most saline waters in the subtropical region, with temperature and salinity averaging 15°C and 34.5psu, respectively (Table 2.2a) (Chiswell et al., 2015). The strength of the EAC varies annually (Ridgway and Godfrey, 1997), mainly influenced by basin-scale changes in wind strength. Stronger years result in greater protrusion of subtropical waters towards Tasmania, and a reduced southward penetration of the Tasman Front (TF) (Hill et al., 2011). The EAC, therefore, has variable salinity and temperature of ~34.4psu and 15°C respectively (Ridgway and Godfrey, 1997).

2.2.2.2 Tasman Front (TF)

A front is a boundary between two distinct water masses but can also refer to a current that defines the boundary over a broad region. The Tasman Front (TF) is the bifurcated tail-end of the much larger and climatically influential EAC (Stanton, 1979), and separates the Coral Sea from the Tasman Sea (Figure 2.2c). It averages 7.6Sv, has a salinity between 35.6-35.7psu (Table 2.2a), and extends to ~1000m depth which is much shallower than the EAC (Sutton and Bowen, 2014).

The TF runs down the east coast of the North Island, and while it's warm (17-19.5°C; Stanton, 1979) waters are mostly depleted in major nutrients it has high concentrations of some micro-nutrient metals – specifically Iron (Boyd et al., 1999). This current represents some of the only outflows of subtropical water from the Tasman Sea, and its waters penetrate as far as the south-western coast of the South Island (Chiswell et al., 2015; Stanton, 1979). This is of great importance, as these waters act as a significant source for bioavailable iron to the iron-depleted sub-polar ocean waters (Boyd et al., 1999; Obata et al., 2008; Smetacek et al., 2012).

2.2.2.3 Sub-Tropical Front (STF)

Moving further south towards Bluff, and over the Chatham Rise on the Eastern side of New Zealand flows the Subtropical Front (STF) (Figure 2.2c). The STF separates the warm

(14-18 °C), salty (35.1 PSU) waters of the subtropical gyre from the cool (10-14°C), fresh (34.6 PSU) (Table 2.2a) upwelled sub-Antarctic waters of the Antarctic Circumpolar Current (ACC) (Belkin and Gordon, 1996; Orsi et al., 1995; Sutton, 2001). The STF defines the northern extent of the Southern Ocean (Belkin and Gordon, 1996; Bostock et al., 2015; Hamilton, 2006), and delineates strong nutrient gradients. Generally, surface water micronutrient content displays a distinct increase in concentration moving across the STF (see Figures 4.2c, 4.2d & 4.2e, Section 4.2.4) into the Sub Antarctic Waters (NB: this is not true for Fe, which displays a distinct decrease in surface concentration). The STF is also thought to be associated with the subduction of central water below the subtropical gyre (Hamilton, 2006) and, resultantly, is known as a region of both high biological productivity and water mass formation (Bostock et al., 2015; Chiswell et al., 2015; Hamilton, 2006).

2.2.2.4 Sub Antarctic Waters (SAW)

The Sub Antarctic Waters (SAW) define the surface waters from latitudes approximately 45°S to 55°S, separated from the warmer, saltier waters to the north by the STF, and the cooler, less saline waters to the south by the sub-Antarctic front (SAF) (Chiswell et al., 2015; Morris et al., 2001; Orsi et al., 1995). Sub-Antarctic Waters are most widespread to the west of New Zealand, with the extent of the waters to the east strongly controlled by the confluence of the STF and SAF (Figure 2.2c). These waters are iron-limited, nutrient-rich and low in chlorophyll (Boyd et al., 1999; Nodder et al., 2016). The average temperature and salinities of the SAW are ~10°C and 34.5psu, respectively (Table 2.2a) (Chiswell et al., 2015).

2.2.3 Intermediate Waters

The intermediate waters to the south of New Zealand are of huge climactic importance, with these water masses acting to ventilate the subtropical gyres, as well as behaving as transfer zones for nutrients, heat and oxygen (Talley, 2003, 2008). Moreover, the sub-Antarctic and Antarctic intermediate waters act as significant sinks for anthropogenic carbon dioxide, ultimately comprising a significant portion of the southern ocean's carbon dioxide sink (Hartin et al., 2014; Mikaloff Fletcher et al., 2006). In general, intermediate waters are expected to have a greater micronutrient content

than the overlying surface waters, given the depth profiles for most nutrient-type TE's show a subsurface maximum at ~1000m depth (see Section 2.5.3).

2.2.3.1 Antarctic Intermediate Water (AAIW)

Antarctic Intermediate Water (AAIW) comprises the main intermediate water masses from 500m-1200m in the Southern Ocean and throughout much of the study region (Hanawa and Talley, 2001; Tsuchiya and Talley, 1998) (Figure 2.2b). It is characterised by a relatively low salinity (~34.45psu) tongue that sinks at approximate 60°S (England, 1992), forming north of the Polar Front (Chiswell et al., 2015) (Figure 2.2b, Table 2.2a). It is considered to be well ventilated and has a mean temperature varying between 3.5°C-10.5°C (Tsuchiya and Talley, 1996) (Table 2.2a). As a result of the AAIW's extent, a great deal of internal variability has been recorded, with Bostock et al. (2013) recognising four distinct subtypes, each characterised by differing degrees of oxygenation and salinity. These subtypes are: Southeast Pacific AAIW (very low salinity, high oxygen, very low nutrients), Equatorial Pacific AAIW (moderate relative salinity, low oxygen, high nutrients), Southern Ocean AAIW (low salinity, mod-high oxygen, low nutrients) and Tasman AAIW (high salinity, high nutrients, low relative oxygen) (see Bostock et al. (2013) & Table 2.2a for further details).

2.2.3.2 Sub-Tropical Mode Waters

Sub Antarctic Mode Waters (SAMW) and Subtropical Mode waters (STMW) together with the AAIW define the intermediate water masses of the New Zealand subcontinent (Figure 2.2b). 'Mode' water usually refers to relatively vertically homogeneous water found over a large geographical area (Hanawa and Talley, 2001).

The South Pacific portion of the STMW is situated to the north of New Zealand, defining a weak layer of near-constant temperature at ~15-19°C (Table 2.2a) (Roemmich and Cornuelle, 1992) with a minimum thickness of 100m (Chiswell et al., 2015; Tsubouchi et al., 2007). The salinity of the STMW is typically 35.5psu at approximately 16.5°C (Roemmich and Cornuelle, 1992). The STMW is thought to form during the winter via convective mixing and overturning (Roemmich and Cornuelle, 1992).

2.2.3.3 Sub-Antarctic Mode Waters

The Sub Antarctic Mode Waters are situated to the south/south-east of New Zealand, defining the intermediate portion of the circumpolar currents of Antarctica (Figure 2.2b).

Similarly to the STMW, the SAMW is a weak layer or mostly constant temperature (7-8.5°C) (Herraiz-Borreguero and Rintoul, 2011; Morris et al., 2001), formed via winter mixing and overturning around the SAF. The salinity of the SAMW is around 34.5psu (Table 2.2a), however, this decreases to the east/south-east of NZ (Morris et al., 2001).

2.2.4 Deep Water

2.2.4.1 Antarctic Bottom Waters (AABW) & Circumpolar Deep Water (CDW, UCDW & LCDW)

The deep-water mass underlying the major ocean fronts of the Southern Ocean is called the Antarctic Bottom Water (AABW) (Figure 2.2d). This water is characteristically cold, dense and salty, with an average temperature ranging between -0.8°C - 2°C, along with a salinity of approximately 34.65psu (Table 2.2a) (Chiswell et al., 2015; Orsi et al., 1995). Sitting above the AABW is another deep-water mass known as Circumpolar Deep Water (CDW). Due to its heterogeneity, CDW is split into Upper Circumpolar Deep Water (UCDW) and Lower Circumpolar Deep Water (LCDW), with each being found from 1450m-2500m and 2500m-AABW respectively (Chiswell et al., 2015; Mantyla and Reid, 1983). Generally, mixing between the LCDW and AABW is necessary to transport AABW northward, as the densities of the AABW alone are much too high to pass over Antarctic sills (Mantyla and Reid, 1983).

2.2.4.2 Deep Western Boundary Current (DWBC)

North of the Southern Ocean, the convergence of the AABW and LCDW water masses creates the Deep Western Boundary Current (DWBC) (Figure 2.2d), which in turn carries this well ventilated, cold and dense concoction northwards, along the eastern flanks of NZ subcontinental landmass up towards the flanks of the Kermadec Arc (Chiswell et al., 2015; Orsi et al., 1995). Other tendrils of LCDW extend northward to the west of New Zealand, flowing along the margins of the Australian continent (Chiswell et al., 2015; Mantyla and Reid, 1983).

2.2.4.3 Pacific Deep Water (PDW)

Pacific Deep Water (PDW) comprises the majority of deep-water inflow from the North of New Zealand and is thought to form via the upwelling of a modified DWBC (LCDW, UCDW and AABW) (Chiswell et al., 2015) (Figure 2.2d). This deep-water is less saline, nutrient-rich, dense and cooler than its southern counterparts.

Oceanographic Fronts	*Temperature (°C)*	*Salinity (psu)*	*Approx. Depth (m)*
TF	17 - 19	35.6 - 35.7	0 - 1000
STF	Δ5	Δ0.5	0 - 500
SAF	5	34.2	0 - 500
PF	0.8 - 3.6	34	0 - 400
Surface Waters			
STW	<15	<34.5	0 - 500
SAW	~10	>34.5	0 - 500
Intermediate Waters			
TS AAIW	3.5 - 10.5	34.5	500 - 1300
SO AAIW	~3.5	34.2	500 - 1300
SEP AAIW	3.5 - 10.5	34.45	500 - 1300
STMW	15 - 19	~35.5	up to 300
SAMW	7 - 8.5	34.2 - 35.8	400-600
Deep Waters			
AABW	0.8 - 2	34.65	2500 +
CDW	~2 - 5	34.7	1450-2500
DWBC	~4	34.7	~1450-2500
PDW	~5	~34.5	1500 - 2500

Table 2.2a. Table of temperatures, salinities and depths of the major oceanographic fronts and water masses in the Southwestern Pacific Region. Data taken from Chiswell et al. (2015) and Heath (1985) and references therein. TF – Tasman Front, STF – Subtropical Front, SAF – Subantarctic Front, PF – Polar Front, STW – Subtropical Waters, SAW – Subantarctic Waters, AAIW – Antarctic Intermediate Waters, STMW – Subtropical Mode Waters, SAMW – Subantarctic Mode Waters, AABW – Antarctic Bottom Water, CDW – Circumpolar Deep Water, DWBC – Deep Western Boundary Current and PDW – Pacific Deep Water. CDW included both Lower CDW and Upper CDW.

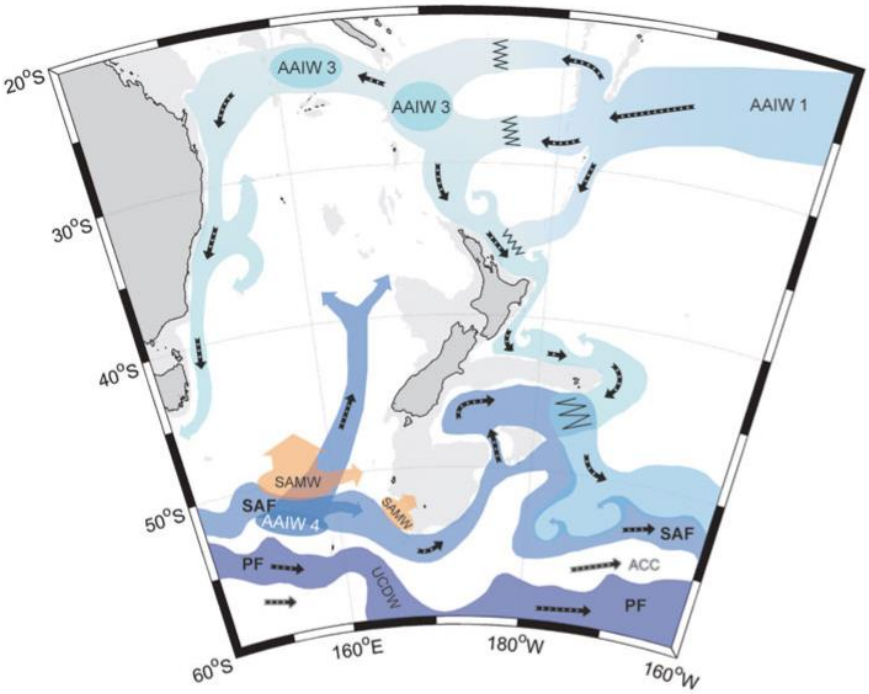

Figure 2.2b. Diagram of intermediate circulation around New Zealand taken from Chiswell et al., (2015). AAIW – Antarctic Intermediate Waters, SAMW – Subantarctic Mode Waters, STMW (not pictured) – Subtropical Mode Waters, SAF – Subantarctic Front. AAIW 4 = Southern Ocean AAIW, AAIW 3 = Tasman AAIW, AAIW 1 = SE Pacific AAIW.

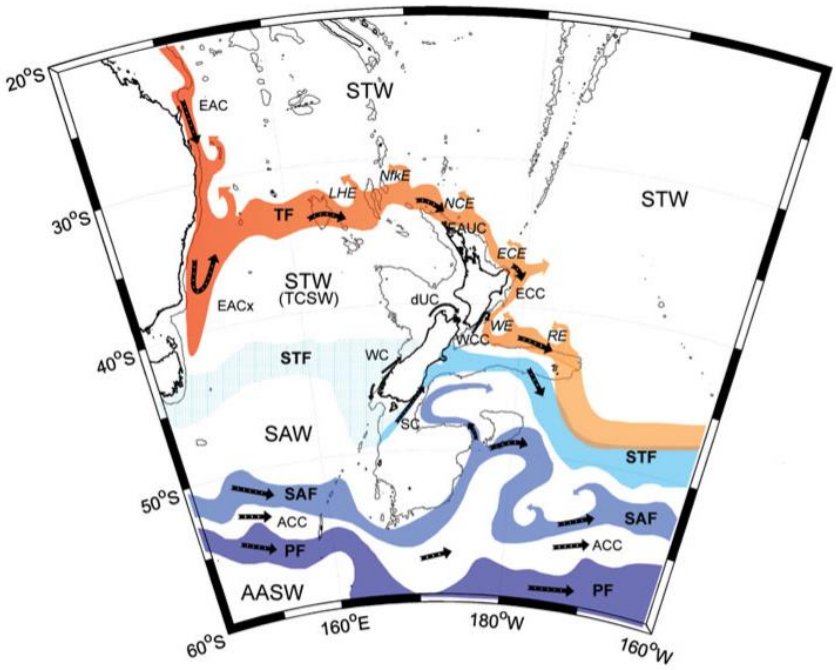

Figure 2.2c. Diagram of surface circulation around New Zealand taken from Chiswell et al., (2015). Oceanographic fronts/flow regions are in colour. Small regional oceanographic features including the LHE, NfkE, NCE, EAUC, ECE, ECC, We, WCC, RE, WC and SC have been ignored for the purposes of this study. TF – Tasman Front, STW – Subtropical Water, STF – Subtropical Front, SAF – Subantarctic Front, ACC – Antarctic Circumpolar Current, PF – Polar Front, AASW – Antarctic Surface Water

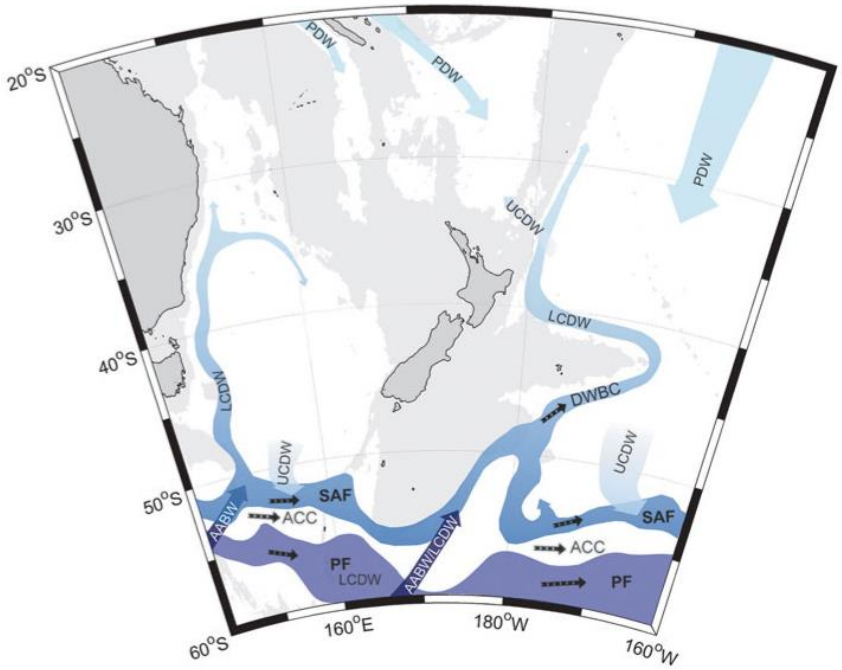

Figure 2.2d. Diagram of deep-water circulation around New Zealand taken from Chiswell et al., (2015). PDW – Pacific Deep Water, UCDW – Upper Circumpolar Deep-Water, LCDW – Lower Circumpolar Deep-Water, DWBC – Deep Western Boundary Current, AABW – Antarctic Bottom Water. DWBC transports both AABW and LCDW north.

2.3 Primary Production

Primary production refers to the production of organic material by primary producers in the ocean, predominantly driven by nutrient (C, N, P, Fe and other micronutrients) input and bioavailability. These primary producers are commonly phytoplankton and bacteria; and comprise the very basis of the ocean food web, serving as a food source for higher marine lifeforms. Primary producers, therefore, are essential in sustaining global fisheries and ultimately life in the ocean as we know it (Pauly and Christensen, 1995). Phytoplankton alone are responsible for over half of net primary production in the global biosphere (Behrenfeld et al., 2001).

During primary production, inorganic compounds (i.e. carbon dioxide (CO_2), carbonate (CO_3^{2-}) and bicarbonate (HCO_3^-) become converted (reduced) into simple organic molecules such as glucose (CH_2O) (Falkowski and Raven, 2013; Falkowski and Woodhead, 2013). These organic molecules comprise the basis of organic compounds,

which are considered to be the building blocks of life and serve as vital mechanisms for storing energy in living organisms (Thornton, 2012). These essential organic molecules are primarily produced by harnessing sunlight in the surface ocean (photosynthesis) but can also be produced by harnessing some chemical reactions such as sulfide oxidation around deep ocean vents (chemosynthesis).

1) $2H_2O + CO_2 + \text{light} \rightarrow (CH_2O) + H_2O + O_2$ (Falkowski and Raven, 2013)

2) $CO_2 + O_2 + 4H_2S \rightarrow CH_2O + 4S + 3H_2O$ (Jannasch & Wirsen, 1979)

1) Equation for photosynthetic reduction of carbon dioxide

2) Equation for chemosynthetic reduction of carbon dioxide

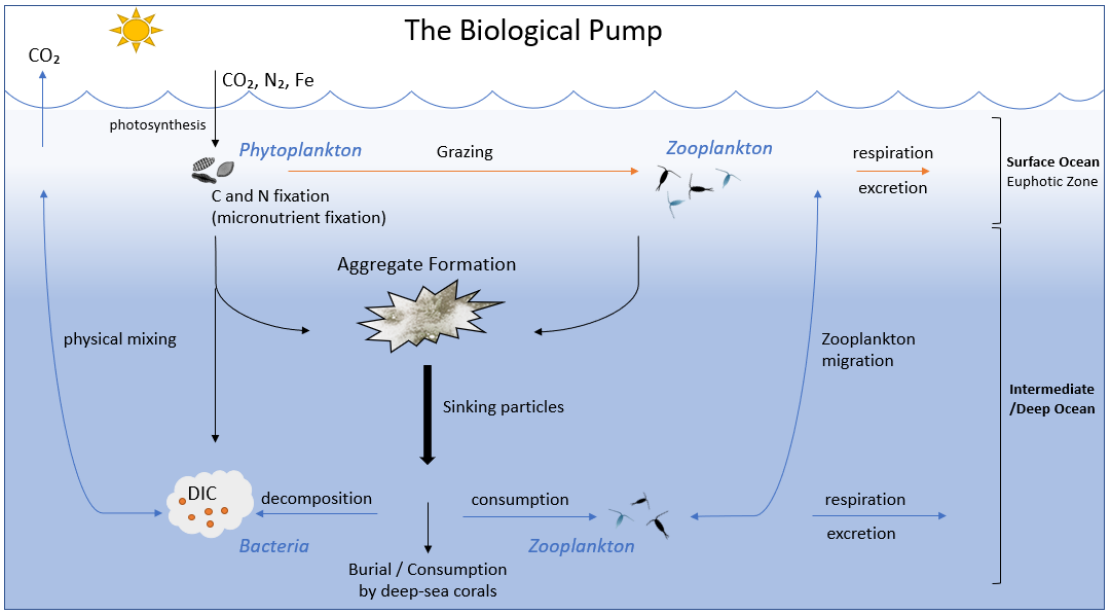

Figure 2.4a. Schematic diagram of the biological pump. Nutrients are up taken by primary producers (phyto/zooplankton) in the euphotic (surface waters) zone. Upon expiration, planktonic remains form aggregates and sink to intermediate depths. Here, nutrients may be remobilised via further consumption or bacterial interaction before becoming buried at the seafloor. Physical mixing (upwelling) and zooplankton migration may return remineralised nutrients/DIC to the surface ocean.

2.4 The Biological Pump

The biological pump is the mechanism responsible for the export of organic particles (including macro and micronutrients in plant parts and animal waste) to the intermediate/deep ocean, and ultimately the biological sequestration of carbon into the

deep ocean (de la Rocha and Passow, 2014b; DeVries et al., 2012) (Figure 2.4a). The pump is driven by photosynthesis at the surface (euphotic zone), during which C, N, P (+ micronutrients) are incorporated into phytoplankton tissues (de la Rocha and Passow, 2014b; Nodder and Boyd, 2001). When the phytoplankton die or are ingested and excreted by consumers, their organic residues sink as particulate organic matter (POM). Breakdown of this organic material below the euphotic zone releases most of these elements, enriching intermediate waters, while some is buried in deep marine sediments (Figure 2.4a). Therefore, biological productivity in the surface ocean and the subsequent export of organic C to the deep ocean play an essential role in regulating atmospheric CO_2, especially on geological timescales. In black corals and other benthic dwelling creatures, this organic material may form their food source.

Nutrients (C, N, P & micronutrients) regenerated at depth cannot return to the surface ocean due to the density barrier that separates the surface from deep waters (pycnocline). Therefore, nutrients are continually depleted from surface waters, leading to low – biolimiting – concentrations; we see this in regions such as the Southern Ocean (Bowie et al., 2009; Bruland et al., 1991). It is only in regions where wind forces upwelling or thermal density stratification breaks down (e.g. polar regions) that deep nutrient-rich waters can mix with surface waters and supply the biolimiting nutrients. It is because of this; the strength and efficiency of the biological pump varies between ocean basins and through time with changing ocean/atmosphere interactions and nutrient supply (de la Rocha and Passow, 2014b; DeVries et al., 2012).

Because this POM is of a surface water origin, its chemistry (with respect to C, N, P, and micronutrients) is expected to reflect the surface water environments from where it is derived. Therefore, a surface-water chemical signature is expected to be imparted on the black coral skeleton (and tissues) as this POM is up taken. However, this relies on the following assumptions: (1) The coral's dominant food source is POM. (2) The trace element composition of the coral skeleton is proportional to the trace element composition of the corals' food. And (3) that the trace metals in the tissues of phytoplankton (& POM) are proportional to the concentration in the surface waters. Given these assumptions are satisfied, this chemical 'surface ocean' signature may

inform us of changes to the nutrient structure, primary productivity and ultimately the strength of the biological pump in the overlying ocean throughout a coral's lifespan.

Considering the biological pump's integral role in the regulation of primary productivity and atmospheric CO_2, understanding the sinks, sources, and transport of nutrients and environmental carbon is critical (Boyd, 2015; Gruber et al., 2009; Passow and Carlson, 2012). The response of the biological pump, CO_2 sequestration and primary productivity to climate change is likely to be complex and non-linear (Boyd, 2015; Chiswell and Sutton, 2020). No definitive conclusion has been reached about whether global warming will increase or decrease the pump (Passow and Carlson, 2012). Typically, the circulation models used to project regional-oceanic responses to changing atmospheric conditions are limited by the data used to inform model boundary conditions, with a paucity of data existing prior to the 1970s. We, therefore, need a way to generate records that can extend our knowledge on phytoplankton dynamics (and by association - CO_2 sequestration) beyond our limited interval of observation. This is where reconstructing past ocean nutrient distributions may be useful.

2.5 Nutrients in the Ocean

Nutrients in the surface ocean ultimately control the abundance of phytoplankton, hence the biological pump and therefore the amount of carbon sequestered into the deep ocean. Understanding the behaviour of nutrients in the ocean is therefore key to understanding phytoplankton carbon flux over broad timescales.

2.5.1 Macronutrients

Carbon, nitrogen and phosphorus are the dominant *macronutrients* required by phytoplankton (de la Rocha and Passow, 2014b; Falkowski and Woodhead, 2013). The relative amounts of each element required by phytoplankton/primary producers can be defined by the Redfield Ratio whereby primary producers require 106 C atoms to 16 N atoms to 1 P atom (Redfield, 1958). When one of these elements is present at a lower ratio to this, phytoplankton can only grow until that element is used up, then growth ceases. The vertical distributions of these dissolved elements in the ocean form predictable patterns in most regions predominantly controlled by phytoplankton productivity and the biological pump (Bruland et al., 2013; De La Rocha and Passow, 2014a; Morel and Price, 2003). Generally, nutrients are aggressively scavenged in euphotic (sunlit) surface regions and exported as particulates to intermediate/deep waters (De La Rocha and Passow, 2014a). This leads to very low surface concentrations. Nutrients become released from settling particulates at intermediate depths primarily via bacterial respiration (de la Rocha and Passow, 2014b; Schneider et al., 2003). This results in an enrichment in most nutrients at intermediate depths (Figure 2.5a).

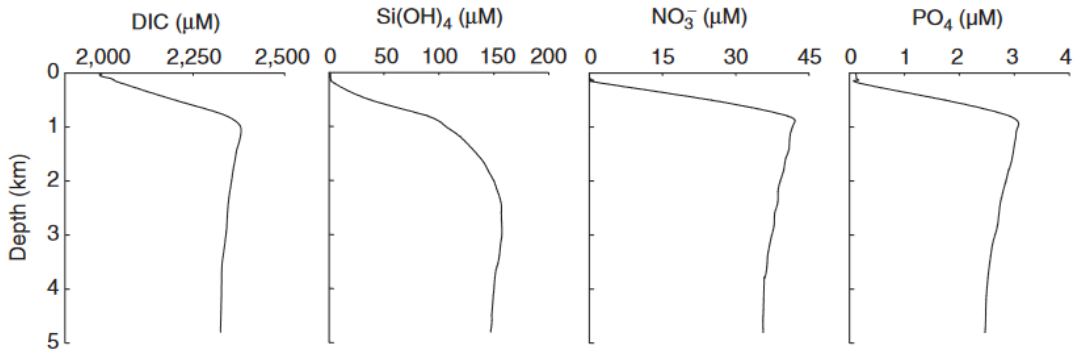

Figure 2.5a. "Idealized" vertical profiles for the distributions of major nutrients in seawater. Figure taken from de la Rocha and Passow (2014b).

*Micro*nutrient trace metals such as Fe, Ni, Zn, Co & Cu are also required by phytoplankton, predominantly as cofactors of metalloenzymes and proteins (Bruland et al., 2013; Morel and Price, 2003; Sunda, 2012). Iron, for example, may be as biolimiting as the macronutrients (Boyd and Ellwood, 2010; Morel et al., 1991; Morel and Price, 2003), although the cellular quotas for these trace element nutrients are significantly lower (Morel, 2008). Because these elements are utilised by phytoplankton in the same

way as macronutrients, the vertical distributions of dissolved elements in the ocean are nearly identical to N and P (Figure 2.5a, 2.5b & 2.5d). These trace metals may therefore serve as proxies for their macronutrient counterparts i.e. see Rosenthal et al. (1997) and Baars et al. (2014).

2.5.2 Trace Elements in Seawater

The following section presents the (bio) geochemistry of various trace elements in the ocean grouped by their distribution types as described in Bruland et al. (2013). There are three general patterns of depth profile: 'conservative', 'nutrient' and 'scavenged' as well as hybrid profiles with features from two of the general profiles. Although loosely defined, the term 'trace element', abbreviated to '**TE**', throughout this research refers to elements present in the Earth's crust in amounts less than 0.1% (Kabata-Pendias and Mukherjee, 2007).

2.5.2.1 Nutrient Type Distributed Trace elements

Elements with nutrient-type depth profiles are predominantly involved in major biogeochemical cycles: taken up by planktonic organisms at the surface, and re-mineralised at intermediate depths (Bruland et al., 2014; Sarmiento, 2013). These processes result in a significant depletion in surface waters, a substantial increase at intermediate depths and a steady decline when approaching abyssal depths (Figure 2.5b), closely approximating the distributions of their macronutrient (C, N and P) counterparts (Figure 2.5a). Typical residence times

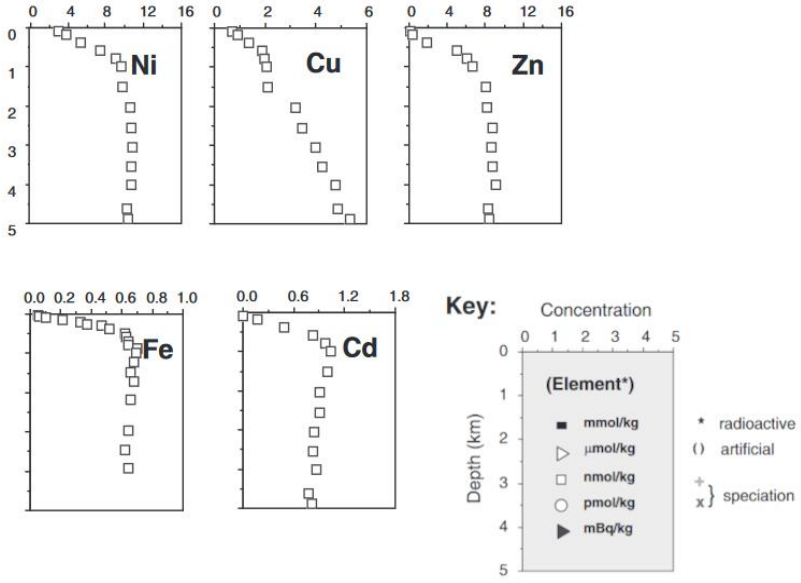

Figure 2.5b. Nutrient-type distributed elements in seawater. Figures adapted from Sarmiento (2013). Distributions are schematic. NB: Fe is included as a nutrient type element despite hybrid behaviour in the South Pacific, see Boyd et al. (1999).

for elements that follow nutrient-type distributions are between thousands to hundreds of thousands of years (Bruland et al., 2014). Iron is included here as a nutrient-type element despite its hybrid behaviour.

Element	*Distribution*	*Source*	*Sink*	*Avg. Concentrations in Seawater (Tasman Sea & Pacific Ocean)*	*Avg. Cellular Concentrations in Phytoplankton*	*Avg. Concentraiton in Calcareous (Hard) Corals*	*Residence Time (years)*
Cd	Nutrient	Terrestrial Hydrothermal Anthropogenic	Seafloor sediment	11.2 - 89.9ppt [1]	~2±0.25ppm [14]	6-58ppb [2] (Poirites) 1.6-170ppb [8] (12x Hard corals around South Africa)	50,000 [18]
Zn	Nutrient	Terrestrial (Rivers and wet/dry dust) Remineralization Anthropogenic	Biological incorperation. Seafloor sediment	>65.4 - 425ppt [3]	~5±1ppm [15]	~322ppm [4] (Poirites) 0.15-4ppm [9] (12x Hard corals around South Africa)	40,000 - 50,000 [19]
Fe	Hybrid (Nutrient/Scavenged) Nutrient in HNLC* locations. Scavenged near terrestrial sources.	Terrestrial (wet/dry dust, windblown) Remineralization	Biological incorperation. Seafloor sediment	5.58 - 41.9ppt [5]	~39±8ppm [16]	111-343ppm [6] (Poirites) 470-2500ppm [10] (12x Hard corals around South Africa)	200 - 500 [20]
Ni	Nutrient	Terrestrial (weathering + rivers + dust) Anthropogenic Hydrothermal	Seafloor sediment. Ferro-manganese Nodules	117-440ppt [7]	N/A	2.7-32ppm [11] (12x Hard corals around South Africa)	10,000 [21]
Cu	Nutrient	Terrestrial Anthropogenic Hydrothermal Remineralization	Seafloor sediment Biological incorperation	31.7-381.2ppt [13]	~2±0.7ppm [17]	210-1100ppb [12] (12x Hard corals around South Africa)	20,000-25,000 [22]

*Table 2.5a. Summary table of nutrient/scavenged-type element distribution, sources, sinks and residence times alongside avg. elemental concentrations in seawater, phytoplankton cells, and hard (calcareous) corals. *HNLC refers to High Nutrient, Low Chorophyll. References: (1, 3, 5, 7 & 13) - Schitzer, 2018, (2,4 & 6) - Hanna & Muir, 1990, (8, 9, 10, 11, 12) - Van der Shyff et al., 2020, (13) - Boyle et al., 1977, (14, 15, 16 & 17) - Ho et al., 2003, (18) - Boyle et al., 1976, (19) - Sinoir et al., 2012, (20) - Boyd & Ellwood, 2010, (21) - Glass & Dupont, 2017, (22) - Richon & Tagliabue, 2019; Little et al., 2013.*

2.5.2.1.1 Zinc

Zinc is present in nanomolar concentrations in the ocean, with most (95-98%) complexed by organic ligands and the rest as free Zn^{2+} (Bruland, 1989; Saito and Goepfert, 2008; Zhao et al., 2014). Much like other trace elements, zinc is present in the ocean in nanomolar concentrations, several orders of magnitude lower than macronutrients (Bermin et al., 2006; Morel and Price, 2003).

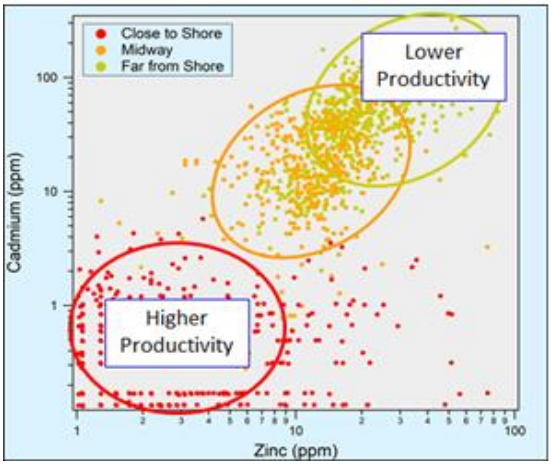

Figure 2.5c. Near linear correlations between Zn and Cd as measured from the skeletons of black corals. Zn and Cd behaviour contradicts traditional behaviour moving away from the coastline, showing a distinct increase in concentrations moving into the open ocean. Original graphics produced by Sinclair, 2018.

Zinc is an important cofactor in the enzyme's carbonic anhydrase (CDCA) and alkaline phosphatase (Coleman, 1998; Sinoir et al., 2012; Zhao et al., 2014). CDCA is essential for uptake of HCO_3^- during organic carbon synthesis (Morel et al., 1994) meaning Zn bioavailability may limit phytoplankton growth. CDCA is also known to play a significant role in the physiology of calcifying corals (Bertucci et al., 2013) and may thereby also be utilised in carbon acquisition by black deep-sea corals.

Prior research has shown Cd and Zn behave similarly in the skeletons of deep-sea corals, as demonstrated by the correlation between skeletal Cd and Zn in Figure 2.5c (Sinclair, unpup 2018). Zinc/Cd concentrations are lowest in samples closest to the coastline, where productivity may be expected to be high and increase with distance from the coastline moving into less productive waters.

2.5.2.1.2 Cadmium

Most (70-80%) of surface water cadmium is complexed with organic ligands, with the remainder (~20-30%) existing predominantly as inorganic chloro-complexes (Bruland, 1992). Due to its nutrient-like behaviour, the vertical distribution of Cd in the ocean strongly correlates with phosphorus (Boyle, 1992; Boyle et al., 1976) and Cd has therefore been used for palaeo-reconstruction (Baars et al., 2014; Marchitto and

Broecker, 2006). In the tests of foraminifera, Cd reflects dissolved Cd concentration of the waters during foram-test formation and has been used as a proxy for oceanic phosphate (Boyle et al., 1976; Cullen, 2001; Marchitto and Broecker, 2006). However, the Cd:P relationship changes across the world's oceans: in the Southern Ocean, for example, enhanced uptake of Cd results in a steepening Cd:P gradient (Baars et al., 2014).

Cadmium has also been found to replace Zn in the Zn-carbonic anhydrase enzyme (Morel, 2013), suggesting it may exhibit co-limiting behaviour (Bruland et al., 2013; Lane, 2000; Morel et al., 1994), and possibly be associated with carbon acquisition in some marine lifeforms such as deep-sea corals. Cadmium may also substitute for Zn in other metalloenzymes, suggesting a functional-replacement mechanism between the two cations (see Morel and Price (2003)). The diatom *Thalassiosira weissflogii* will preferentially uptake Cd under low-Zn conditions (see Lane (2000)), increasing cellular carbonic anhydrase production. However, recent work suggests that Cd uptake may be incidental, with minimal effect on carbonic anhydrase activity (Horner et al., 2013).

This potential co-limiting behaviour between Cd and Zn may be responsible for driving the tight Zn-Cd correlations previously observed in deep-sea corals (Figure 2.5c) (Sinclair, unpub 2018).

Cadmium is also a major anthropogenic pollutant and is considered one of the most toxic heavy (trace) metals (Engel and Fowler, 1979; Okocha and Adedeji, 2011; Wahyu et al., 2020). Despite its toxicity, Cd can accumulate in large concentrations in the skeletons of black corals accumulating at up to 400ppm (Komugabe, 2015a; Raimundo et al., 2013), 10^7 times above its concentration in seawater (Schlitzer, 2018). These large Cd concentrations suggest the black corals may be utilising Cd for some unknown biological purpose *or* that the skeletons may form a metabolic dump/storage/detoxification location for trace metals present in large, toxic concentrations such as Cd (Rainbow, 2002).

2.5.2.1.3 Nickel

In seawater, up to 50% of dissolved Ni is in its free ion inorganic (Ni^{2+}) form and 10-30% is complexed by strong organic ligands (Achterberg and Van Den Berg, 1997; Donat et al., 1994; Glass and Dupont, 2017). Nickel is known to be an essential trace element for several terrestrial plants and microorganisms, however, comparatively little is known

of its biological utility for marine organisms (Biscéré et al., 2017; Cempel and Nikel, 2006).

Nickel forms the active metal centre in the urease enzyme and is therefore involved in nitrogen acquisition by some primary producers and calcifying corals (Biscéré et al., 2018; Biscéré et al., 2017; Morel and Price, 2003; Twining et al., 2012). In locations where urea is the sole nitrogen source (such as in regions with low upwelling and nutrient supply (Remsen, 1971), the growth of some phytoplankton species is dependent on the Ni concentration of seawater (Dupont et al., 2008). Here, large Ni concentrations may enhance the growth rates of phytoplankton.

Assuming that coral Ni faithfully reflects the Ni concentration in the settling organics, then an elevated skeletal Ni concentration in black corals may indicate surface water conditions where nitrogen supply is low, and phytoplankton are forced to use urea as a nitrogen source. This would set up an anticorrelation between coral Ni and surface water productivity.

2.5.2.1.4 Iron

Iron has been long known to behave as a major biolimiting trace nutrient in the ocean. Low surface concentrations mean that it is the limiting nutrient in ~30% of the world's oceans (Moore et al., 2004), such as the South Pacific (Boyd et al., 1999; Martin and Fitzwater, 1988). In most locations, Fe has a nutrient-type profile, with intense depletion at the surface and regeneration with depth (Johnson et al., 1997). However, in areas with high aeolian dust input, Fe instead displays a scavenged depth profile with a surface maximum and depletion at depth (Bruland et al., 2014). The hybrid nature of Fe's behaviour may be observed in the Southern, Atlantic and Pacific Oceans as a lack of increase in Fe with depth (in contrast to the major nutrients) (Boyd and Ellwood, 2010) due to scavenging (Bruland et al., 2014).

More than 99% of dissolved Fe is bound to complexing organics (Gledhill and Buck, 2012), characterised as either strong binding ligands ('L1') or weak binding ligands ('L2'). L2 ligands are ubiquitous throughout the water column, whereas the L1 ligands are mostly confined to the upper ocean (Boyd and Ellwood, 2010). These ligands play an

integral role in keeping Fe dissolved in solution (hence bioavailable) (Rue and Bruland, 1995; Wu et al., 2001).

Iron-containing molecules are essential in electron-transport processes occurring within phytoplankton, so Fe heavily affects the efficiency of photosynthesis (Morel and Price, 2003). Low Fe concentrations result in lower conversion rates of inorganic carbon into biomass hence slower growth rates (Martin and Fitzwater, 1988; Martin et al., 1990). Iron is also essential for N_2 fixation, and so the distribution of Fe also controls oceanic fixed N content (Sunda, 2012). Consequentially, Fe plays an integral role in regulating key biological cycles for C and N and, ultimately - the biological pump (Sunda, 2012). Therefore, understanding the dynamics of dissolved Fe in seawater through time is essential to tracking changes to the biological pump, especially in Fe limited regions.

Iron has also been observed to preferentially concentrate within the organic cement regions in between successive skeletal layers of coral skeleton (Nowak et al., 2009), implying black corals have some biological use for Fe, or Fe occupies some structural role in the skeletal organics.

2.5.2.1.5 Copper

Approximately 95-99.8% of oceanic Cu is complexed by organic matter (Little et al., 2013; Moffett and Dupont, 2007). Copper is an essential micro-nutrient for phytoplankton and diatoms, involved in both iron and oxygen acquisition (Annett et al., 2008; La Fontaine et al., 2002; Maldonado et al., 2006). Despite this, high Cu concentrations are highly toxic to marine life, so Cu is considered a “goldilocks” element (Bruland et al., 2013). Phytoplankton regulate seawater Cu by releasing strong Cu-binding ligands (Bruland et al., 2013; Little et al., 2013; Richon and Tagliabue, 2019) which can considerably reduce free ion Cu^{2+} concentrations down to non-toxic levels, favouring phytoplankton growth (Moffett and Brand, 1996).

In some cases, Cu may be co-limiting with Fe as it behaves as a part of the high-affinity Fe uptake system in diatoms (Annett et al., 2008; La Fontaine et al., 2002; Maldonado et al., 2006). By association with Fe, Cu is also likely an important component in regulating key biochemical cycles, and may, therefore, be utilised by black corals for some biological purpose or possibly occupy some structural role in the skeletal organics.

2.5.2.2 Conservative Type Distributed Elements

Conservatively distributed elements tend to be unreactive and thus have residence times longer than ocean mixing times (Bruland et al., 2014). Therefore, their concentrations have become homogenized throughout all ocean basins, resulting in minimal change with latitude or depth (Figure 2.5d), aside from remaining at a constant ratio to salinity (Bruland et al., 2014; Sarmiento, 2013). Conservatively distributed elements are typically present as either large monovalent cations or oxyanions (Bruland et al., 2014). Unlike their nutrient-type counterparts, the behaviour/distributions of conservative elements in seawater do not correlate with macronutrients. Thus, these elements (except for I, see below) offer little utility in reconstructing ocean nutrients. Instead, many of the elements listed below are redox-sensitive (Bennett and Canfield, 2020; Brüske et al., 2020; Emerson and Huested, 1991; Morford and Emerson, 1999) and may, therefore, serve as tracers for the redox state of the environment surrounding the coral upon their consumption.

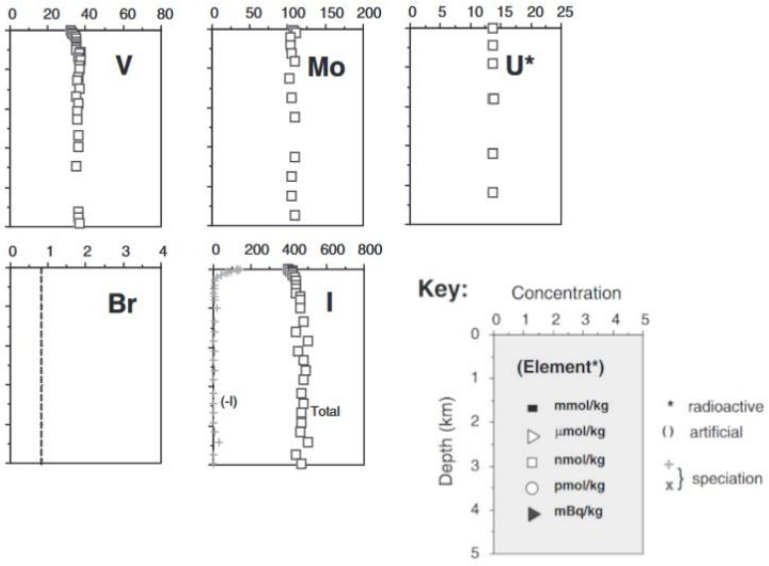

Figure 2.5d. Conservative-type distributed elements. Figure adapted from Sarmiento (2013).

2.5.2.2.1 Molybdenum

The main dissolved form of Mo in the ocean is molybdate (MoO_4^{2-}, Mo(VI)), which is released during weathering and subsequently transported to the ocean via rivers (Morford and Emerson, 1999; Siebert et al., 2003). In seawater, Mo is an essential trace element for some phytoplankton, with Mo-containing proteins being key components in the two nitrogen and dinitrogen reducing enzymes: algal nitrate reductase and nitrogenase (Collier, 1985; Dellwig et al., 2007; Tuit, 2003). Despite this biological

function, uptake of Mo by organisms is not high enough to significantly affect its oceanic distribution. Therefore, in most cases, Mo behaves conservatively (Collier, 1985). However, Mo may exhibit non-conservative (scavenged) behaviour nearby to major terrestrial sources and in regions of intense primary productivity (Dellwig et al., 2007). For example, there is some evidence to suggest Mo may be biolimiting under the right conditions, with depth profiles from the Wadden Sea showing distinct non-conservative behaviour (Dellwig et al., 2007).

Because water column sulfide levels control Mo scavenging (Brüske et al., 2020; Morford and Emerson, 1999; Tessin et al., 2019), palaeoceanographers may utilize Mo in deep-sea sediments to indicate ocean redox states. When sulfide concentrations are high (i.e. under reducing conditions), Mo removal from seawater is greatest. Therefore, large Mo concentrations in seafloor sediments may be used as an indicator for changes to the redox state at the seafloor (see Tessin et al. (2019)). Assuming coral Mo reflects the concentration of the ambient seawater surrounding the coral, then low skeletal Mo concentrations may indicate enhanced Mo removal at the seafloor. This, in turn, potentially could be used to track changes to seafloor redox conditions through time.

Element	*Distribution*	*Source*	*Sink*	*Avg. Concentrations in Seawater*	*Avg. Concentrations in Phytoplankton*	*Avg. Concentraiton in Corals*	*Residence Time (years)*
Mo	Conservative	Terrestrial. May be remobilized at depth in seawater.	Seafloor sediment	9-13ug/L (107nmol/kg)[1]	2-2.5ppm [2]	-	700,000 - 800,000 [12]
V	Conservative	Terrestrial. Anthropogenic. May be remobilized at depth in seawater.	Seafloor sediment	35-45nmol/kg [3]	0.08-49ppm [4]	119.4ppb [5] Poirites coral avg.	120,000[13]
U	Conservative	Terrestrial. Anthropogenic.	Seafloor sediment. Carbonates	3.3ppb [6]	14-20ppb [7]	~33ppb [8] (deep-sea coral, family: Isdidae)	350,000 - 400,000 [14]
Br	Conservative	Seawater	Sea-spray/Evaporation	~65ppm [9]	-	-	130,000,000 [15]
I Tot	Conservative/Nutrient	Seawater	Sea-spray/Evaporation	58-60ppb [10] (may increase with depth)	~3600ppm [11]	-	340,000 [16]

Table 2.5b. Summary table of conservative-type element distribution, source, sink, and residence times along with avg concentrations in phytoplankton, seawater and hard corals. References: (1) - Collier, 1985; Morris, 1975, (2) - Tuit, 2003, (3) - Barceloux & Barceloux, 1999, (4)- Kutter et al, 2014, (5) - Saha et al., 2019, (6) - Andersen et al., 2010; Ku et al., 1977, (7) - Russel et al., 2004, (8) - Sinclair et al., 2011, (9) - Eggenkamp, H. , 2014; Stumm & Brauner, 1975, (10) - Carpenter, 2003; Elderfield & Truesdale, 1980; Moreda-Pineiro et al., 2011., (11) - calculated from observations in Elderfield & Truesdale (1980), (12) - Siebert et al., 2003, (13) - Andersen et al., 2010, (14) - Schlesinger et al., 2017, (15) - Eggenkamp, H., 2014, (16) - Broeker & Peng, 1982.

2.5.2.2.2 Vanadium

Vanadium is present in seawater predominantly in its +4 to +5 oxidation states (Barceloux and Barceloux, 1999; Huang et al., 2015; Schlesinger and Bernhardt, 2013; Wang and Wilhelmy, 2009), existing as the vanadyl ion (VO_2/VO^{2+}) under reducing conditions, and the vanadate ion (VO_4^{3-}) under oxidising conditions (Barceloux and Barceloux, 1999; Emerson and Huested, 1991).

Although normally conservatively distributed, vanadium may exhibit non-conservative (scavenged) behaviour in some coastal waters (Wang and Wilhelmy, 2009).

Vanadium may be considered relatively non-toxic compared to other trace metals (Barceloux and Barceloux, 1999; Huang et al., 2015). This low toxicity and multiple oxidation states mean that V acts as a trace nutrient for phytoplankton and macroalgae (Barceloux and Barceloux, 1999; Huang et al., 2015; Wang and Wilhelmy, 2009). Some microorganisms have been observed to utilise Vanadyl ions (VO^{2+}) instead of Fe(III) as electron acceptors during respiration (Huang et al., 2015; Lyalkova and Yurkova, 1992; Zhang et al., 2014). Additionally, V is involved in the metal centres for nitrogen reducing enzymes such as nitrate reductase and nitrogenase (Schlesinger and Bernhardt, 2013; Wang and Wilhelmy, 2009)

As with Mo, V is redox-sensitive and can be used as a palaeo-redox indicator in seafloor sediments (Bennett and Canfield, 2020). Here, oxic bottom waters limit V removed into sediments, and sub-oxic/anoxic seawater enhance V removal. Assuming V uptake by black corals is passive, and skeletal V concentrations reflect that of the ambient seawater surrounding the coral, significant changes in V concentration throughout the coral skeleton may provide an insight into changes to the redox conditions of the seafloor surrounding the coral.

2.5.2.2.3 Uranium

Uranium is primarily present in seawater in a highly soluble U(VI) state but may be reduced to a highly insoluble U(IV) state through biological mediation and in reducing environments (Andersen et al., 2010; Klinkhammer and Palmer, 1991; Lovley and Phillips, 1992; Markich, 2002). Typically, free metal ion form U(IV) and UO_2^{2+} form complexes with inorganic ligands (such as carbonates or phosphates) in dissolved,

colloidal or particulate forms (Markich, 2002). Organisms tend to take up U(VI) as UO_2^{2+} and UO_2OH^+ ions rather than the more strongly complexed species (Markich, 2002).

Uranium is readily incorporated into the calcareous structures of carbonate lifeforms due to its ability to form strong complexes with carbonates (Klinkhammer and Palmer, 1991; Markich, 2002). As such, uranium is concentrated in most carbonate corals in levels very similar to that of its ambient seawater concentrations (Gothmann et al., 2019). Similarly, U is concentrated in black corals in isotopic equilibrium with seawater uranium, with δU^{234} values throughout the coral skeletons remaining within the range of modern seawater (Komugabe et al., 2014; Roark et al., 2009a). Therefore, assuming black corals source U from an ambient seawater source (and it is passively uptaken), changes in isotopic uranium concentrations (U^{234}/U^{238}) may reflect changes in the U isotope content of seawater. Because uranium is redox-sensitive, this may inform us about the redox state of the seawater surrounding the coral.

2.5.2.2.4 Bromine

In seawater, Br is present mainly as the soluble bromide (Br^-) ion (Grinbaum and Freiberg, 2000). Bromide is easily oxidised to oxyanions (such as perbromate [BrO_4^-] and hypobromite [BrO^-]) by sunlight and ozone (Eggenkamp, 2014; Grinbaum and Freiberg, 2000). Marine organisms commonly convert Br to several organic forms such as bromo-ketones, bromo-alkanes and bromo-phenols via a number of abiotic (Keppler et al., 2000) and enzymatic (Butler and Carter-franklin, 2004; Leri et al., 2010) pathways, with these organic compounds becoming removed from the surface ocean to the atmosphere (Sander et al., 2003).

As such, inorganic Br has some biological utility and may be converted to organic forms by marine organisms, usually to increase the biological activity of secondary metabolites (i.e. the end products of primary metabolites such as toxins, pheromones and enzyme inhibitors) (Dembitsky, 2002; La Barre et al., 2010) or as a means of chemical defence (Dembitsky, 2002; Leri et al., 2010). Additionally, biophilic bromine has been found to correlate with total organic carbon (TOC) in some marine sediments and may be used to approximate TOC in deep-sea sediment cores (Ziegler et al., 2008).

Bromine is a known structural (organically-bound) component of proteinaceous deep-sea coral skeletons and is present in the form of a halogenated scleroprotein (Nowak et al., 2009; Williams et al., 2006), namely bromotyrosine and dibromotyrosine (Ehrlich, 2019). As such, the proteinaceous skeletons of deep-sea corals contain some of the largest concentrations of halogens (specifically Br and I) in a biological material (Nowak et al., 2009; Williams, 2020). Interestingly, these concentrations vary throughout the deep-sea coral skeletons and thus must be controlled by their biological availability (Juárez-de la Rosa et al., 2007; Prouty et al., 2011; Williams, 2020; Williams and Grottoli, 2011). Considering Br is predominantly present in seawater in a dissolved phase and is accumulated in large proportions by black corals, it seems unlikely the coral would source Br from any minor particulate phase – such as POM. Therefore, skeletal Br may be uptaken by the corals from some additional, possibly dissolved ambient seawater source, strongly suggesting that biologically-utilised TE's can be sourced from ambient seawater in addition to POM

2.5.2.2.5 Iodine

Over 96% of iodine in seawater is in its thermodynamically stable iodate form (IO_3^-) (Fuge and Johnson, 1986; Moreda-Pineiro et al., 2011; Wadley et al., 2020). The remainder is present in its free ion form as iodide (I^-) and organically bound particulate states (Fuge and Johnson, 1986; Moreda-Pineiro et al., 2011; Wadley et al., 2020). Iodide is predominantly formed via the biologically mediated reduction of iodate and is considered to be biophilic, accumulating in the tissues of some phytoplankton at up to 600,000x its concentration in seawater (Elderfield and Truesdale, 1980; Tsunogai, 1971; Tsunogai and Henmi, 1971; Wadley et al., 2020; Wong et al., 1976). Dissolved organic iodine (in its reduced I^- form) is thought to be the main species up taken by corals due to iodate (the more abundant oxidised species) being generally obstinate, less soluble and therefore less biologically available (Elderfield and Truesdale, 1980; Fuge and Johnson, 1986). As a result, the presence of iodide in the ocean can be linked to primary productivity, with regions of increased iodide concentrations generally correlating with regions of increased productivity (Elderfield and Truesdale, 1980; Tsunogai and Henmi, 1971; Wadley et al., 2020). This relationship to productivity may be expressed by an I:C ratio (Elderfield and Truesdale, 1980; Wadley et al., 2020).

Also, as with bromine, iodine forms one of the only known structural components in the skeletons of proteinaceous deep-sea corals (Nowak et al., 2009). Here iodine is present in the form of an iodinated-scleroprotein, preferentially concentrating in the glue regions between successive layers of the coral skeleton (Ehrlich, 2019; Nowak et al., 2009). Iodine concentrations, therefore, vary throughout the deep-sea coral skeletons and may be controlled by their biological availability in seawater (Juárez-de la Rosa et al., 2007; Prouty et al., 2011; Williams, 2020; Williams and Grottoli, 2011). This suggests skeletal Iodine may offer some utility as a tracer for primary productivity in black coral skeletons (assuming its uptake is not under heavy metabolic control).

Chapter 3 - Methods

3.1 Specimen Selection

The primary goal of this research is to study whether corals display element concentrations that reflect the composition of surface or intermediate (ambient) water masses around New Zealand. Therefore, the main selection criteria for specimens was to get a broad distribution of specimens from around the New Zealand subcontinent. However, since there remains much uncertainty about factors affecting coral skeletal chemistry (see Chapter 2), specimens were also selected (within the constraints of available specimens) to allow controlled subsets that isolate the effects of:

- Geographic Location
- Species/Genus
- Water Depth
- Coral Size
- Location within a Colony

Approximately 50 black coral colonies were selected from the National Institute of Water and Atmospheric Research (NIWA) Invertebrate Collection (NIC) (Figure 3.1a). Descriptions of the selected subsets are presented in the following sections.

3.1.1 Geographic Location

Samples were collected from all around New Zealand, aiming for a broad distribution around the New Zealand region, ideally sampling colonies representative of both the northern subtropical waters (STW) and southern subantarctic waters (SAW). Unfortunately, limited specimen availability means that a majority of colonies were located around New Zealand's East Coast, predominantly across the Chatham Rise and in the Bay of Plenty (Figure 3.1a). Only two black coral colonies were sampled from south of the STF (below 47˚S).

The lack of corals on the West Coast of New Zealand likely represents a lack of suitable seafloor substrates. Black corals exclusively grow on harder surfaces such as dense rubble and bedrock (Anderson et al., 2014) (see Section 2.1.3). These substrates are largely absent on New Zealand's more geologically passive west coast (Bostock, 2019). The lack of black coral samples to the south of NZ may be reflective of the limited

micronutrient supply in NZ's subantarctic waters (SAW) (Nodder et al., 2016) which restricts the availability of phytoplankton (the coral's food source).

In addition to sampling broadly, we also selected specimens to examine the effects of proximity to the New Zealand coastline (Section 4.2.2). Corals were sampled along two transects moving away from the shoreline in the Bay of Plenty and across the Chatham Rise from Banks Peninsula (Figure 3.1a). These transects offer the ability to compare coral chemistry at an increasing distance from the coast - something that is traditionally known to have a considerable effect on surface ocean chemistry (Bruland et al., 2013).

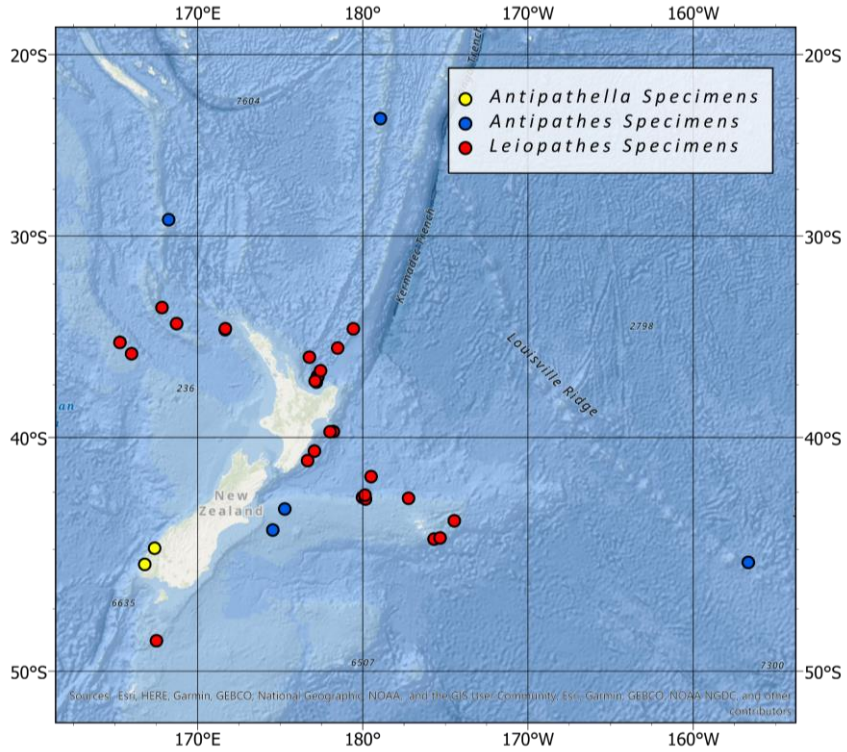

Figure 3.1a. Map of the distribution of sampled coral specimens around New Zealand. Classified by genus.

3.1.2 Species

This subset of corals was selected to investigate whether there is a taxonomic control on coral geochemistry. Of the 50 black corals sampled from the NIC dry store, 39 were of the *Leiopathes* genus, including the species *acanthophora*, *bullosa* and *secunda*, with 20 of the sampled *Leiopathes* corals not identified beyond the genus level (*Leiopathes* spp.). The *Leiopathes* corals sampled were identified by Dennis Opresko and Tina Molodtsova from 1998-2012. Five *Antipathella* genus corals were sampled, all of which were identified as the species *Antipathella fiordensis* by Dennis Opresko (1998) and Ken

Grange (1990). The remaining six corals were identified to the genus *Antipathes*, two of which were identified to the species *Antipathes sarothrum* by Dennis Opresko (2006).

The *Leiopathes* and *Antipathes* corals sampled are of broadly similar form, with both genera forming arborescent, bush-like and fan-shaped structures, with relatively robust main stems (Nowak et al., 2009; Wagner et al., 2012) (Table 3.1a). The *Antipathella* corals were slightly different in form, not exceeding a skeletal long-axis diameter of

	L. acanthophora	*L. bullosa*	*L. secunda*	*A. fiordensis*	*Antipathes* spp.
Corallum	Irregularly branched	Irregularly branched	Sinusoidal stem and larger branchlets with flabellate	Regularly branched	Irregularly branched
Spine form	Conical acute	Hemispherical blister like spines	Conical	Acicular, occasionally bifurcated	Steep sinistrose
Spines on larger branchelts	Present	Absent	Present	Present	Present
Polyps per cm	4-6	3-5	6-9	6-8	7-12
Growth rate (µm/yr)	1.3 - 40	1.3 - 40	~9.2	~53	90.9 - 142.9

Table 3.1a. Comparison of sampled coral species and genera. Table adapted from Molodtsova (2011), with additional Antipathella, Antipathes and growth rate data from Grange (1990); Warner (1981), and Hitt et al. (2020) respectively

Figure 3.1b. Comparison of Leiopathes (left) and Antipathella (right) skeletal surfaces. Note the typical smooth polished finish on the Leiopathes coral compared to the rough spine covered surface of the Antipathella.

2.5cm and forming much more pronounced skeletal spines (visible as a rough skeletal surface in Figure 3.1b). Both *Leiopathes* and *Antipathes* colonies are densely branched, without distinct pinnules, however, *Antipathes* colonies tend to be more flabellate with irregular yet alternating branches (Opresko et al., 2014; Tracey et al., 2014). The

Leiopathes colonies are generally more loosely spreading, with thicker branches, usually smooth and polished (Opresko et al., 2014; Tracey et al., 2014)(see Figure 3.1b & 3.1c).

3.1.3 Collection Depth

In order to test whether water depth has a significant influence on skeletal chemistry, several suites of coral samples were selected from different depths within the same region (within a ~25km radius). These comparisons may provide further insight into the black coral food source, taxonomy and/or whether their element concentrations reflect the surface or ambient water chemistry.

The sampled coral colonies were predominantly dredged up by commercial and research trawling vessels, with the *A.fiordensis* corals being collected by SCUBA divers. *Leiopathes* and *Antipathes* corals in the NIC exist across a similar depth range up to ~1600m (Tracey and Hjorvarsdottir, 2019); however, *Antipathella* corals are generally confined to much more shallow waters, existing from ~1m to over 400m water depth (Tracey and Hjorvarsdottir, 2019). While the *Antipathes* and *Leiopathes* corals have similar depth ranges, *Antipathes* corals have been found in waters as shallow as 10m, including one of the sampled *Antipathes sarothrum* specimens (NIWA Catalogue no. 15060). The sampled *A.fiordensis* corals were collected from shallow, relatively consistent depths between 34-85m, whereas the sampled *Leiopathes* and *Antipathes* corals collection depths ranged between 10m and 1500m. Despite the broad depth range of the *Antipathes* and *Leiopathes* corals, three groups of 3-4 corals were sampled within ~100 metres depth of each other, allowing the comparison of trace element concentrations at the same (within a ~25km radius) location and depth.

3.1.4 Size

Coral specimens of varying size (as defined by stem diameter) were sampled from the same geographic location (within a ~25-50km radius) and genus. This comparison set allows us to test if an ontogenetic factor (or some other size-related factor) affects coral chemistry.

The coral size was difficult to control during specimen collection due to the corals rarely being whole. The sizes of the sampled specimens varied greatly, with some black coral specimens being whole (basal root to branchlets ~2m long) and others being little more than branchlets – the equivalent of twig ends from a tree branch (<3cm long) (Figure 3.1c). The skeletal trunk diameters ranged from 0.5mm to 95mm, with an average of 30mm and a median of 12.5mm.

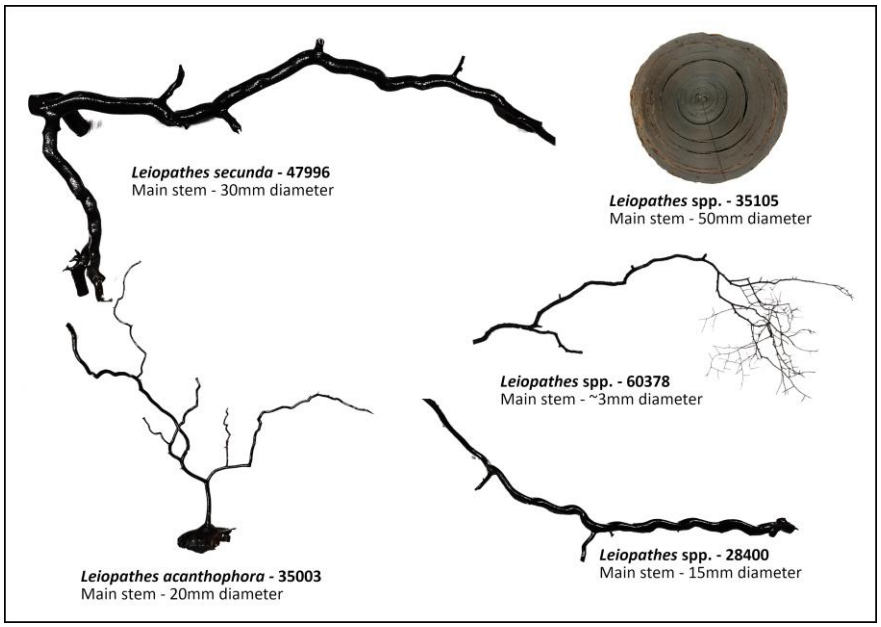

Figure 3.1c. Example of the different size and forms of the sampled black coral specimens. Note varying structures between Leiopathes species. Size measurements refer to the coral long axis diameter.

Many of the additional specimens in the NIC were found to be too small to sample reliably (>0.5mm skeletal diameter). On average, the *Leiopathes* corals were ~15-35mm in base/main stem diameter, and the *Antipathes* & *Antipathella* corals between 15-40mm.

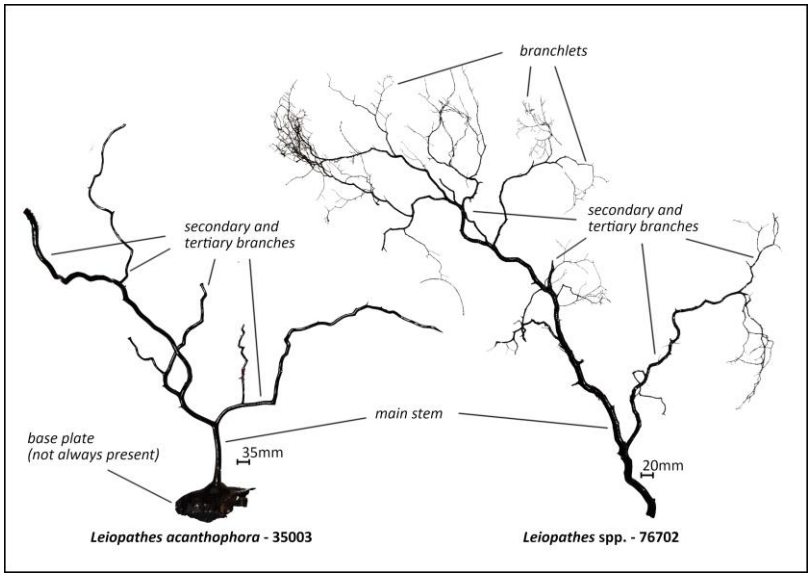

Figure 3.1d. Morphology of sampled black coral specimens L. acanthophora (35003 – left) and L. spp. (76702 – right).

3.1.5 Location Within a Colony

In order to determine whether the coral chemistry is consistent throughout the skeleton (or whether some form of ontogenetic effect might control skeletal composition), a subset of coral samples was taken from various parts of the same specimen (Figure 3.1d), including main stem and outer (tertiary) branches. This controlled subset is referred to in the text as the 'intra-colony test' (Section 4.1.2).

3.2 Sample Preparation

All sample preparation and analytical techniques were developed in-house with Dan Sinclair (VUW) in consultation with Bruce Charlier (VUW), Luisa Ashworth (VUW), Peter Marriott (NIWA), Di Tracey (NIWA), Nick Hitt (VUW) and Ashley Davis (VUW). Samples were collected from the NIC and milled in a Laboratory space at NIWA.

3.2.1 Milling

Sampling commenced by first cleaning the outside of the specimen by shaving off a thin layer using the side of a 1mm diameter carbide bit in a Dremel tool. This removed any residual tissue and/or potentially chemically altered surficial material. Following this, the working surface & drill were cleaned with compressed air. On corals with highly degraded (e.g. flaky/crumbly) skeletal surfaces, care was taken to remove additional surface material prior to drilling the target area to avoid contamination of the sample.

Once the skeleton surface had been cleaned, powder subsamples were taken using a slightly larger (1.5mm) tungsten carbide drill bit. A small ~4mm wide and ~4mm deep hole was milled, and ~10 mg of powdered sample was collected on waxed weighing paper. During milling, the Dremmel was set to its lowest setting, and minimal pressure was applied to avoid frictional heating of the skeletal material. On corals with smaller skeletal diameters (less than 8mm), multiple small (~2mm) surficial holes were drilled to obtain a sufficient amount of coral powder.

Powders were transferred to small polypropylene vials, ensuring that any large flakes of coral material were removed, including larger swarf-like strands of coral material. These flakes may be contaminated as they come from the unclean outer skeletal surface. After milling each sample, the surfaces and drill bit were thoroughly cleaned using ethanol, Kimwipes and compressed air to prevent sample cross-contamination.

In total, 111 powder samples were taken from the 50 black coral specimens. These samples include the control subsets described in Section 3.1.

3.3 Laboratory Procedure

3.3.1 Milling

The powder samples were weighed into Teflon vials at the VUW Geochemistry lab. Weighing is a precision-limiting step in the analytical protocol (see Section 3.3.2 below) because there are no elements that can be used as internal standards. Initial tests showed that the fine-grained organic powder was highly susceptible to static electricity, despite the use of an anti-stat gun, making it necessary to investigate alternative weighing methods to avoid compromising analytical precision.

Initially, small aluminium foil squares were folded into custom weighing boats; however, static caused the coral powder to stick to the foil, making it nearly impossible to fully transfer all weighed powder to digestion vessels. In addition, transferred powder often became stuck around the rims and on the base of the polycarbonate centrifuge vials. Ultimately, samples were weighed into ultra-pure 99.999% purity gold-foil weighing boats that had been pre-cleaned in boiling concentrated nitric acid. The powder and weighing boat were then transferred to the vials to undergo the complete digestion protocol (see Section 3.3.2). Gold is expected to be insoluble under the digestion conditions used here, so leaving the powders in the gold foil avoids sample loss during transfer. The gold-foil weighing boats were exclusively handled using plastic forceps to reduce contamination and avoid static charging.

Approximately 1 mg of coral powder was weighed on a high precision ultra-microbalance with a precision of approximately +/- 0.001%. This is expected to be equal to, or less than, the analytical uncertainty of the ICP-MS method (nominally around 5% RSD). After weighing, the powders – still in the gold foil weighing boats – were placed into clean, labelled 2ml Teflon beakers.

3.3.2 Digestion

All digestion was undertaken in ultraclean facilities within the VUW geochemistry lab. Powders (and the gold foil weighing boats) were initially reacted with 400µl of 50% nitric acid over a hotplate at 120˚C for 4hrs. Once powders were dissolved, the samples were dried down at 120˚C over ~6 hrs until a small orange-brown bead had formed (Figure 3.3a).

Figure 3.3a. Photo of first stage dried down coral standard material, including distinct orange colour and bubbly gelatinous form. The orange colour was maintained in solution through subsequent digestion procedures.

The samples were then re-digested in 1ml of 3% Nitric acid, which had been spiked with 0.5ppb Indium as an internal standard (this solution is hereafter referred to as the 'diluent'). Samples were then refluxed on a hotplate at 120˚C for 24hrs. As a way of testing whether the digestion protocol completely digested all material, a digested coral sample was centrifuged at 5000 rpm for 5 minutes and then carefully inspected for signs of insoluble residue. No particulate material was observed. Note that the gold foil weighing boats remained in the vials for this entire procedure.

150µl of each digested coral sample solution was pipetted (and precisely weighed) into clean, labelled polycarbonate sample cups. To these, 1350µl of 0.5ppb Indium spiked 3% nitric acid was added, resulting in a 10,000x mass dilution of the original coral powder.

With each batch of ~27 coral samples, approximately five procedural blanks were prepared, all of which underwent the exact digestion procedure as the coral powder samples, including the addition of the gold foil weighing boats.

3.3.3 Peroxide test

Following the digestion protocols, the solutions had a noticeable yellow/brown colour. To test whether this represents residual (soluble or colloidal) organic material, two aliquots of coral solution were taken. The first was kept as is. The second was reacted with 200ul of 30% H_2O_2. After 15minutes, the H_2O_2 containing solution was compared to the untouched coral solution with no colour difference observed. The stability of the colour to a strong oxidizing agent implies the colouration is not based on organic

material, but instead may represent high concentrations of a dissolved ion. These ions are possibly iodine (iodide) and/or bromine (bromide), which are known to be present at percentage levels within the coral (see Nowak et al. (2009) and Goldberg et al. (1994)).

3.3.4 Coral Standard Preparation

To calibrate the coral analysis, an in-house coral standard solution was prepared. 50mg of coral powder was initially digested in 50% nitric acid over a hot plate at 120˚C for 24hrs. Following dry-down, the coral was taken up in 50ml of diluent and left to dissolve on a hotplate overnight. After cooling, 4.92mls of solution was then transferred to a new clean Teflon beaker, into which an additional 44.28 ml of diluent was added, resulting in a 10,000x mass dilution of the original powder.

Elemental Spike	Units	Concentration
Li	*µg/kg*	18.9
P	*µg/kg*	7674.7
Ti	*µg/kg*	163.3
Cr	*µg/kg*	327.6
Fe	*µg/kg*	4255.8
Si	*µg/kg*	3179.0
As	*µg/kg*	16.0

Table 3.3a. Concentrations (ppb = ugkg^{-1}) of spikes added to the 10k coral standard to improve the respective trace element analytical signals.

Preliminary ICP-MS measurements revealed a number of elements (Li, P, Ti, Cr, Fe, Si and As – see Table 3.3a) were present in the coral standard at low concentrations which may result in poor quantification by ICP-MS. Therefore, a spike comprising these elements was added to the coral standard to boost the concentrations to a more measurable level. The spike was prepared using 1000ppm element stock solution of each Li, P, Ti, Cr, Fe, Si and As, diluted to the desired concentration (Table 3.3a) using 3% nitric acid. Phosphorus, Fe and Si required a single stage dilution, whereas Li, Ti, Cr and As required a two stage dilution. 134.8ul of the elemental spike was then pipetted into the 44.28ml vial of 10,000x diluted coral standard solution.

Throughout the analyses two batches of coral standard were made from the original coral dissolution. The first batch was used for the first two ICP-MS days (see Section 3.4.1). However, insufficient solution remained, so a second batch was prepared and used for the third ICP-MS day. Although the two coral standards came from the same initial coral digestion, slight differences in concentration between them had to be

accounted for. This was achieved via cross-calibration by running five replicates of old and new standard during the third day of analyses.

3.3.5 Standard Additions

The coral solution described above (Section 3.3.4) was used as a drift correction standard because its chemical matrix is a close match to the unknown corals. However, because its trace element composition was also unknown, it could not be used as a primary calibration standard until it had itself been calibrated.

Calibration was undertaken by Standard Additions for a selected subset of trace elements of particular interest, including Cd, B, Mn, Fe, Ni, Cu, Zn & U. Standard Additions is a very accurate technique that avoids the problem of calibrating a sample with a complex matrix where no matrix-matched standard is available. Multiple aliquots of the unknown solution are spiked with varying amounts of a trace element standard and measured. The concentration of the element in the original unknown solution can then be calculated from the slope and intercept of the resultant graph (e.g. see Figure 3.5a).

An initial semi-quantitative estimate of element concentrations in the coral standard was obtained by analysing the coral solution against the Canadian SLRS-5 river water standard. Based on this, concentrations of Standard Addition spikes were calculated. The target was that one 50uL aliquot of spike added to 4.9mL of coral solution would approximately double the element concentration in solution. Standard Addition spikes were prepared using serial dilutions of 1000ppm pure element

Element	*Units*	*Standard Addition 0*	*Standard Addition 1*	*Standard Addition 2*	*Standard Addition 3*
Li	*µg/kg*	0	0.05	0.11	0.17
Cd	*µg/kg*	0	12.4	25.3	38.3
B	*µg/kg*	0	6.27	12.8	19.4
P	*µg/kg*	0	0.47	0.96	1.45
Ti	*µg/kg*	0	0.50	1.03	1.56
Cr	*µg/kg*	0	0.95	1.93	2.92
Mn	*µg/kg*	0	0.14	0.29	0.43
Fe	*µg/kg*	0	12.7	25.9	39.2
Ni	*µg/kg*	0	0.77	1.57	2.38
Cu	*µg/kg*	0	2.41	4.92	7.45
Zn	*µg/kg*	0	37.4	76.4	116
U	*µg/kg*	0	3.20	6.52	9.87
Si	*µg/kg*	0	8.97	18.3	27.7
As	*µg/kg*	0	0.05	0.10	0.15

Table 3.3b. Concentrations of spiked elements in each standard addition solution. Each consecutive standard addition sample (i.e 0, 1, 2 & 3) increases in concentration linearly (i.e. for Ti, stadd0 = 0, stadd1=0.5, stadd2 = 1, stadd3 = 1.5). Units ugkg^{-1} = ppb.

standard solutions using the diluent (see Table 3.3b). Four aliquots of the spike + diluent were prepared, with 0, 1, 2, and 3 aliquots of the Standard Addition spike added, respectively (Table 3.3b). The Standard Addition solutions were run twice per ICP-MS day, once near the beginning and once near the end of each batch. For other elements that were not included in the Standard Additions, we rely on calibration using the (non matrix-matched) SLRS-5 standard (see Section 3.5.1 for details). It is acknowledged that this may introduce calibration uncertainty as the SLRS-5 is not a good matrix-match to the corals. We investigate the potential error resulting from this in Section 3.6.

3.3.6 Pipette Calibration

Since solution weights during sample preparation and dilution were potentially important contributors to the overall analytical precision, pipettes were carefully calibrated prior to use. Tests were carried out using 10µl, 200µl and 5ml (Table 3.3c) pipettes, measuring 10 aliquots of Milli-Q water each time. Weights of water were measured after each aliquot on a 5 dp. microbalance. Analytical precision was no worse than 0.78% for the smallest pipette (see Table 3.3c).

Pipette	RSD (%)
10µl	0.78
200µl	0.20
5ml	0.13

Table 3.3c. Pipette calibration results. Represented as relative standard deviation as a percentage of the average. Pipette uncertainty remains below 1% for all pipettes used.

3.4 Solution ICPMS Methodology

3.4.1 Solution Sequence

All solution ICP-MS analyses were made using the Thermo Scientific 'Element 2' ICP-MS at the VUW Geochemistry laboratory. The Element 2 has the advantage of allowing measurement of transition metals while avoiding isobaric interferences. These interferences are common across the transition metal portion of the mass spectrum. Elements were therefore analysed at three levels of resolution, low, medium and high (Table 3.4a), depending on the nature and severity of isobaric interferences.

Resolution	Trace Elements
Low Resolution	^{7}Li ^{89}Y ^{95}Mo ^{105}Pd ^{111}Cd ^{121}Sb ^{138}Ba ^{139}La ^{140}Ce ^{141}Pr ^{146}Nd ^{182}W ^{202}Hg ^{208}Pb
Medium Resolution	^{11}B ^{27}Al ^{29}Si ^{31}P ^{47}Ti ^{52}Cr ^{55}Mn ^{59}Co ^{60}Ni ^{63}Cu ^{66}Zn ^{75}As ^{88}Sr ^{127}I ^{238}U
High Resolution	^{25}Mg ^{34}S ^{43}Ca ^{51}V ^{56}Fe ^{72}Ge ^{77}Se ^{78}Se ^{79}Br

Table 3.4a. Isotopes monitored, and analytical resolution used for various trace elements measured.

Before commencing analysis, the ICP-MS was tuned for high sensitivity, low oxides (< 5%) and an even mass response. Accurate mass offsets were determined by running a mixture of SLRS-5 and the coral standard (to ensure all elements were present and measurable). Unknown solutions were then analysed.

A total of three separate batches of unknowns were run through the ICP-MS. Each batch typically included:

- ~ 27 unknown coral samples
- ~ 5 analytical replicate coral samples
- ~ 5 procedural blanks
- ~ 7 coral standard samples
- 13-15 diluent blanks
- 2-3 SLRS-5 standards
- Two sets of the 4 Standard Additions solutions
- Two sets of 4 replicates of a coral solution

Diluent blanks and coral standard samples were run between every seven samples. The diluent blank provided a subtraction blank and the coral standard provided

additional drift control while also acting as the primary standard. The 0.5ppb of indium used in the diluent acts as an internal standard for all solutions analysed. Replicated unknowns used coral sample U (NIWA catalogue ID: 15131) for the first batch, sample 2B (NIWA catalogue ID: 47996) and U for the second and 2B exclusively for the third.

3.4.2 Initial Data Processing

Instrument sensitivity typically changed by less than 20% across each batch. A first pass drift correction was applied to the data by dividing element signal intensities by the known indium concentration in each sample (0.5ppb in the diluent). The presence of a 'memory effect' was then assessed by examining signal intensities in two diluent blanks run back-to-back following a high-concentration unknown. No significant memory effect was detected.

Element	**Li**	**Y**	**Mo**	**Pd**	**Cd**	**Sb**	**Ba**
Diluent Blank	49%	1%	0.1%	55%	0.01%	10%	18%
Element	**La**	**Ce**	**Pr**	**Nd**	**W**	**Hg**	**Pb**
Diluent Blank	15%	6%	7%	13%	4%	33%	3%
Element	**B**	**Al**	**Si**	**P**	**Ti**	**Cr**	**Mn**
Diluent Blank	12%	21%	59%	5%	11%	2%	5%
Element	**Co**	**Ni**	**Cu**	**Zn**	**As**	**Sr**	**I**
Diluent Blank	7%	2%	0.3%	7%	20%	0.5%	0.2%
Element	**U**	**Mg**	**S**	**Ca**	**V**	**Fe**	**Ge**
Diluent Blank	0.003%	0.3%	8%	4%	0.1%	6%	4%
Element	**Se**	**Br**					
Diluent Blank	2%	0.2%					

Table 3.4b Percentage contribution of the dilution blanks to the coral signal.

Blank subtraction was carried out by interpolating between diluent blanks and subtracting from the signal intensity (Figure 3.4a). The signal-to-blank ratios for coral solutions were assessed as a potential measure of data quality. Elements with the highest percentage blank contribution were Li, Pd, Hg, B, Al, Si, P, Ti, Fe, Si and As (Table 3.4a). Elements I, Cd and Mo produced high signal intensities with counts per second upwards of 1,000,000. Elements As and Ti produce low signal intensities with counts per second below 100.

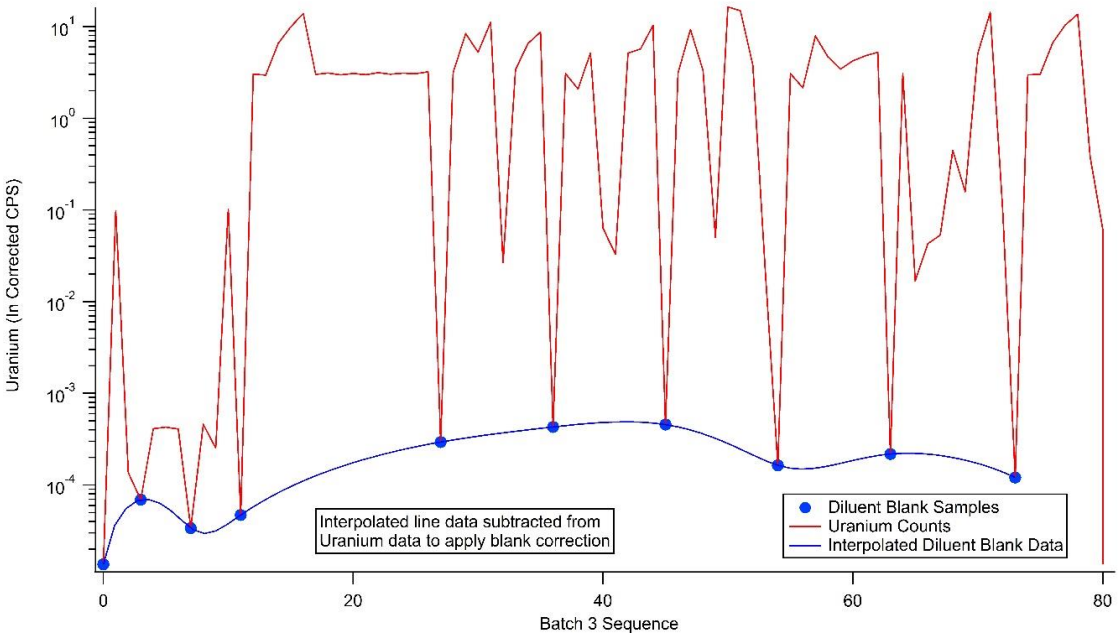

Figure 3.4a. Example of diluent blank interpolation for uranium using a cubic spline interpolation. Each interpolation was carried out individually for each batch of analysed corals. CPS = counts per second. X axis = ICP-MS sequence (each point represents some measurement). Y axis = uranium concentration (units = indium corrected CPS). Blue points represent diluent blank

The blank subtracted coral standards were interpolated between measurements (Figure 3.4b). The signal for each unknown solution was then divided by the interpolated coral standard signal to generate a ratio of the unknown relative to the coral standard.

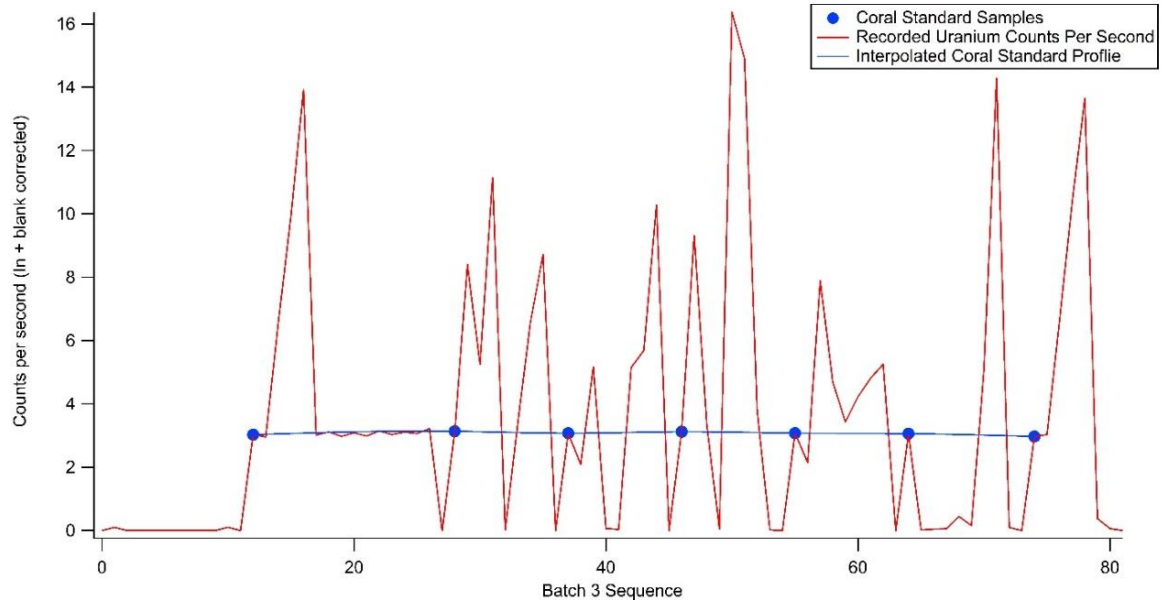

Figure 3.4b. Coral standard interpolation for Batch 3 uranium. NB: The interpolated coral standard profile (blue) extends to the start and beginning of the sequence (not pictured). X axis – ICP-MS sequence. Y axis = uranium concentration (units = indium corrected CPS).

This achieves a secondary drift correction and means that final data calibration is now simply a matter of multiplying all unknown solution data by the element concentrations determined for the coral standard (see Section 3.5).

3.4.3 Procedural Blank Subtractions

Procedural blank subtractions were not carried out on the drift corrected coral data due to significant differences between Batch 1+2 and Batch 3 procedural blank samples for some elements and little contribution from others (Table 3.4c). Most elements of interest – specifically U, V, Cd, Ni, Fe, Br, Mo and I - displayed a procedural blank contribution less than 10% of the coral signal; however, others were over 100% of the coral signal. The rare earth elements (REE's) appear to be significantly impacted by procedural blank differences between Batch 1+2 and Batch 3. With La, Ce and Pr are recording over 50% higher concentration in B3 relative to B1+2 (Table 3.4c).

Element	*Batch 1 +2*	*Batch 3*	*Element*	*Batch 1 +2*	*Batch 3*
Li	3%	13%	**Cr**	231%	10%
Y	2%	5%	**Mn**	8%	50%
Mo	0.03%	0.05%	**Co**	10%	97%
Pd	564%	360%	**Ni**	1%	1%
Cd	0.01%	0.01%	**Cu**	6%	6%
Sb	24%	3%	**Zn**	42%	12%
Ba	1%	467%	**As**	11%	2%
La	14%	61%	**Sr**	0.3%	0.4%
Ce	13%	77%	**I**	0.2%	0.1%
Pr	10%	72%	**U**	0.02%	0.01%
Nd	792%	189%	**Mg**	0.2%	0.2%
W	6%	5%	**S**	1%	1%
Hg	8%	17%	**Ca**	12%	3%
Pb	8%	148%	**V**	0.03%	0.02%
B	1%	1%	**Fe**	7%	27%
Al	177%	31%	**Ge**	8%	4%
Si	17%	440%	**Se**	101%	1%
P	0.3%	5%	**Br**	0.2%	0.2%
Ti	30%	272%			

Table 3.4c. Procedural blank counts. Presented as percentage averages of the average unknown coral signal from all batches. Note the difference in %procedural contribution between B1+2 and B3.

As the blank subtractions were not carried out, the data for some elements are likely to be heavily influenced by procedural blank contamination. These elements include Pd, Nd, Ba, Pb, Si, Al, Ti, Cr, Co, & Se and will be excluded from further analysis (see Section 3.6.4 for additional details).

3.5 Data Calibration

The coral standard prepared (Section 3.3.4) is well matched to the unknowns both in bulk chemical matrix and trace element concentration. Thus, this is the preferred

solution to act as the primary reference standard for our analytical method. However, because this solution was prepared from an unknown coral, the composition of the coral standard needed to be assessed. This was done either using Standard Additions (Section 3.5.2) (for selected elements) or by intensity-ratio to SLRS-5 (Section 3.5.1).

3.5.1 Calibration of the Coral Standard by SLRS-5

The coral standard was measured ~ 7 times per batch of solutions (see Section 3.4.1) while the SLRS-5 standard was typically measured 2-3 times per batch. These data were averaged to produce a signal-intensity ratio of coral standard to SLRS-5 and then multiplied by the known SLRS-5 composition (adjusting for slight dilution of the SLRS-5 solution when it was spiked with 0.5 ppb indium as an internal standard).

$$C_{in\ 10k\ Coral\ Solution} = \frac{I_{Coral}}{I_{recorded\ SLRS5}} \times C_{in\ SLRS5}$$

Where: I = recorded elemental intensity (in counts per second), C = elemental concentration

Element	*SLRS5 Calibrated*	*Uncertainty (±%)*	*Std. Adtn. Calibrated*	*Uncertainty (±%)*	*Discrepancies*
As	0.034	*1%*	0.057	*13%*	40%
Si	13.10	*1%*	17.87	*30%*	27%
Zn	71.19	*7%*	202.0	*2%*	65%
Cu	1.749	*5%*	1.908	*3%*	8%
Ni	0.601	*2%*	0.697	*4%*	14%
Fe	12.97	*12%*	14.15	*9%*	8%
Mn	0.146	*17%*	0.161	*7%*	9%
Cr	0.918	*8%*	1.095	*4%*	16%
P	26.87	*1%*	0.535	*2%*	4921%
Ti	0.556	*1%*	0.550	*6%*	1%
B	5.378	*2%*	7.011	*6%*	23%
Cd	14.86	*0.4%*	23.84	*2%*	38%
Li	0.057	*6%*	0.068	*4%*	16%
U	2.766	*13%*	2.783	*2%*	1%

Table 3.5a. Comparison of SLRS5 and Standard Addition calibrations for the Coral Standard (units ppm). Column 6 shows the discrepancies between the calibrations, relative to the Standard Addition calibration. Discrepancies are likely representative of introduced matrix error (see Section 3.6.3).

Trace element data for SLRS5 were obtained from the Geological and Environmental Reference Material (GeoReM) database. Where multiple published values were presented, we selected the GeoReM 'Preferred Values'. Concentrations of, and comparisons between SLRS-5 and Standard Addition calibrated coral standard concentrations are presented in Table 3.5a.

3.5.2 Calibration of the Coral Standard by Standard Additions

For a subset of elements (Li, Cd, B, P, Ti, Cr, Mn, Fe, Ni, Cu, Zn, U, Si and As), the coral standard was also calibrated by Standard Additions. The four Standard Addition solutions were plotted, with the known amount of each element added plotted on the y-axis and the measured drift corrected signal intensity plotted on the x-axis (see Figure 3.5a). Plotted this way, the true concentration of the element in the un-spiked coral solution is simply the negative of the y-intercept.

Element	Avg. Intercept	Uncertainty (%)
As	0.054	13%
Si	17.23	30%
Zn	195.6	2%
Cu	1.827	3%
Ni	0.668	4%
Fe	13.61	9%
Mn	0.155	7%
Cr	1.052	4%
P	25.27	2%
Ti	0.529	6%
B	6.740	6%
Cd	23.03	2%
Li	0.066	4%
U	2.669	2%

Table 3.5b. Standard Addition y-intercept values and uncertainty. Uncertainty represented as percentage relative standard deviation.

Standard Addition solutions were run twice in each batch for six measurements of the four solutions. However, a solution preparation error meant that the first two measurements were incorrect and had to be discarded. This provided a total of four linear fits, producing four intercept values (e.g. see Figure 3.5a), from which an average was taken and uncertainty calculated (see Table 3.5b). Linear fits were usually very precise, with r-square values typically being 0.999 or better. Uncertainty on the calibrations was better than 6% for all elements apart from As, Si and Fe, which were 13%, 30%, and 9%, respectively (Table 3.5b).

The intercepts calculated represent the trace element concentrations in the first Standard Addition solution (spiked with four aliquots of diluent). These values were converted into concentrations for the primary coral standard solution by adjusting for the minor dilution resulting from the diluent addition. Standard Addition calibrated coral standard concentrations for Li, Cd, B, P, Ti, Cr, Mn, Fe, Ni, Cu, Zn, U, Si and As are presented in Table 3.5a (alongside the SLRS-5 calibrated values).

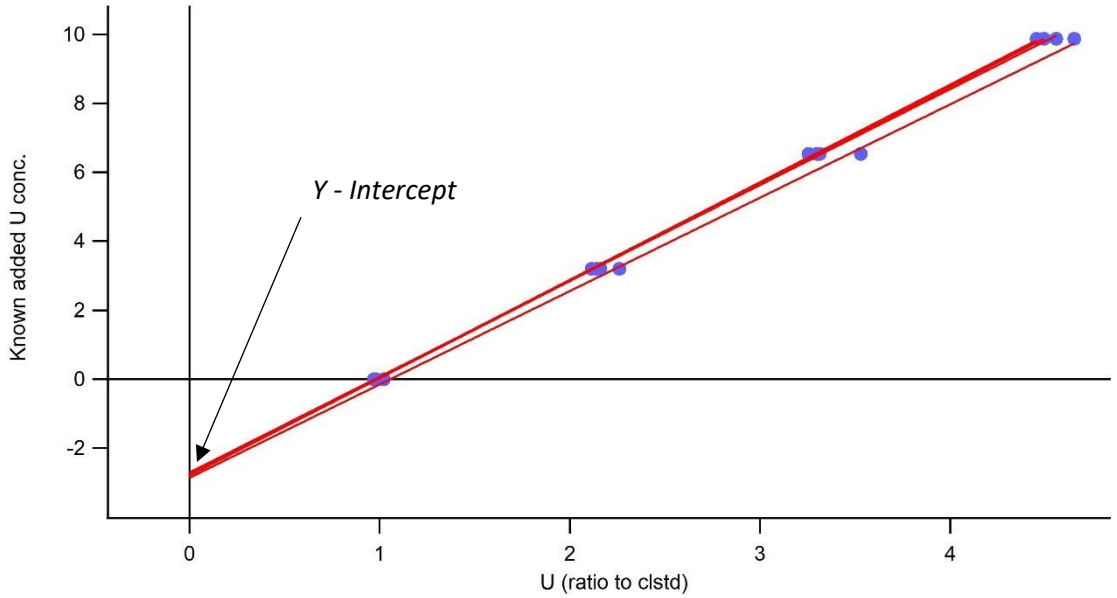

Figure 3.5a. Example of a Standard Addition plot for calculating the concentration of an element (uranium) in solution. The Standard Addition calibration factor is represented by the y-intercept. Note that the slopes of the 4 lines differ due to slight uncorrected sensitivity drift in the ICP-MS, but the lines all converge on the same y-intercept, demonstrating why this is a very robust method for solution calibration. Y axis = Known added uranium concentration, X -axis = measured U concentration (as a ratio to the coral standard).

3.5.3 Standardising Unknowns

Unknown coral solutions were standardised using the coral standard calibrations presented in Sections 3.5.1 and 3.5.2, favouring estimates obtained by Standard Additions over SLRS-5 calibrations. The final step in drift correction (see Section 3.4.2) results in a signal intensity ratio to the coral standard. Standardization was, therefore, simply a matter of multiplying this ratio by the coral standard. This gives the concentration of elements in the unknown solutions. To convert these back to concentrations in the solid coral, it was necessary to multiply the solution concentration by the mass dilution factors calculated from the initial weights of coral powder dissolved

(approximately a factor of 10,000). The resulting data were converted to part per million where divisible by 1000 and left as part per billion otherwise.

3.6 Method Statistics and Evaluation

3.6.1 Limits of Detection

The limit of detection (LOD) quantifies the concentration an element has to have in the unknown sample in order for it to have a high chance of being resolved over the levels in the blanks. Therefore, the LOD is a function of the intrinsic variability of the blank rather than the signal/blank ratio (an element may have a low LOD even if it has a high blank provided the blank is highly reproducible). Formally, the LOD is defined as 3x the standard deviation of the blanks converted into concentration. Assuming that we are calibrating using SLRS-5, this would be:

$$\mathrm{LOD} = \frac{3 \times \mathrm{Stdev}_{\mathrm{blank}}}{\mathrm{SLRS5}_{\mathrm{meas}}} \times \mathrm{SLRS5}_{\mathrm{known}}$$

Where: LOD = Limit of Detection, $\mathrm{Stdev}_{\mathrm{blank}}$ = the average standard deviation of the indium-normalised diluent blank data, $\mathrm{SLRS5}_{\mathrm{meas}}$ = blank corrected SLRS5 data and $\mathrm{SLRS5}_{\mathrm{known}}$ = known SLRS5 data from Yeghicheyan et al. (2013) and the GEOREM database.

LODs calculated this way represent limits of detection in solution. Limits of detection in the solid coral would be approximately 10,000x higher than this due to the mass dilution for analysis (see Table 3.6a). LODs were calculated for all trace elements in the dataset apart from elements I, Hg and Se, where no corresponding known SLRS-5 values exist

(Table 3.6a). In almost all cases, the average measured coral concentrations are much greater than the LODs.

Element	**Li**	**Y**	**Mo**	**Pd**	**Cd**	**Sb**	**Ba**
LOD (solid coral)	74.69	1.506	151.9	4.261	7.014	30.18	51.55
Avg. Measured Concentration	97.38	54.14	91827	3.090	119773	180.0	242.5
Element	**La**	**Ce**	**Pr**	**Nd**	**W**	**Hg**	**Pb**
LOD (solid coral)	3.124	3.587	0.470	2.082	35.46	n/a	13.40
Avg Measured Concentration	7.866	23.57	17.49	10.81	2206	69911	380.3
Element	**B**	**Al**	**Si**	**P**	**Ti**	**Cr**	**Mn**
LOD (solid coral)	7129	61778	16299	6562	63.83	28.06	154.1
Avg Measured Concentration	64686	30757	122114	33772	1409	1172	1469
Element	**Co**	**Ni**	**Cu**	**Zn**	**As**	**Sr**	**I**
LOD (solid coral)	4.307	358.8	86.94	5326	23.08	160.7	n/a
Avg Measured Concentration	101.2	13601	17139	167524	147.7	25142	14670
Element	**U**	**Mg**	**S**	**Ca**	**V**	**Fe**	**Ge**
LOD (solid coral)	3.643	24481	34583	143376	79.71	2079	12.57
Avg Measured Concentration	38680	1937937	1506599	2784299	46227	28691	60.61
Element	**Se**	**Br**					
LOD (solid coral)	n/a	33920					
Avg Measured Concentration	21371	7062641					

Table 3.6a. Calculated limits of detection in the solid coral for elements analysed on the Element 2 ICP-MS. Units = ppb.

3.6.2 Analytical Precision and Reproducibility

The precision of the analytical method – i.e. the reproducibility of a single measurement under ideal conditions – was estimated from replicated measurements of two of the unknown solutions (see Section 3.4.1). The relative standard deviation (RSD) was calculated for each set of analytical replicates from each batch, then averaged into a composite for each trace element over the three ICP-MS days (n = 18). These data are presented in Table 3.6b and range from 1-36% but are generally within 1-15% RSD. This is reasonably typical for an ICP-MS intensity-ratio method (D. Sinclair pers comm.)

Analytical precision only quantifies the reproducibility intrinsic to the analytical method. In practice, multiple external factors can contribute to a lower effective sample reproducibility. Examples are compositional heterogeneity within a coral specimen or

colony-to-colony variation in trace element incorporation. These additional constraints on reproducibility are considered further in Chapter 4, Section 4.1, where we specifically examine the results of the controlled sample subsets discussed in Section 3.1 and 3.7. In those discussions, we refer to the analytical precision as 'Tier 1' reproducibility to distinguish it from intra-colony, inter-colony and total (general) variability.

Element	**Li**	**Y**	**Mo**	**Pd**	**Cd**	**Sb**	**Ba**
Analytical RSD	12%	4%	1%	23%	2%	14%	10%
Element	**La**	**Ce**	**Pr**	**Nd**	**W**	**Hg**	**Pb**
Analytical RSD	26%	23%	14%	23%	2%	6%	19%
Element	**B**	**Al**	**Si**	**P**	**Ti**	**Cr**	**Mn**
Analytical RSD	3%	36%	20%	22%	8%	2%	21%
Element	**Co**	**Ni**	**Cu**	**Zn**	**As**	**Sr**	**I**
Analytical RSD	4%	2%	6%	4%	7%	2%	2%
Element	**U**	**Mg**	**S**	**Ca**	**V**	**Fe**	**Ge**
Analytical RSD	2%	4%	3%	6%	3%	8%	25%
Element	**Se**	**Br**					
Analytical RSD	34%	4%					

Table 3.6b. Relative standard deviation (as a %) for analytical reproducibility as estimated from replicate measurements of a coral solution. Later in the text this is referred to as 'Tier 1' error. n = 18.

3.6.3 Comparing SLRS-5 vs Standard Addition Calibrations (Accuracy)

A little over half of the elements in the coral standard were calibrated using only the river-water standard SLRS-5. This standard is not matrix matched to the coral. Therefore, the potential exists for matrix effects (differential instrument response resulting from injection of solutions with different major ion compositions) to affect the accuracy of the method.

One way to estimate the potential magnitude of calibration uncertainty is to look at the subset of elements that were calibrated by Standard Additions. For these elements, the coral standard has two calibrated values: one calculated from SLRS-5 calibration, and one by Standard Additions (Table 3.5a). This allows us to compare values to estimate inaccuracies arising from the SLRS-5 calibration. Implicit in this is the assumption that the Standard Additions calibration is intrinsically the more accurate because it uses matrix-matched solutions and primary reference standards.

This uncertainty was calculated by taking the difference between Standard Addition and SLRS-5 calibrations of the coral standard and expressing it as a percentage:

$$Calib.Uncertainty = \frac{|Stadd - SLRS5|}{Stadd} \times 100\%$$

Where: Stadd = Coral standard calibrated by Standard Additions, SLRS5 = Coral standard calibrated by SLRS-5.

These data are presented in Table 3.6c. Matrix effects likely dominate the calibration error; however, other factors may contribute to the uncertainty. These include uncertainties in the reported concentrations for SLRS-5, sample weighing errors, the Standard Addition measurement and instrument sensitivity drift. We cannot estimate the calibration error for elements that were only calibrated using SLRS-5; however, based on the data from Table 3.6c, we can infer that these could also be subject to a calibration uncertainty of around 30-40%. Note that calibration uncertainty affects all measurements equally. Thus, it does not affect analytical reproducibility, so it does not impact the ability to distinguish relative differences between solutions.

Element	Calibration Error
^{7}Li	24%
^{111}Cd	39%
^{11}B	27%
^{29}Si	71%
^{31}P	98%
^{47}Ti	3.6%
^{52}Cr	18%
^{55}Mn	25%
^{60}Ni	15%
^{63}Cu	94%
^{66}Zn	81%
^{75}As	38%
^{238}U	0.7%

Table 3.6c. Calibration error for SLRS5 calibrations. Error represented as a percentage. Calibration error values were calculated from the average calibrated values from a complete dataset of SLRS 5 calibrated data and Standard Addition calibrated data. This included the average calibrated value for each element from all measured coral samples across all batches.

3.6.4 Procedural Blanks and Contamination

3.6.4.1 Trace elements in the Procedural Blanks

The procedural blanks quantify several possible sources of contamination, including dust/detritus during milling and subsequent sample handling, contaminants from reagents, contaminants from the gold weighing boats, etc. Therefore, it is expected that procedural blanks will have higher concentrations than diluent blanks. However, trace elements were higher in the procedural blanks than expected, based on prior experience of reagent blanks and clean-room digestion procedures (D. Sinclair, pers. comm.).

	Li	Y	Mo	Pd	Cd	Sb	As
Diluent Blank	49%	1%	0.1%	55%	0.01%	10%	20%
Procedural Blank	56%	4%	0.1%	319%	0.02%	14%	18%
	Pb	**B**	**Al**	**Si**	**P**	**Ti**	
Diluent Blank	3%	12%	21%	59%	5%	11%	
Procedural Blank	36%	12%	29%	127%	7%	92%	
	Sr	**I**	**U**	**Mg**	**S**	**Ca**	
Diluent Blank	0.5%	0.2%	0.003%	0.3%	7.8%	3.6%	
Procedural Blank	0.6%	0.2%	0.01%	0.4%	10.0%	13.5%	
	Ba	**La**	**Ce**	**Pr**	**Nd**	**W**	
Diluent Blank	18%	15%	6%	7%	13%	4%	
Procedural Blank	184%	35%	30%	34%	539%	14%	
	Cr	**Mn**	**Co**	**Ni**	**Cu**	**Zn**	
Diluent Blank	2%	5%	7%	2%	0.3%	7%	
Procedural Blank	238%	17%	34%	3%	6%	29%	
	V	**Fe**	**Ge**	**Se**	**Br**	**Hg**	
Diluent Blank	0.1%	6.4%	3.7%	2.1%	0.2%	33%	
Procedural Blank	0.1%	20.5%	1.6%	1.3%	0.3%	87%	

Table 3.6d. Diluent blank and procedural blank contributions presented as a percentage of the average coral signal. Data has been averaged across all batches.

Procedural blank contamination was greatest for Li, Pd, Pb, Al, Si, Ti, Ba, La, Ce, Pr, Nd, Cr, Co, and Hg, with the blank contributing over 30% of the coral signal in some cases (Table 3.6d). Yttrium, Mo, Cd, P, Sr, I, U, Mg, S, Ni, Cu, V, Ge, Se and Br all showed low contamination levels, with blanks contributing less than 10% to the coral signal (Table 3.6d). Compared to the diluent blanks, the procedural blanks contribute considerably more Pd, Pb, Si, Ti, Ba, Nd, Cr and Hg. Most of these elements record an order of magnitude higher than the diluent blanks.

Because the analytical reproducibility was measured on splits of only one digest, any contamination from the gold foil would be constant for these replicates and therefore not captured in the reproducibility statistics presented in Section 3.6.2. This may explain

(some of) the significant jump in reproducibility from Tier 1 (analytical) to Tier 2 (intra-colony) (see section 3.6.2 and 4.1.2).

3.6.4.2 Possible Contamination from Gold Weighing Boats

We know from experience that reagents and Teflon beakers are negligible sources of contamination. The main new feature in our analytical protocol is the use of the gold foil weighing boats which went through the complete digestion procedure alongside the coral powders. Therefore, it is suspected that this is the likely origin of contaminants. Gold is supposed to be unreactive to nitric acid, and weighing boats were rigorously pre-cleaned in boiling ultra-pure nitric acid and Teflon distilled milli-Q water prior to use, so it was surprising to see that they may be appreciable sources of contamination. However, some of our observations (Figure 3.6a, and see below) point to the possibility that the gold is more reactive than previously thought. Although this gold is of very high purity (99.999%), even minor reactivity could potentially release contaminants at part-per-billion levels.

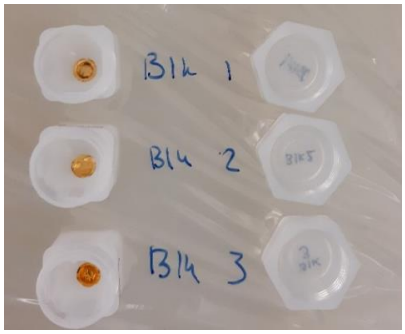

Figure 3.6a. Photo of black/brown material covering the procedural blank gold foil vessels. Procedural blanks shown are from ICP-MS Batch 2. Gold foil vessels were expected to remain unaltered through all coral dissolution and digestion steps due to their high (99.999%) purity.

After sample digestion and dry-down was complete, we noted a dark brown-black material had formed on the edges of the gold foil weighing boats used in the procedural blanks that was not observed on any of the weighing boats for samples containing coral (Figure 3.6a). This was consistent except for two procedural blanks from Batch 2. The trace element chemistry of those two procedural blanks was found to be within a similar range to their blackened counterparts, with the exception of few elements such as Fe and Zn of which were a few orders of magnitude higher in the blackened procedural blank samples. The origin of this black material remains a mystery. At no point during sample handling was any additional material introduced to the workspace, nor was anything done to the procedural blanks samples that was not already done to the coral samples. It is because of this; the procedural blanks may be a source of the high uncertainty.

Fortunately, for most elements of interest, the procedural blank signal remained relatively low, with elements such as U, V, Cd, Br, I, Cu, Ni and Mo all accumulating in the procedural blanks at less than 15% of the coral signal. As such, any lack of reproducibility introduced by this contamination is insignificant relative to the wide range of natural sample-to-sample variability and is therefore unlikely to impact the project.

3.6.4.3 Contamination of the Old Coral Standard

A new coral standard solution was prepared for Batch 3 by diluting a new aliquot of the original digestion solution. Five replicates of the new and old coral standards were run at the start of Day 3 as a cross-calibration (see Section 3.3.4 for further information). Initial inspection of the data for the old vs new coral standards revealed that the old standard had increased in concentration for many elements, with enrichments ranging from just a few % to over 600% for some elements (Table 3.6e). Therefore, it appears that the old coral standard had become contaminated between Days 1+2 and Day 3 (which were separated by ~ 3 months). The source of this contamination is unknown; the laboratory suffered an air-filtration failure just before Day 3, but the standard coral vial remained closed during this time. The coral solution was previously tested for particulate residues, and none were found (see Section 3.3.3 & 3.3.4), ruling out the possibility of slow leaching/dissolution of an undigested solid phase. Another possibility is the leaching of elements from the walls of the Teflon container. Although these Teflon containers are re-used within the lab and may have previously held a high-concentration solution, they were rigorously cleaned before use by refluxing in concentrated nitric acid multiple times. Therefore, contamination from the Teflon seems implausible.

Element	*Old:New Ratio*	*Element*	*Old:New Ratio*
I	1.01	**Ge**	1.21
Br	1.02	**Ce**	1.22
Cd	1.03	**Ba**	1.30
Cu	1.04	**Pb**	1.31
U	1.04	**Pd**	1.35
Ni	1.04	**S**	1.41
V	1.04	**Y**	1.44
Mo	1.05	**Mn**	1.46
Cr	1.05	**Hg**	1.51
Mg	1.05	**Sb**	1.66
As	1.07	**Ca**	1.72
W	1.07	**Si**	3.03
Fe	1.08	**Co**	3.26
Sr	1.12	**Zn**	3.43
Ti	1.12	**Pr**	4.18
P	1.13	**La**	5.38
Se	1.13	**Nd**	6.46
B	1.13	**Al**	9.09
Li	1.15		

Table 3.6e. Ratio of the old Coral Standard to the newly prepared Coral Standard in Batch 3. Elements Si, Co, Zn, Pr, La, Nd and Al are most significantly impacted.

This contamination made the old vs new coral standard cross-calibration invalid. However, as the new coral standard was prepared by diluting the same stock solution as the old coral standard, the only difference between the two would have been weighing errors on the solution aliquots, which are expected to be well under 1%. The new coral standard was therefore used without cross-calibration. This may introduce minor additional uncertainty, which is captured in the analytical reproducibility estimates presented in Table 3.6b.

3.6.5 Comparison to a Previous Analysis

Comparisons between measured solution ICP-MS concentrations to a previous laser-ablation ICP-MS analysis by Hitt (2020) reveal some similarities and differences between analyses. The samples analysed from the LA-ICP-MS analyses include *Leiopathes* corals 35104, 15131, 64334 and 47996, along with the *Antipathes* coral 80784. The laser-ablation analyses results show averaged trace element concentrations over a multiple radial transects of black coral skeletons. Therefore, the concentrations recorded represent the whole black coral skeleton, not just the most recently deposited skeletal layers. Because of this, some deviation in recorded concentrations is expected between analyses.

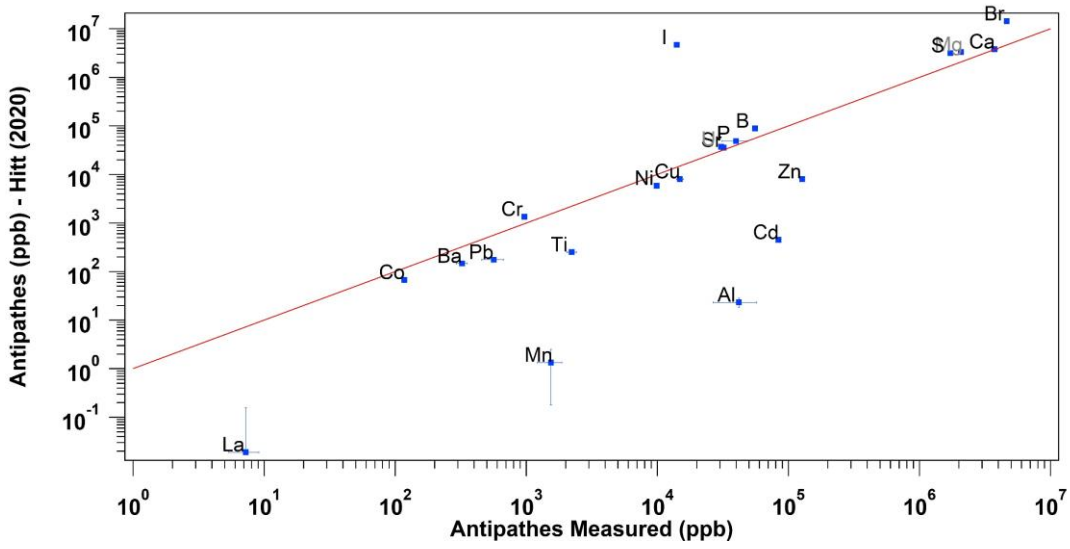

Figure 3.6b. Comparison of average ICP-MS measured Antipathes concentrations to average LA-ICP-MS measured concentrations from Hitt (2020). Error represented by analytical RSD and one standard deviation for measured (ICP-MS) and previously calculated (LA-ICP-MS) values, respectively. NB: Elements compared are limited to those chosen in the Hitt (2020) analysis and therefore do not include the full measured suite of elements analysed in solution. Presented elements include Cd, Ba, La, Pb, B, Al, P, Ti, Cr, Mn, Co, Ni, Cu, Zn, Sr, I, U, Mg, S & Br.

Solution ICP-MS concentrations for Cd, Zn, Al, Mn, Ti and La in *Antipathes* corals are 1-3 orders of magnitude higher than measured by laser-ablation (Figure 3.6b). However, the iodine concentrations measured by solution are over two orders of magnitude lower than those recorded by laser-ablation. In general, 11/21 elements record higher concentrations in the solution ICP-MS results relative to the laser ablation results.

Solution ICP-MS concentrations for La & Mn in *Leiopathes* corals are over three orders of magnitude higher than those measured by laser-ablation (Figure 3.6c). Zinc, Co, Cd and P are up to one order of magnitude higher in solution compared with laser-ablation. As with the *Antipathes* corals, iodine in the *Leiopathes* corals is recorded at much higher (<2 orders of magnitude) concentrations in the laser-ablation analysis relative to solution. In general, the solution ICP-MS *Leiopathes* concentrations are slightly higher than those measured by Hitt (2020), with 13/21 elements plotting below the 1:1 line in red.

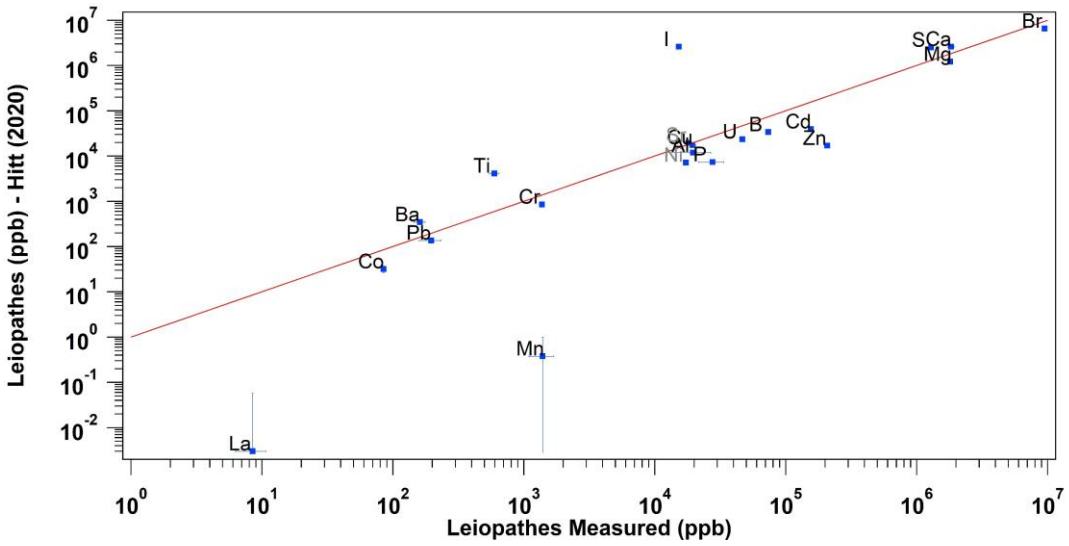

Figure 3.6c. Comparison of average ICP-MS measured Leiopathes concentrations to average LA-ICP-MS measured concentrations from Hitt (2020). Error represented by analytical RSD and one standard deviation for measured (ICP-MS) and previously calculated (LA-ICP-MS) values, respectively. NB: Elements compared are limited to those chosen in the Hitt (2020) analysis and therefore do not include the full measured suite analysed in solution.

Solution Mn and I concentrations likely deviate from equivalent laser-ablation data recorded due to iodine being among the only non-matrix matched elements (thereby accruing up to 98% calibration error) and manganese undergoing a considerable amount of contamination from the old coral standard (Section 3.6.4). Iodine is also known to accumulate in the 'glue' regions between successive layers of coral skeleton and

accumulate in larger proportions in older parts of the coral skeleton relative to younger parts (Goldberg et al., 1994; Komugabe, 2015a; Nowak et al., 2009). Considering samples were taken only from the younger, outer skeletal layer of the coral specimens avoiding any glue regions, this may also explain the low recorded I concentrations relative to the LA-ICP-MS analyses.

3.7 Data Processing

3.7.1 Data Cleaning

3.7.1.1 Contaminated Samples

After initial data processing (blank subtraction, drift correction and calibration to part-per-million values) was complete, elemental regression plots revealed the presence of

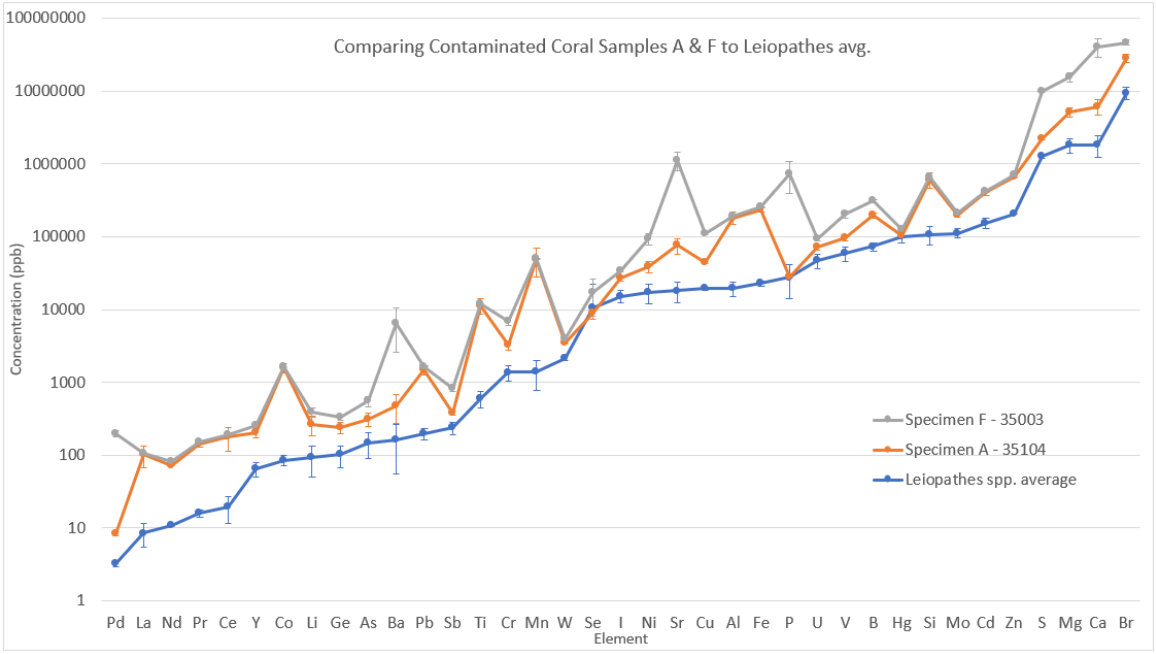

Figure 3.7a. Comparison of coral samples A(+B) & F to average Leiopathes spp. concentrations. All elements (in both samples A & F) are consistently elevated beyond the bounds of uncertainty of the Leiopathes avg. Error represented by analytical RSD. Units = ppb.

consistently outlying values related to potentially contaminated samples. These corals included the first two sampled from the NIC (Coral 35104 – samples A & B) along with sample 35003 (Sample F). Figure 3.7a compares the elemental concentrations for corals A and F against average *Leiopathes* concentrations (averaged using all *Leiopathes* corals, n = 37). Both specimens A & F consistently show elevated concentrations in all elements, with many elements accumulating at over an order of magnitude higher than in the

averaged *Leiopathes* data. Therefore, coral specimens A (+ B) & F are thought to be contaminated and have been excluded from further analysis.

3.7.1.2 Antipathella fiordensis Corals

Antipathella fiordensis corals were exclusively sampled from the waters of Fiordland. These waters are characterised by high sedimentation rates, steep watersheds, short residence times for most elements and circulation restricting sills at inlet entrances (Cui et al., 2016; Howe et al., 2010). Because of this it is likely the *A. fiordensis* corals record a chemical signature unique to the other corals sampled, separate from that of the ocean waters around New Zealand. Therefore, *A.fiordensis* corals were removed from most datasets, specifically when testing for the effects originating from environmentally and/or endogenous factors such as distance from the coastline and coral size.

3.7.1.3 Replicate Measurements

Repeated samples taken from the same coral specimen, such as analytical replicates and intra-colony replicates, were averaged into a single value for that coral for use in clean datasets. Repeated samples taken from different parts of the same coral were generally excluded from most clean datasets, apart from those concerned with coral size or intra-colony variation.

3.7.1.4 Data Transformations

Data tended to have a positive skew, with a minority of specimens having highly enriched concentrations relative to the majority. In situations that required data to be normally distributed (e.g. statistical analyses) we applied a square-root or logarithmic transformation to achieve a normal distribution.

3.7.2 Elemental Maps

3.7.2.1 The Empirical Bayesian Kriging function

A number of elemental maps were created in ArcGIS Pro to visualise spatial relationships in the coral TE data. The maps were created using the empirical bayesian kriging (EBK) interpolation method developed by Krivoruchko (2012) available in ArcGIS Pro. The main benefit of the EBK interpolation method over others such as ordinary kriging and nearest neighbours is that it allows for accurate predictions/interpolations for moderately non-stationary data (data showing moderate heterogeneity – random walks, cycles and trends) while offering more accurate standard errors of prediction

than any other kriging method (Krivoruchko, 2012). This method creates and evaluates multiple semivariograms (see Section 3.7.2.3), increasing the interpolation accuracy on smaller datasets and improving standard error. The EBK function provides a surface map output and a geospatial statistics layer that allows testing whether a spatial distribution is significantly different from random noise. Therefore, the EBK method is a robust non-stationary algorithm for spatial interpolation (Krivoruchko and Gribov, 2014). The EBK interpolation method has successfully been used to map trace elements in groundwater (Magesh et al., 2017) and soils (Gribov and Krivoruchko, 2020) as well as isotopes (C and N) in seawater as recorded in the tissue of Loggerhead Turtles (Ceriani et al., 2014). Because of this, it is thought that the EBK function is suited to the trace element data for black coral skeletons.

3.7.2.2 Data Transformations

While the EBK function can handle non-normal data, its performance improves considerably when the data is normally distributed (Krivoruchko and Gribov, 2014). Therefore, when non-normal, the data was transformed using the available empirical or logarithmic transformations offered within the EBK function. The suitability of the transformations was assessed using histograms and qq-plots of the model residuals provided by the geostatistical wizard feature in ArcGIS Pro.

3.7.2.3 Semivariograms

Semivariograms are graphical representations of spatial autocorrelation (the closer things are together in space, the more related they are) (Figure 3.7b). Distance between points is represented on the x-axis, and semivariance (a measure of spatial dependency of measured values between different locations, see equation below) on the y-axis (Figure 3.7b). The point at which semivariance stops increasing on the semivariogram is called the range; beyond this, samples are no longer spatially autocorrelated (i.e. show no relationship with distance). A single semivariogram is calculated during a standard kriging interpolation and used to interpolate a surface between points. The EBK function instead computes multiple (>50) semivariograms based on regional (samples with a ~500km radius, as defined by search radius – see below) subsets of the data to suit large, non-normally distributed datasets better.

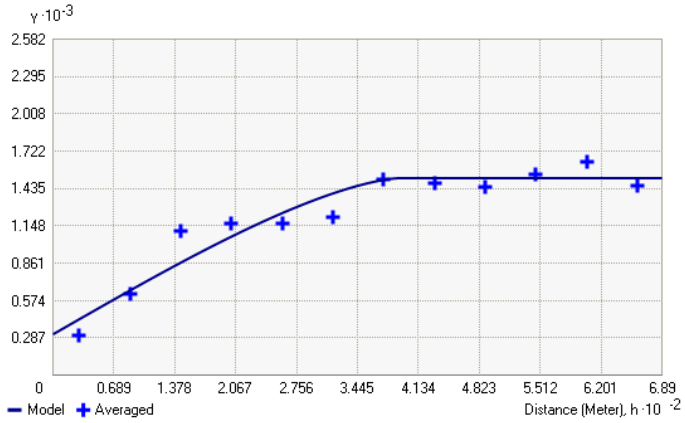

Figure 3.7b. Example of a semivariogram (Screengrab from ArcGIS Online). X axis = distance, Y axis = semi variance. Blue crosses = input data. Example represents a single semivariogram whereas the EBK function will compute upwards of 50 for a data set. Terminology: range = distance where the semi-variance stops increasing, sill = semi-variance at the range.

Semivariance is calculated by the EBK function using the following equation:

$$Semivariance\ y(h) = \frac{1}{2N}\sum_{(i,j)}^{n}(z_i - z_j)^2$$

Where: N = no. of observation pairs, Zi= value of observation (i.e. elemental concentration) at one location, Zj = value of observation at another location

The EBK function offered multiple semivariogram types, each of which operates under a different assumption of autocorrelation. For example, an exponential semivariogram assumes any similarity between data diminishes quickly over distance and the whittle semivariogram assumes the similarities diminishes slowly. Semivariogram types were chosen based on their ability to accommodate all plotted empirical semivariances. The

best performing semivariograms contain empirical semi variances within the middle of the plot and flatten out at the greatest distance. The semivariogram types available are as follows: Power, Exponential, Linear, Thin-plate-spline, K-Bessel and Whittle.

3.7.2.4 EBK Model Parameters

Model parameters for the maximum number of points in each local model, local model area overlap and number of simulated semivariograms were tweaked, favouring a balance between optimal model performance and faster processing times. Search neighbourhood parameters were changed to "smooth circular" to improve the aesthetics of the model output, this has no bearing on the model output – just the display. Additionally, the search radius was decreased from 15˚ to 5˚ (5˚ being the lowest available search radius), ensuring that the influence of corals between regionally distinct water masses such as the Tasman Front dominated northwest of the North Island and SAF dominated waters south of the South Island were minimal.

3.7.2.5 Model Quality Assessment

The quality of each elemental map was assessed using the simulated semivariograms, measured vs predicted regression models, and root mean square error (RMSE) statistics provided in a statistical output map layer. The best performing models had empirical semi variances (represented by blue crosses) that plotted within the middle of all simulated semivariograms, were not flat-lying and produced the most statistically significant regression models. The geostatistical output for the EBK function did not provide any r-square or p-values, so we could not test the statistical significance of the regression models. Instead, model performance was assessed qualitatively by visual inspection of the best fit line on the regression plots, and range length on the semivariograms.

Spatial relationships in element distribution revealed by the EBK analysis were then compared to element transects generated by the GEOTRACES cruises GIPY06 and GP13, which span the waters NW and NE of New Zealand. Although the elemental data from these cruises are limited to Cd, Cu, Fe, Ni, and Zn, additional knowledge on the behaviour and (bio)geochemistry of NZs regional water masses from Chiswell et al. (2015) and Nodder et al. (2016) was drawn on to help interpret the behaviour of other (conservative) trace elements (i.e. U, V, Mo, Br and I).

3.7.3 Trace Element Regression

Trace elements were regressed against each other (Figure 2.5c) as a way of examining common behaviour and to compare with relationships identified in other studies (Komugabe (2015a), Sinclair (unpup 2018)). Elements with similar ocean or biogeochemical behaviour such as cadmium and zinc and uranium and vanadium were plotted against each other. A high correlation (i.e. with an r-square value greater than 0.7) might imply that the elements behave similarly in seawater or that corals are systematically up taking the trace elements for some purpose.

3.7.4 Statistical Tests and Studies

3.7.4.1 Internal Variations

Endogenous processes which are unique to each coral colony may obscure any environmental reconstruction using TEs (trace elements). Therefore, quantifying any such variation is an important first step in determining whether the TE's in the coral skeleton offer any utility as palaeo-proxies. A total of six subsets of samples were selected to control for intra-colony variations, inter-colony variations, inter-species variations, inter-genus variations and variations in TE content with coral size.

3.7.4.2 Environmental Variations

A relationship between coral TE and an environmental parameter not only highlights a potential environmental proxy, but also offers insights into how that TE enters the coral's skeleton (e.g. whether it is taken up via a food source or absorbed from ambient seawater).

A total of five studies using uncontrolled and controlled subsets of the samples were set up to explore relationships between coral TEs and water depth, proximity to the New Zealand landmass, surface primary productivity, location around New Zealand and proximity to the STF. Multiple methods of comparison were employed, as detailed in Sections 3.7.4.1 and presented in Section 4.2.

3.7.4.3 Living Tissue

Comparisons between the TE content of coral living tissues and skeleton can provide us with an insight into the functional roles of TEs in black coral colonies and the differences in TE compositions between them. A number of the NIWA specimens included both skeletal material and adhering (dried) tissue, and in these cases, tissue

material was analysed alongside the skeletal material using the same protocols. Skeleton-tissue enrichment factors were then calculated from skeleton-tissue pairs.

3.7.5 Statistical Analyses

All presented statistical tests (linear regression, ANOVA, hierarchical linear regression) present p values that have been adjusted for post-hoc analysis (accounting for the running of multiple different comparisons, which increases the probability of finding a positive outcome purely by chance). P values adjustments were carried out in R using Holms method (Holm, 1979).

Similarly, r-squared values produced by statistical models have been adjusted to account for the number of predictors in the model. In all linear models testing for a 1:1 relationship, these adjustments are inconsequential; however, in the HLR and ANOVA tests, the r-square adjustment ensures the increase in r-square with the addition of each new predictor is not artificial. R-square adjustments were carried out in R using the Wherry method, see Field et al. (2012).

3.7.6 Map Data

All maps were produced in Arc GIS Pro v2.6. Default ESRI global ocean base maps were used alongside bathymetric data from the National Institute for Water and Atmospheric Research (NIWA) data service portal. Additional New Zealand landmass shapefiles and subcontinental data was sourced from the Land Information New Zealand Data Service. Satellite chlorophyll-a data was also sourced from the NIWA Satellite Data Service. Oceanographic shapefiles were sourced from the Australian Antarctic Data Centre (AADC).

Chapter 4 - Results

In Section 4.1 we present relative standard deviations (RSDs) as a way of quantifying the magnitude of the different effects studied with the controlled sample subsets described in Sections 3.1 & 3.7. These results are presented for all elements analysed by ICP-MS, and this is then used to narrow down to a reduced suite of trace elements for further investigation (such as testing for the effects of depth, coral size, coral genus, coral species, coastal proximity, and general location on skeletal chemistry). Criteria for narrowing the element selection were low contamination, low endogenous variability, and potential for use as a palaeoceanic proxy or for elucidating coral uptake pathways. Final selected elements were: Cd, Zn, I, Br, U, V, Mo, Cu, Ni and Fe, and are the focus of Sections 4.2, 4.1.4, 4.1.5 and 4.1.6.

Variability calculated throughout Section 4.1 and 4.2 is presented as four tiers of variability: Tier 1 (T1) – Analytical RSD, Tier 2 (T2) – intra-colony RSD, Tier 3 (T3) – inter-colony RSD and Tier 4 (T4) – Total RSD. Here, each successive tier of variability encapsulates all of the variation associated with the previous tier(s), i.e. Inter-colony variability includes the variability within a colony (intra-colony), as well as the analytical reproducibility for an element (analytical RSD).

4.1 Intrinsic Elemental Variations

In this section we examine the magnitude of *intrinsic* TE variability – i.e. variability originating from processes internal to the coral, rather than driven by the corals' environment. Intrinsic variabilities are described in Sections 4.1.1, 4.1.2, 4.1.3, 4.1.4 & 4.1.5 and quantified using % RSD (Table 4.1a).

Element	**Li**	**Y**	**Mo**	**Pd**	**Cd**	**Sb**	**Ba**	**La**	**Ce**	**Pr**	**Nd**	**W**	**Hg**
T1 - Analytical RSD	12%	4%	1%	23%	2%	14%	10%	26%	23%	14%	23%	2%	6%
T2 - Intra-colony RSD	45%	27%	37%	60%	47%	26%	74%	41%	56%	21%	80%	38%	105%
T3 - Inter-colony RSD	56%	38%	40%	34%	46%	41%	48%	59%	60%	39%	41%	28%	48%
T4 - General RSD	99%	47%	45%	181%	71%	61%	131%	97%	71%	64%	99%	54%	376%

Element	**B**	**Al**	**Si**	**P**	**Ti**	**Cr**	**Mn**	**Co**	**Ni**	**Cu**	**Zn**	**As**
T1 - Analytical RSD	3%	36%	20%	22%	8%	2%	21%	4%	2%	6%	4%	7%
T2 - Intra-colony RSD	10%	61%	18%	58%	66%	32%	40%	15%	44%	12%	25%	29%
T3 - Inter-colony RSD	13%	46%	59%	88%	53%	29%	74%	37%	47%	27%	34%	41%
T4 - General RSD	46%	260%	116%	151%	136%	45%	146%	50%	62%	33%	38%	99%

Element	**U**	**Mg**	**S**	**Ca**	**V**	**Fe**	**Ge**	**Se**	**Br**	**I**	**Pb**	**Sr**
T1 - Analytical RSD	2%	4%	3%	6%	3%	8%	25%	34%	4%	2%	19%	2%
T2 - Intra-colony RSD	21%	41%	11%	51%	26%	14%	58%	33%	24%	32%	43%	48%
T3 - Inter-colony RSD	30%	40%	12%	43%	33%	31%	62%	74%	33%	30%	57%	44%
T4 - General RSD	46%	48%	22%	74%	51%	48%	86%	261%	57%	40%	157%	67%

Table 4.1a. Summary table of the different tiers of variability. T1 – Analytical variability (RSD)(n=18), T2 – Intra-colony variability (RSD)(n = 14), T3 – Inter-colony variability (RSD)(n=11) and T4 – Total (general) variability RSD (1sd)(n=34). NB: Where T3 variability is less than T2 variability is indicative of changing sample sizes (T3 n = 11, T2 n = 14) and contamination (Pd, Ba, Nd, W, Hg, Al, Ti, Cr, & Ca all show evidence of contamination from the procedural blanks and the old coral standard (see Section 3.6.4 & 4.1.3.1)).

4.1.1 Analytical Reproducibility

Analytical reproducibility was quantified from multiple measurements on splits of the same digested material (see Section 3.6.2) and is presented in Table 3.6b & 4.1a. We refer to this as "T1 – Analytical RSD". Here 'T1' denotes the first tier of variability – that introduced by the analytical method itself (and expected to be common to all corals). Most of the elements have RSDs below 10% indicating that the analytical method is sound despite issues described in Section 3.6, we are confident that the method is good enough to resolve small TE differences between sample sets. A few elements with RSDs above 20% are likely impacted by high procedural blanks (see Section 3.6.4).

4.1.2 Intra-colony Reproducibility

The next tier of reproducibility is that occurring *within* a single colony. This is referred to as "Tier 2 Intra-colony RSD" (T2 RSD). It incorporates analytical reproducibility and reflects the intrinsic variability of a trace element sampled at random from a colony. It becomes a lower bound on trace element differences we could expect to resolve between any two separate measurements (both within and between specimens).

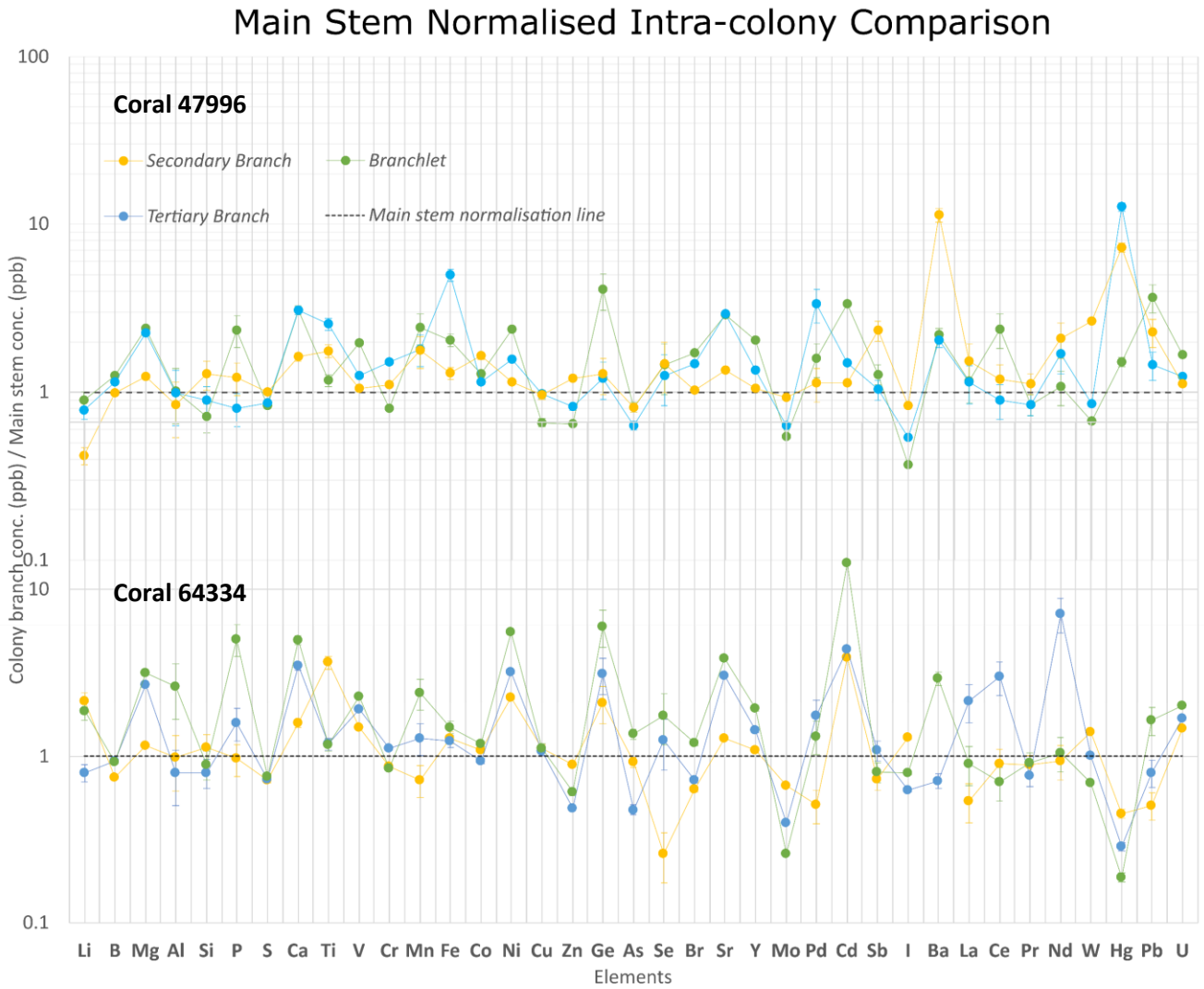

Figure 4.1a. Intra-colony comparison between different parts of the same colony (Leiopathes spp. coral 47997 (top) and 64334 (bottom). Data has been normalised to the main stem. Points plotting above the normalisation line are enriched relative to the main stem, and those plotting below are depleted relative to the mainstem. See Figure 3.1d for image displaying the different parts of the coral colony. Uncertainty is represented by analytical RSD values.

These statistics are defined from two sample subsets: Seven subsamples from *Leiopathes* coral 63443 and seven subsamples from *Leiopathes* coral 47996. Results reveal a moderate (~40%) variation in trace element chemistry between different parts

of the coral skeleton (Table 4.1a, Figure 4.1a). Most range from 26-56% (interquartile range).

The elemental variation within coral colonies is significantly larger than analytical reproducibility for all elements indicating that these are real compositional variations: clearly corals are not internally homogenous with respect to their trace element concentrations.

The patterns displayed in Figure 4.1a suggest that some elements are systematically different in composition in different parts of the coral skeleton. These variations, however, rarely exceed an order of magnitude difference relative to the main coral stem. Magnesium, Cd, Fe, Ca, Ti, Ni, Sr and Ge are consistently slightly elevated in all parts of the coral relative to the main stem (Figure 4.1a). RSDs for these elements are above 40%, suggesting they are among the most heterogeneous within the coral skeleton. Considering coral size may also affect elemental concentrations (Williams and Grottoli, 2011), the intra-colony differences likely represent an upper bound, and true intra-colony variability may be slightly lower than presented.

Intra-colony variability has been quantified in several other studies (Table 4.1b), and these data show some similarities to ours. This adds evidence that the differences are real. Laser-ablation, being intrinsically higher spatial resolution, tends to result in greater intra-colony RSDs, reflecting the sampling of fine – compositionally-distinct – substructures within the coral such as glue regions.

Element	*Hitt, N. 2020. LA ICP MS*	*Komugabe, A. 2015 LA ICP MS*	*Williams & Grottoli, 2011 Solution ICP MS*	*This Study Solution ICP MS*
Br	39%	-	14%	24%
Zn	139%	25%	4%	25%
U	48%	18%	-	21%
I	53%	-	144%	32%
Cu	93%	23%	-	12%
Ni	186%	25%	-	44%
Cd	126%	28%	4%	47%
Mo	-	14%	-	37%
Fe	-	31%	-	14%
V	-	20%	-	26%

Table 4.1b. Table comparing intra-colony RSD (as a percentage) from this study to other solution and LA ICP-MS analyses.

4.1.3 Inter-colony Reproducibility

The next tier of variability we consider is the inter-colony variability – the variation between individuals (all other things being constant). We denote this 'Tier 3 (T3)' reproducibility, as it should encapsulate both Tier 1 (analytical) and Tier 2 (intra-colony) variability. Inter-colony reproducibility was assessed by comparing averages between three groups of 4-5 *Leiopathes* spp. corals from the same location, depth and of a similar size.

Inter-colony RSDs are presented in Table 4.1a. Most elements have RSDs in the range 38-59% (interquartile range) (Table 4.1a), which is broadly similar to the range found within a specimen (T2 Intra-colony RSD). Because corals used in this study were not identified to species level, some of the variations between the coral colonies may reflect an inter-species effect (see Section 4.1.4). Therefore, the inter-colony RSDs presented in Table 4.1a are likely to representative upper limits of inter-colony variation.

We would generally expect inter-colony (T2 RSD) variability to be equal to or larger than intra-colony variability (T3 RSD) given that the latter includes the former. This was the general pattern (Table 4.1a); however, in some cases the variability within corals was larger than the variability between colonies (Table 4.1c). It should be noted that the corals for the inter-colony comparison were mostly sampled near the base, possibly avoiding some of the Tier 2 trace element variability associated with thinner branches (see Section 4.1.2 & 4.1.6). It is also possible that high analytical variability (e.g. due to high procedural blanks for Pd, Ba, Hg, Nd, Al and Ti) may also result in Tier 2 variability being higher than Tier 3 variability just by chance.

Element	*T2 RSD Intra-colony*	*T3 RSD Inter-colony*
W	38%	28%
Pd	60%	34%
Al	61%	46%
Ti	66%	53%
Ba	74%	48%
Nd	80%	41%
Hg	105%	48%

Table 4.1c. Table of elements showing intra-colony reproducibility RSD values greater than inter-colony equivalents.

4.1.4 Inter-species Reproducibility

Data presented in Table 4.1d show RSD's calculated by comparing the average of all *L.acanthophora* data to the averages of all, *L. bullosa* and all *L. secunda* samples. RSDs were less than 25% for 23/37 elements analysed, including those we judged to have the greatest potential for reconstructing surface ocean processes (Mo, U, V, Cd, Zn Br, I, Cu and Fe). Only 2/37 elements analysed produced an RSD over 50%. The species reproducibility for these elements of interest was tested with a one-way analysis of variance (ANOVA) model. All elements produce (adjusted) p-values greater than 0.05, implying there is no significant difference in mean elemental concentrations between corals of different species within the *Leiopathes* genus.

Element	**Li**	**Y**	**Mo**	**Pd**	**Cd**	**Sb**	**Ba**
Inter-species RSD	46%	22%	14%	10%	17%	18%	65%
Element	**La**	**Ce**	**Pr**	**Nd**	**W**	**Hg**	**Pb**
Inter-species RSD	36%	40%	11%	3%	6%	18%	17%
Element	**B**	**Al**	**Si**	**P**	**Ti**	**Cr**	**Mn**
Inter-species RSD	13%	22%	27%	49%	26%	23%	44%
Element	**Co**	**Ni**	**Cu**	**Zn**	**As**	**Sr**	**I**
Inter-species RSD	16%	31%	4%	2%	39%	31%	19%
Element	**U**	**Mg**	**S**	**Ca**	**V**	**Fe**	**Ge**
Inter-species RSD	23%	23%	6%	33%	23%	7%	33%
Element	**Se**	**Br**					
Inter-species RSD	111%	20%					

Table 4.1d. Inter-species RSD. Calculated using data from all L. bullosa, L. secunda, and L. acanthophora corals, n = 3.

Coral species (within the *Leiopathes* genus) therefore has a minimal effect on skeletal chemistry.

Test:	*ANOVA - Species*		
Element	*p value*	*F statistic*	*DoF*
log **Ni**	1	2.73	3
log **Br**	1	2.43	3
log **Cd**	1	1.95	3
Mo	1	2.15	3
log **I**	1	1.55	3
log **U**	1	1.44	3
V	1	1.05	3
log **Zn**	1	0.15	3
Fe	1	0.13	3
log **Cu**	1	0.06	3

Table 4.1e. Results from one-way ANOVA experiments comparing the differences in mean elemental concentrations between different species of the Leiopathes genus. All data (except for Fe, V, and Mo) have been logarithmically transformed. DoF = degrees of freedom. n = 3.

4.1.5 Higher Taxonomic Comparisons

In order to test for the presence of a genus-effect on skeletal chemistry, RSDs were calculated using averages for *Antipathes*, *Leiopathes* and *Antipathella* corals (n = 3).

Here, 30/37 analysed elements return an inter-genus RSD greater than 20% (Table 4.1f) suggesting black coral taxonomy exerts some control on the elements taken up by the coral. Note that this comparison does not control for size, depth or location.

Element	**Li**	**Y**	**Mo**	**Pd**	**Cd**	**Sb**	**Ba**
Inter-genus RSD	14%	36%	24%	22%	79%	43%	40%
Element	**La**	**Ce**	**Pr**	**Nd**	**W**	**Hg**	**Pb**
Inter-genus RSD	42%	22%	28%	53%	32%	84%	51%
Element	**B**	**Al**	**Si**	**P**	**Ti**	**Cr**	**Mn**
Inter-genus RSD	24%	71%	9%	18%	47%	15%	27%
Element	**Co**	**Ni**	**Cu**	**Zn**	**As**	**Sr**	**I**
Inter-genus RSD	8%	59%	40%	57%	20%	30%	60%
Element	**U**	**Mg**	**S**	**Ca**	**V**	**Fe**	**Ge**
Inter-genus RSD	29%	16%	10%	31%	37%	20%	94%
Element	**Se**	**Br**					
Inter-genus RSD	87%	29%					

Table 4.1f. Inter-genus RSD. Calculated using total averages for Antipathes, Leiopathes and Antipathella genera. n = 3.

Some elements vary more than others, with Li, Si, Cr, Co, Mg and S all remaining below 20% and Cd, Al, Ge, and Se remaining above 70%. ANOVA testing (Table 4.1g) for 10 elements of interest reveals that all (except for Fe & U) produce (adjusted) p-values less than 0.05 (supported by F-statistics > 5) confirming the presence of a genus effect on these elements.

Test:	**Genus ANOVA**		
Element	*p value*	*F statistic*	*DoF*
log **Cd**	2.56E-09	450.8	2
I	4.44E-06	93.2	2
log **Ni**	0.016	34.1	2
log **Cu**	0.016	40.4	2
log **Br**	0.018	9.7	2
log **Zn**	0.025	15.7	2
log **V**	0.036	9.1	2
log **Mo**	0.036	5.0	2
log **U**	0.06	5.8	2
log **Fe**	0.118	3.0	2

Table 4.1g. Results from one-way ANOVA experiments comparing the differences in mean elemental concentrations between Antipathes, Antipathella and Leiopathes genus corals. All data (except for I) have been logarithmically transformed to satisfy the assumption of data stationarity. DoF = degrees of freedom.

4.1.6 Effect of Colony Size

The next test is for the effects of coral size on trace element content of black coral skeletons. Coral size refers to the length (diameter) of the coral long axis measured during specimen sampling (Figure 4.1e). These tests use a cleaned subset of the data with all replicates, contaminated and *A. fiordensis* samples removed (n=40).

Statistical results yielded r-squares with insignificant p-values (greater than 0.05) for all elements (Table 4.1h).

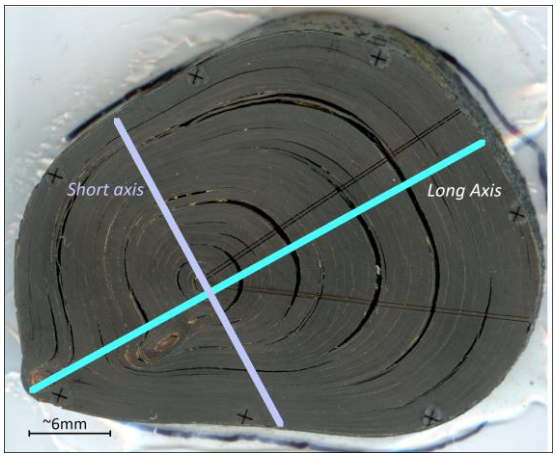

Figure 4.1b. Example of long (white/grey line) and short (pink/purple line) coral axes on coral 64334.

Test:	*Size*		
Element	*p value*	*F statistic*	*Adj r-square*
I	1.000	0.01	-0.025
sqrt **Zn**	1.000	0.03	-0.024
sqrt **Cd**	1.000	0.52	-0.012
sqrt **Fe**	1.000	0.64	-0.009
sqrt **Br**	1.000	1.65	0.016
log **Ni**	0.945	2.33	0.031
sqrt **Cu**	0.945	2.33	0.031
U	0.306	4.69	0.083
log **V**	0.306	4.85	0.086
sqrt **Mo**	0.210	5.80	0.105

Table 4.1h. Table presenting the results from linear regressions testing for the effect of coral size concentrated elements. P values less than 0.05 with F values greater than 5 indicate a statistically significant R-square value. The "log" or "sqrt" prefix denotes data transformation type. n=40. Degrees of freedom (DoF) = 1 & 39.

Linear regression models reveal insufficient evidence in support of a relationship between coral size (main stem diameter) and elements concentrated.

4.2 Environmental Elemental Variations

In this section we explore the relationships within and between corals that may be interpreted as environmentally driven (i.e. exogenous effects). These tests include relationships between coral TEs and water depth, proximity to the New Zealand landmass, surface primary productivity, location around New Zealand and proximity to the STF.

4.2.1 Testing for Depth Induced Elemental Variations

The presence of a depth relationship in corals for elements with a known depth dependency (i.e. nutrient-type and biologically active conservative TE's) may

Test:	*Depth*		
Element	*p value*	*F statistic*	*Adj r-square*
log **U**	0.546	1.2	0.005
sqrt **Cd**	0.546	1.8	0.02
log **Ni**	0.546	1.9	0.02
log **V**	0.546	2.3	0.03
sqrt **Fe**	0.504	3.0	0.05
I	0.504	3.1	0.05
log **Zn**	0.101	6.6	0.12
log **Br**	0.019	10.6	0.19
sqrt **Cu**	0.005	14.0	0.25
sqrt **Mo**	0.00009	25.9	0.38

Table 4.2a. Table presenting the results from linear regressions testing for the effect of coral collection depth (assumed habitat depth) on concentrated elements. The "log" or "sqrt" prefix denotes data transformation type. n = 40. DoF = 1 & 39.

indicate an ambient seawater origin. The presence of a depth relationship in conservative elements with no depth dependency (i.e. U and Br) may provide evidence in support of the presence of some taxonomic effect because coral genera are somewhat controlled by depth (Tracey and Hjorvarsdottir, 2019; Tracey et al., 2014).

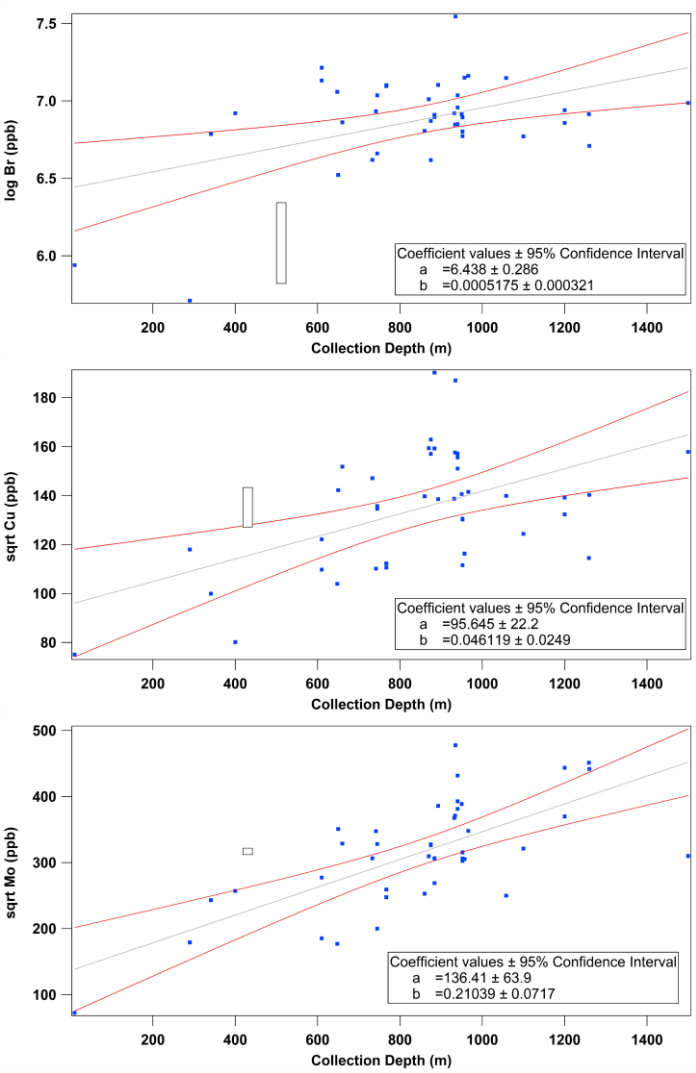

Figure 4.2a. Plots of elemental concentration (Cu, Br and Mo) vs collection depth (assumed habitat depth). Uncertainty is proportional to the size of the black rectangle. Linear fit achieved using orthogonal distance regression and is shown in grey. Upper and lower 95% confidence intervals are in red. Data presented for Cu and Mo have been square-root transformed. Data for Br has been log transformed n = 40.

Large scale tests (Section 4.2.1.1) use the 'cleaned' sample set (replicates averaged and contaminant unknowns removed; n=40). Regional-scale tests (Section 4.2.1.2) use 'cleaned' data but from corals of the same genus and from the same location (within a 25km radius; n=5). For regional tests, we aim to remove inter-genus and location-based effects on coral chemistry; however, this limits the sample pool.

4.2.1.1 Large scale (using full, clean dataset)

Table 4.2a presents statistical results for linear regressions of each trace element vs depth. Bromine, Cu and Mo produce the only statistically-significant ($p < 0.05$, $F > 10$) r-square values indicating the presence of a relationship with depth. Concentration vs depth plots (Figure 4.2a) show that Br, Cu and Mo all increase with depth.

Collection depth appears to have a considerable effect on Mo, explaining up to 38% of the variation (Figure 4.2a, Table 4.2a). Depth explains 25% and 19% of variation in Cu and Br respectively.

4.2.1.2 Regional scale (location, and genus controlled.)

Regional scale depth tests were carried out clusters of 4-5 *Leiopathes* spp. corals in 1) the Bay of Plenty (Table 4.2c) and 2) the Central Chatham Rise (Table 4.2b). Copper, Br and Mo were the subjects of these tests as they showed the strongest evidence for a depth effect in Section 4.2.1.1. No statistically-signficiant depth effects were observed in either the central Chatham Rise or Bay of Plenty subsets (Tables 4.2b & 4.2c), possibly because of the small sample numbers.

While there is evidence supporting the existence of some depth effect on coral chemistry, especially on a broad scale, more data are required to resolve this effect on a regional scale.

Test:	***Depth - BoP***		
Element	*p value*	*F statistic*	*Adj r-square*
Mo	0.6	1.6	0.12
Br	0.6	6.1	0.56
log **Cu**	0.159	9.7	0.68

Table 4.2c. Table presenting the results from regionally (Bay of Plenty) controlled linear regressions, testing for the effect of coral collection depth (assumed habitat depth) on concentrated elements Mo, Cu and Zn. Concentration data are from 5 Leiopathes spp. corals from the same general location in the Bay of Plenty. n = 5. DoF = 1 & 4.

Test:	***Depth - Chathams***		
Element	*p value*	*F statistic*	*Adj r-square*
Mo	0.074	39.2	0.93
Br	0.614	2.7	0.36
Cu	0.614	0.4	-0.27

Table 4.2b. Table presenting the results from regionally (Chatham Rise) controlled linear regressions, testing for the effect of coral collection depth (assumed habitat depth) on concentrated elements Mo, Cu and Zn. Concentration data are from 4 Leiopathes spp. corals from the same general location in the central Chatham Rise. n = 4. DoF = 1 & 3.

4.2.2 Coastal Proximity Tests

Because many trace metals are from terrestrial sources, their concentrations are expected to be greater nearer to the coast, specifically in surface waters of coastal regions around large catchments and river basins such as North Canterbury and Hawkes Bay. Here we present both large and regional scale tests assessing whether proximity to the coast affects coral trace elements. The large-scale tests exclude data from *A. fiordensis* corals because their unusual, fjordic location may bias any patterns. The regional scale tests used two regional subsets pertaining to the 1) Bay of Plenty (n = 8) and 2) the Chatham Rise (n = 9). These subsets include corals from both *Leiopathes* and

Antipathes genera. Distance from the coast was calculated using the near function in ArcGISPro in combination with a NZ coastline shapefile from LINZ.

Statistical results from large scale (n = 40) linear regression models (Table 4.2d) yield little evidence for a costal proximity effect on black coral chemistry (all r-squares <0.001, F < 5 and p values > 0.05).

Test:	*Distance from coast*		
Element	*p value*	*F statistic*	*Adj. r-square*
Cu	0.895	0.02	-0.025
log **Ni**	0.837	0.04	-0.025
log **U**	0.670	0.18	-0.021
log **Zn**	0.662	0.19	-0.021
Br	0.618	0.25	-0.019
log **V**	0.555	0.35	-0.016
log **Cd**	0.537	0.39	-0.016
Mo	0.512	0.44	-0.014
log **Fe**	0.424	0.65	-0.009
I	0.314	1.04	0.001

Table 4.2d. Table presenting results from linear regression models testing for the effect of coastal proximity on skeletal chemistry. DoF = 1 and 39. n = 40. The "log" or "sqrt" prefix denotes data transformation type.

As this experiment utilised data from all coral unknowns (excluding *A. fiordensis*), a number of additional endogenous and exogenous factor such as coral size, chlorophll-a (surface productivity), location and genus have not been controlled for. Therefore, there is a possibility that these effects may be shrouding an underlying coastal proximity effect for some elements. As

Test:	*Coastal Proximity - BoP*		
Element	*p value*	*F statistic*	*Adj r-square*
Br	1	0.01	-0.12
log **V**	1	0.13	-0.11
Fe	1	0.18	-0.10
U	1	0.25	-0.09
log **Ni**	1	0.50	-0.06
log **I**	1	0.73	-0.03
log **Zn**	1	1.76	0.08
Mo	0.94	3.07	0.19
Cu	0.85	3.60	0.22
Cd	0.27	7.26	0.41

Table 4.2f. Table presenting results from linear regression models testing for the effect of coastal proximity on skeletal chemistry. DoF = 1 and 8. Data are regional subsets for the Bay of Plenty. The "log" prefix denotes logarithmically transformed data. n=8.

Test:	*Coastal Proximity - Chatham Rise*		
Element	*p value*	*F statistic*	*Adj r-square*
log **Fe**	1	0.01	-0.14
Cu	1	0.39	-0.08
Mo	1	0.42	-0.08
Br	1	0.49	-0.07
log **I**	1	1.25	0.03
log **Cd**	0.9845	2.53	0.16
Zn	0.9845	3.12	0.21
U	0.9845	3.15	0.21
log **V**	0.9845	3.43	0.23
log **Ni**	0.9845	3.63	0.25

Table 4.2e. Table presenting results from linear regression models testing for the effect of coastal proximity on skeletal chemistry. DoF = 1 and 7. Data are regional subsets for the Chatham Rise. The "log" prefix denotes logarithmically transformed data. n=9.

such, two additional regionally controlled (regional subsets) experiments are presented (Table 4.2f & 4.2e).

Regression results (Table 4.2e & 4.2f) yield no evidence in support of a coastal proximity effect on the elements of interest in the BoP and Chatham Rise (all r-squares <0.41, F < 7 and p values > 0.05). There is therefore insufficient evidence on both large and regional scales in support of the presence of a coastal proximity effect on the TE content of black coral skeletons.

4.2.3 Surface Productivity

If biologically active trace elements were obtained by corals from the surface ocean we would expect to see a negative relationship with overlying productivity. This is because aggressive scavenging in the surface waters of productive regions would deplete the surface ocean in these elements, resulting in lower surface concentrations. Therefore, corals up taking nutrients derived from surface waters are expected to have a lower skeletal TE content in regions of increased productivity. Conversely, if corals were sampling TEs from ambient seawater then we may expect to see a positive correlation with surface productivity. This is because heightened surface water productivity is expected to result in an increase in remineralized (micro)nutrients at depth. Therefore, corals up taking TEs from intermediate waters are expected to have a higher skeletal TE content in regions of increased productivity.

Test:	*Chlorophyll a*		
Element	*p value*	*F statistic*	*Adj. r-square*
log **Br**	1.000	0.1	-0.024
Cu	1.000	0.3	-0.016
log **Zn**	1.000	0.7	-0.008
log **U**	1.000	0.8	-0.004
log **V**	1.000	0.8	-0.004
Mo	1.000	0.9	-0.001
log **Ni**	1.000	1.1	0.001
Fe	1.000	1.1	0.002
log **Cd**	0.920	2.6	0.038
log **I**	0.018	10.7	0.191

Table 4.2g. Table presenting results from linear regression models testing for the effect of surface productivity (chlorophyll a) on skeletal chemistry. DoF = 1 and 39. n = 40.

The surface productivity data used are average annual chlorophyll-a (Chl-a) data from the MODIS satellite from 2009 to 2013. This Chl-a dataset has a pixel resolution of 2.5 minutes (as in 2.5/60ths of a degree or 0.0416667 degrees) resolution. Each Chl-a data point was taken from a box 7 x 7 pixels in size(or about 1/3 of a degree) centred on the

coral GPS location. The Chl-a content of seawater is a measure of the amount of the green chlorophyll pigment directly associated with photosynthesis.

Linear regression results for the relationship between concentrated trace elements and Chl-a of the overlying surface waters (Table 4.2g) produce low and statistically insignificant r-square values for all elements except iodine.

Figure 4.2b displays logarithmically transformed iodine data against chlorophyll-a showing a weak negative relationship. The 95% confidence intervals for the plot include zero, implying there is no relationship between iodine concentrations and surface water Chl-a content.

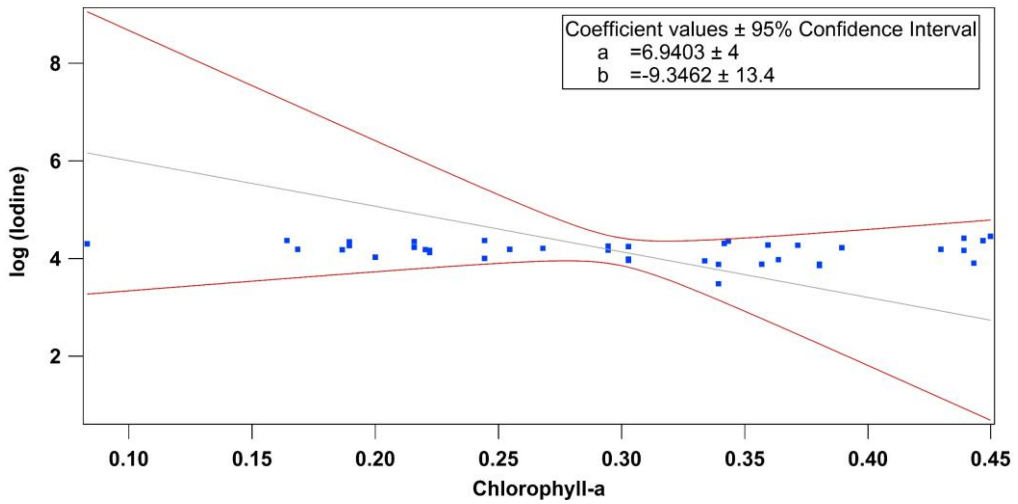

Figure 4.2b. Plot of Iodine vs. Chl-a content of the waters overlying each unknown sample. The iodine data has been logarithmically transformed to normalise its distribution. Upper and lower 95% confidence intervals are in red, and the line of best fit is presented in grey. Curve fitting was carried out using the orthogonal distance method.

4.2.4 Distance from the Subtropical Front

The STF separates the warm, micronutrient-poor waters of the subtropics from the cold, micronutrient-rich sub-Antarctic waters. Therefore, over the NZ region, the STF represents a zone of water mixing, inciting high levels of productivity (Murphy et al., 2001).

GEOTRACES data from transects Gipy06 and GP13 (Figures 4.2c, 4.2d & 4.2e) demonstrate the relationships between nutrient TEs and the STF in surface and intermediate waters. Here, nutrient elements in surface waters show a significant change (an increase for Ni, Cu, Zn and Cd, and a decrease for Fe) in concentration across the front. In contrast, the change in nutrient elements across the STF at intermediate depths is minimal, with little to no relationship with STF proximity moving south. Unfortunately, no GEOTRACES data was available for conservative trace elements in the study region; however, biologically active conservative elements (i.e Mo, V and I) could possibly show similar behaviour across the front to their nutrient counterparts (i.e. a larger change in concentration in surface waters relative to intermediate, and a general increase in concentration across the front). Otherwise, less-biologically active conservative elements (such as U) are expected to show little change in concentration across all depths.

Test:	**Distance from the STF**		
Element	*p value*	*F statistic*	*adj r-square*
log **Br**	0.02	11.3	0.200
I	0.51	3.8	0.065
log **Zn**	0.51	3.8	0.063
log **U**	1.00	0.02	-0.024
log **V**	1.00	0.2	-0.021
Mo	1.00	2.2	0.029
sqrt **Cd**	1.00	0.6	-0.009
log **Fe**	1.00	0.3	-0.018
sqrt **Cu**	1.00	0.1	-0.022
log **Ni**	1.00	0.002	-0.025

Table 4.2h. Table presenting results from linear regression models testing for the effects of distance from the STF on trace element chemistry. Degrees of freedom = 1 & 39. n = 40. The "log" or "sqrt" prefix denotes data transformation type.

Based on Figures 4.2c, 4.2d and 4.2e, if trace elements in black corals skeletons are obtained from surface water environments, then we would expect to see some relationship with proximity to the STF; namely, a significant increase in micronutrient content of surface waters approaching and moving over the STF (from the North) for all elements except for Fe (which shows a decrease in concentration, see Figure 4.2e – lowermost plot). Trace elements from intermediate waters are likely to show little change in concentration across the STF and therefore no relationship with STF proximity. Uranium is expected to behave similarly across all depths.

Statistical results from the linear regression models are presented in Table 4.2h. Distance from the STF (in km) was calculated using the near function in ArcGISPro in combination with a STF shapefile from Orsi et al. (1995).

No evidence was found for a relationship between concentrations and distance from the STF ($p > 0.05$, $f < 5$) for most elements. However, there is some evidence to suggest that Br concentrations are weakly related to STF proximity ($p < 0.05$, $f > 5$). Plotted Br data against STF proximity (in km) (Figure 4.2f) suggest this relationship is weak as indicated by the zero-inclusive 95% confidence interval.

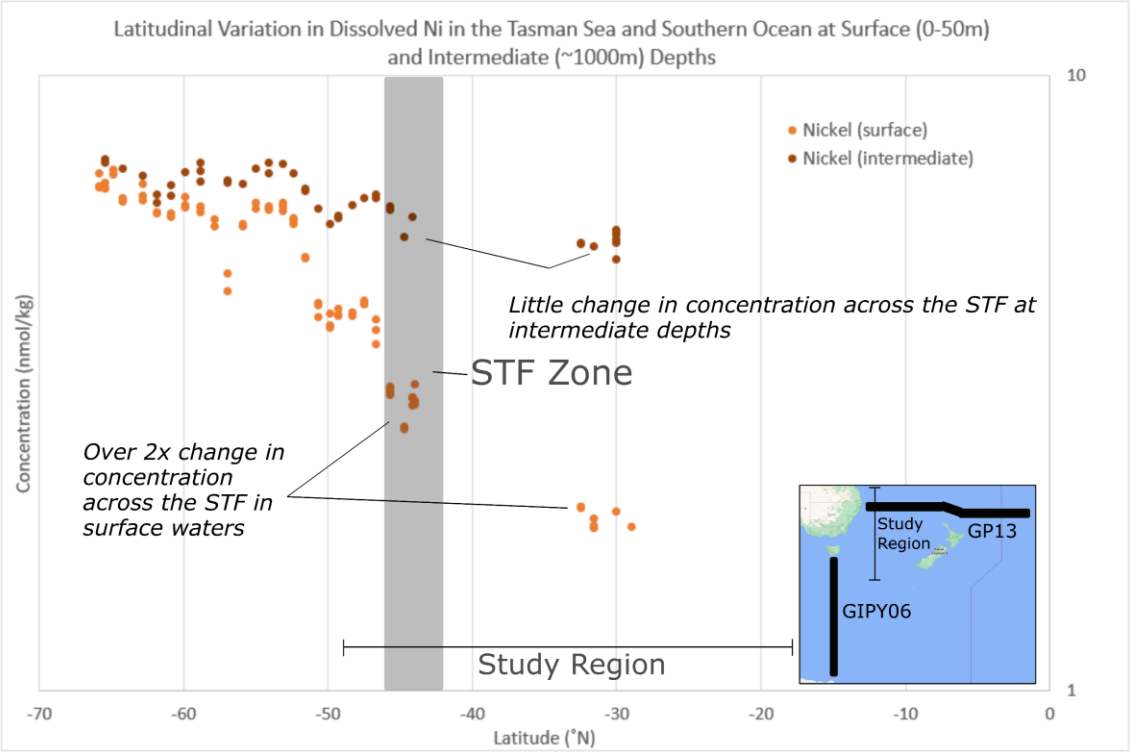

Figure 4.2c. Latitudinal plots of dissolved Nickel concentrations from Geotraces cruises Gipy06 and GP13 (Schlitzer, 2018). Data from north of ~-33˚N are from transect GP13 and data south of ~-43˚N are from transect Gipy06 (pictured in inset map). The gap from ~-33˚N to ~-43˚N represents the latitudinal offset between transects. It is acknowledged that this gap may represent a significant degree of uncertainty in the expected gradients, however, the change in concentration approaching the STF in surface waters is still clearly more significant than in intermediate waters. "Study Region" is indicative of latitudinal extent of coral distribution.

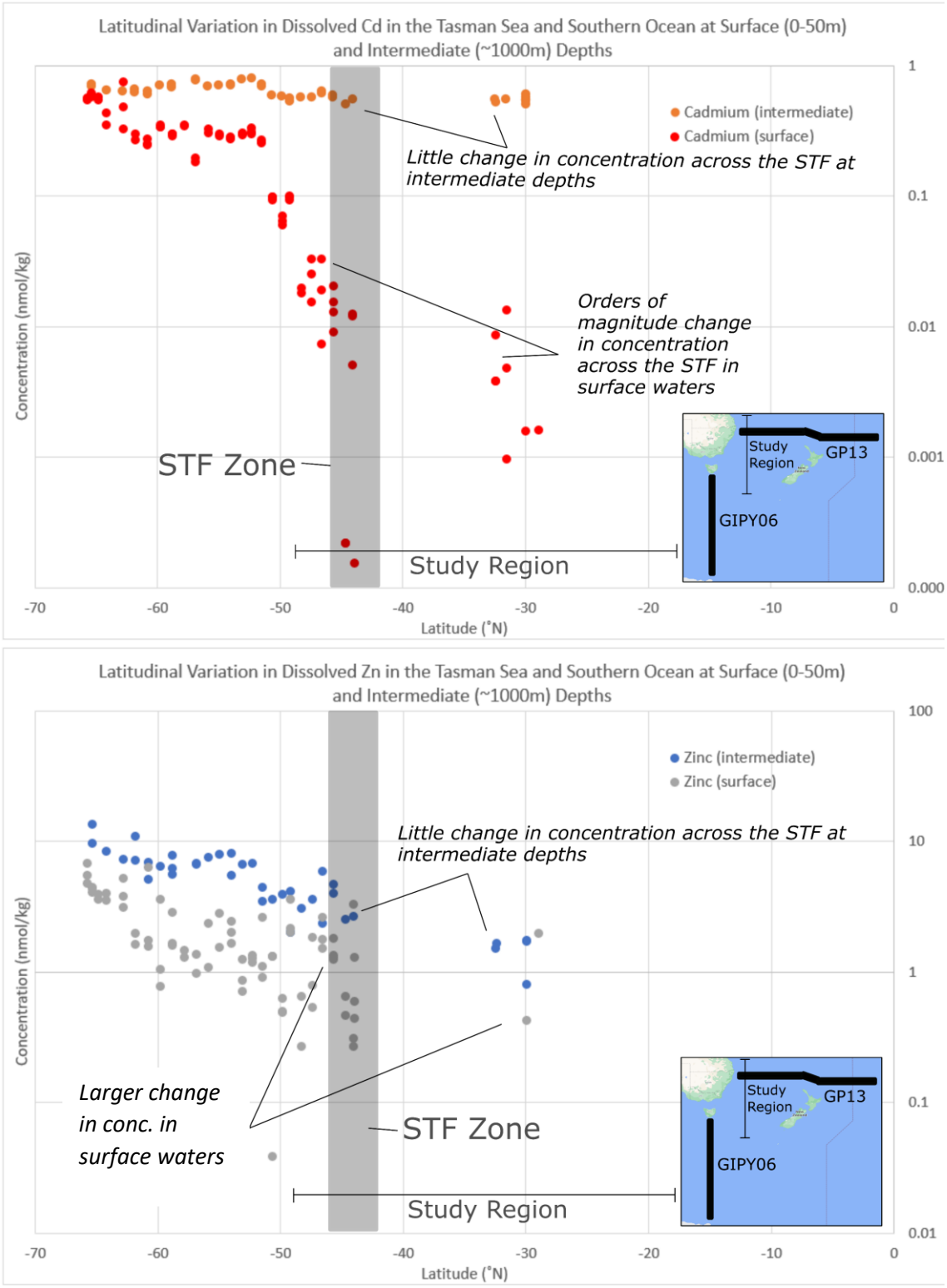

Figure 4.2d. Latitudinal plots of dissolved nutrient element concentrations (Cd top, Zn bottom) from GEOTRACES cruises Gipy06 and GP13 (Schlitzer, 2018). Data from north of ~-33˚N are from transect GP13 and data south of ~-43˚N are from transect Gipy06 (pictured in inset map). The gap from ~-33˚N to ~-43˚N represents the latitudinal offset between transects. It is acknowledged that this gap may represent a significant degree of uncertainty in the expected gradients, however, the change in concentrations approaching the STF in surface waters is still clearly more significant than in intermediate waters (less so for Zn). "Study Region" is indicative of latitudinal extent of coral distribution.

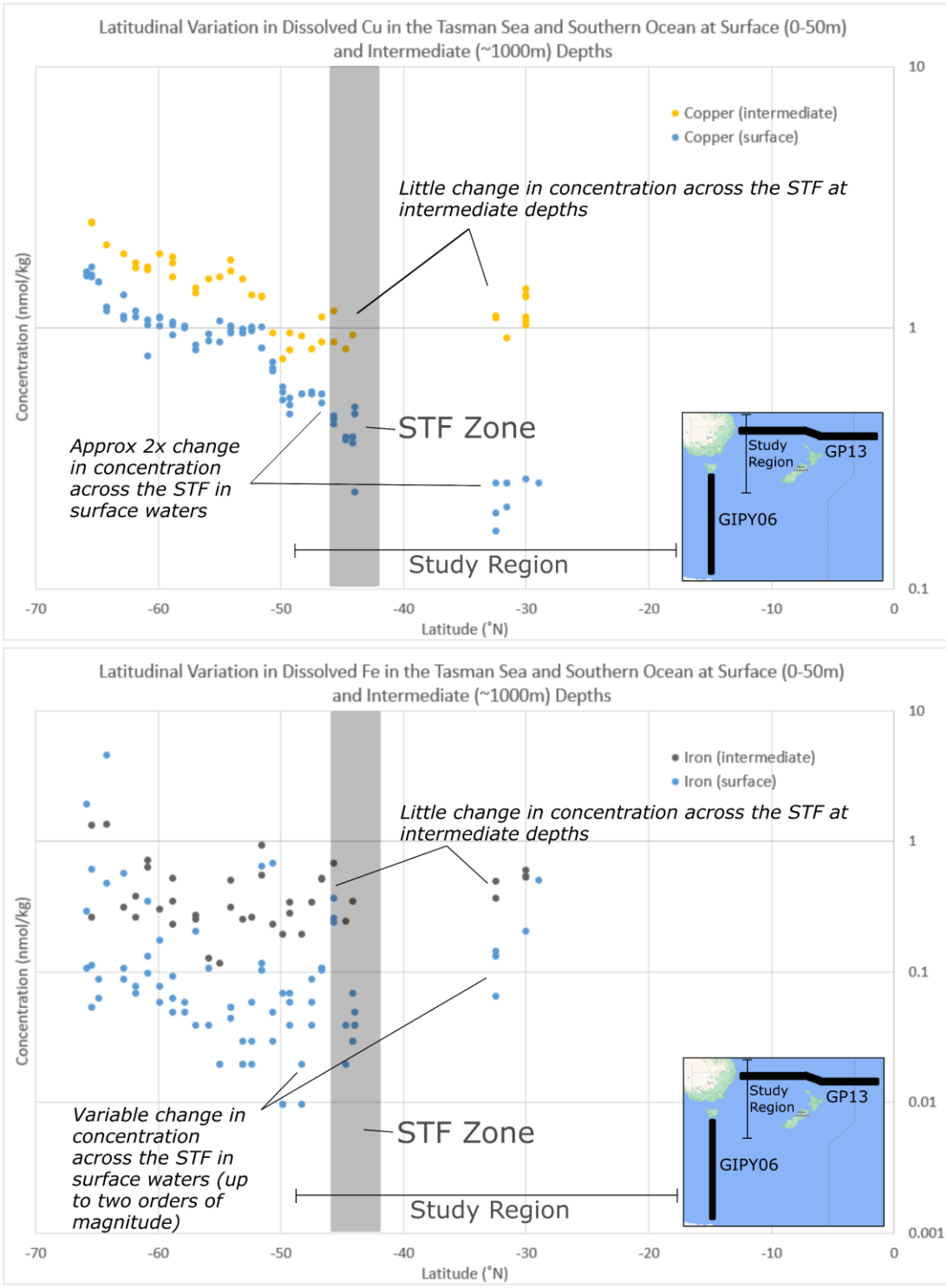

Figure 4.2e. Latitudinal plots of dissolved nutrient element concentrations (Cu top, Fe bottom) from Geotraces cruises Gipy06 and GP13 (Schlitzer, 2018). Data from north of ~-33˚N are from transect GP13 and data south of ~-43˚N are from transect Gipy06 (pictured in inset map). The gap from ~-33˚N to ~-43˚N represents the latitudinal offset between transects. It is acknowledged that this gap may represent a significant degree of uncertainty in the expected gradients, however, the change in concentration approaching the STF in surface waters is still clearly more significant than in intermediate waters. "Study Region" is indicative of latitudinal extent of coral distribution.

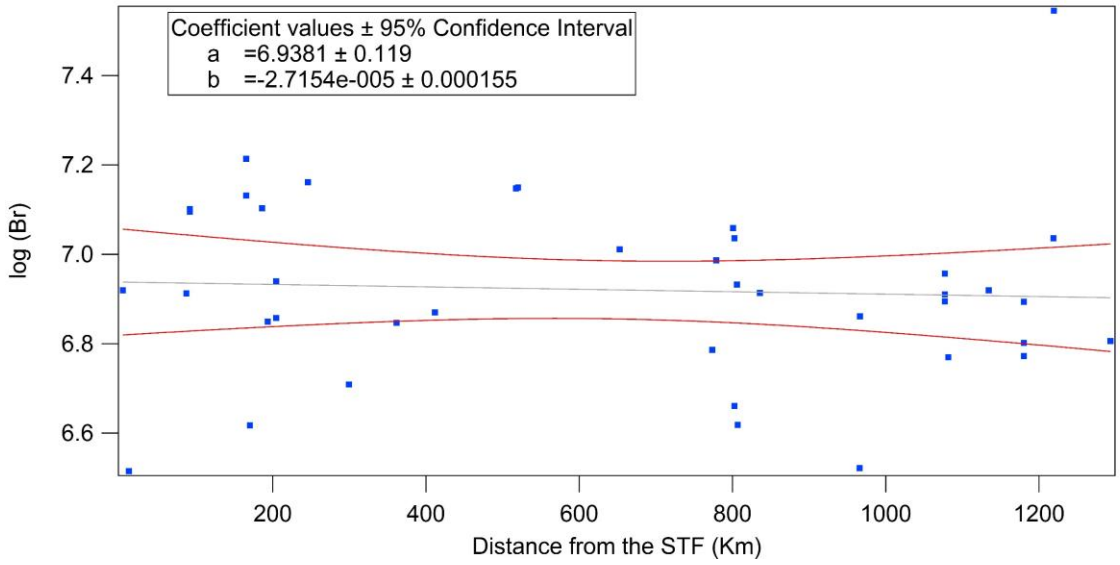

Figure 4.2 f. Plot of log(Br) (ppb) vs. distance from the STF (Km). Upper and lower 95% confidence intervals are in red. The line of best fit (using ODR) is presented in grey. N=40. Each blue square is representative of the log(Br) (y-axis) concentration and distance from the STF (x-axis).

4.2.5 Total Sample Variation

The final tier (Tier 4) of replication is represented by the total variation between all *Leiopathes* and *Antipathes* samples around New Zealand (as a percentage, 1sd) (Table 4.1a – T4 General RSD). This represents the differences in trace element content between all samples arising from both intrinsic and environmental effects, encapsulating T1, T2 and T3 variability. *Antipathes* corals are included despite sufficient evidence supporting a taxonomic effect, as their exclusion significantly narrows the sample distribution.

4.2.6 Location & EBK Maps

This section presents comparisons and an analysis of variance (ANOVA) between average trace element concentrations in *Leiopathes* spp. corals from three regions representing three distinct water masses around New Zealand – The Bay of Plenty, west Cape Reinga and The Chatham Rise. These regions, in turn, represent the waters of the Tasman Front (TF) (west Cape Reinga), the confluence of the TF and the STF (Chatham Rise) and southward extension of the TF/Subtropical Waters (BoP) per (Chiswell et al., 2015; Orsi et al., 1995). This section also presents a suite of elemental maps, interpolated from the measured TE data for each coral specimen. These maps are designed to help discern the environmental origin of the observed variation in elemental

concentration between samples by comparing their trends to known patterns in regional oceanography and known trace element distributions around the New Zealand subcontinent.

4.2.3.1 Comparisons between corals from regionally distinct water masses

Table 4.2i presents RSDs calculated by comparing the average of all Bay of Plenty (BoP) coral data to all Chatham Rise data and all Cape Reinga data (n = 3). Note that each region represents an average from a sample pool of n = 12. RSDs were less than 40% for 25/37 elements analysed.

Element	**Li**	**Y**	**Mo**	**Pd**	**Cd**	**Sb**	**Ba**
Location RSD	39%	36%	29%	33%	32%	27%	52%
Element	**La**	**Ce**	**Pr**	**Nd**	**W**	**Hg**	**Pb**
Location RSD	60%	61%	39%	26%	16%	30%	50%
Element	**B**	**Al**	**Si**	**P**	**Ti**	**Cr**	**Mn**
Location RSD	19%	57%	58%	102%	72%	29%	45%
Element	**Co**	**Ni**	**Cu**	**Zn**	**As**	**Sr**	**I**
Location RSD	21%	49%	18%	29%	51%	26%	25%
Element	**U**	**Mg**	**S**	**Ca**	**V**	**Fe**	**Ge**
Location RSD	34%	24%	12%	24%	38%	33%	68%
Element	**Se**	**Br**					
Location RSD	14%	16%					

Table 4.2i. Table of location RSD values as a percentage. Representative of variability between corals of the same genus from three different locations around New Zealand. n =3.

The ANOVA model (Figure 4.2j) results imply there is no significant difference in the mean elemental concentrations between corals from The Chatham Rise, Cape Reinga and The BoP.

4.2.3.2 Elemental Maps

A suite of six maps of elemental concentrations in the corals around NZ were created using the Empirical Bayesian Kriging (EBK) geospatial interpolation method in ArcGIS pro (see Section 3.7.2 for further information).

Interpolating the skeletal trace element concentrations using the EBK function provides us with a visual representation of spatial patterns in skeletal trace element content around NZ. This may indicate that environmental parameters influence skeletal TE concentrations or, assuming that surface

Test:	*ANOVA - Location*		
Element	*p value*	*F statistic*	*DoF*
log **V**	1	0.6182	2
log **U**	1	0.3171	2
sqrt **Br**	1	0.3659	2
I	1	0.2542	2
sqrt **Mo**	1	0.8169	2
Cd	1	1.2761	2
log **Zn**	1	1.7257	2
log **Ni**	1	0.2122	2
sqrt **Cu**	1	0.788	2
log **Fe**	1	1.7609	2

Table 4.2j. Table presenting results from a one-way ANOVA test for the relationship between elements concentrated and location of the coral samples around the NZ subcontinent. "log" or "sqrt" prefix denotes the transformation type carried out on the elemental data.

waters have higher spatial gradients (per Figures 4.2c, 4.2d & 4.2e), a surface origin of TEs.

Data used has been cleaned to exclude all repeat and contaminant unknowns as well as *A.fiordensis* corals. *Antipathes* corals were included to maintain a broad sample distribution despite evidence in support of a taxonomic control on trace element uptake.

4.2.3.2.1 Elemental Maps: Issues and Unwanted Features

In all EBK map outputs, the EBK function produced some unavoidable, and unwanted features. For example, the models ignored New Zealand landmass and occasionally carried through concentrations on the West Coast to the East (and vice versa) without considering the continental boundary. This occurs around the North Island, where corals to the West of Cape Reinga have their concentrations carried through to the Bay of Plenty. This also occurs on the West Coast of the South Island. In these cases, we recommend ignoring the coast proximal regions on the map outputs around the West Coast of the South Island and from Farewell Spit up to the Taranaki Basin. This feature is also likely to complicate the finer details in more local oceanographic features such as regional offshoots of the Tasman Front like the East Auckland Current.

The poor distribution of coral samples below 45˚S is also problematic for the EBK function and map outputs. Here (within a ~500km radius), the interpolated/predicted concentrations are controlled by two *Leiopathes* spp. corals which are distinctly elevated in most elemental concentrations. Therefore, the EBK model adds significant 'weight' to these samples, manufacturing a gradient of increasing elemental concentration moving south from the Chatham Rise that may not be real.

The most informative regions of the interpolated maps are generally around the areas with the most coral samples, such as around west Cape Reinga, the Chatham Rise and the Bay of Plenty. Interpolation quality generally decreases where data become more sparsely distributed.

4.2.3.2.2 Assessing the Quality of the Surface Maps

Semivariograms

The EBK function offers multiple semivariogram types to choose from (see Section 3.7.2 for further information on semivariograms). Elements I, Cd, Zn, and V use an

exponential semivariogram type, and Mo, Fe and U use a power semivariogram type. Elements Br and Ni use a whittle semivariogram type.

The visual fit for the semivariograms presented in Figures 4.2h & 4.2i are not ideal with many of the empirical semi-variances (blue crosses) plotting outside the semivariograms for most elements (I, V, Cu, Ni, Cd and Zn). Semivariograms for I, V, Cu and Ni are also flat-lying beyond ~250 -500 km, implying these elements are not spatially autocorrelated at great distances. This provides preliminary evidence for these elements (I, V, Cu and Ni) having no spatial relationship between black coral colonies.

The semivariograms perform the best for U, Br, Fe and Mo, (Figure 4.2g and 4.2h) where most empirical semi-variances fall within the plotted semivariograms. The semivariograms for these elements (excluding Fe) also have a large range, suggesting these elements are spatially autocorrelated between black coral specimens across the study region.

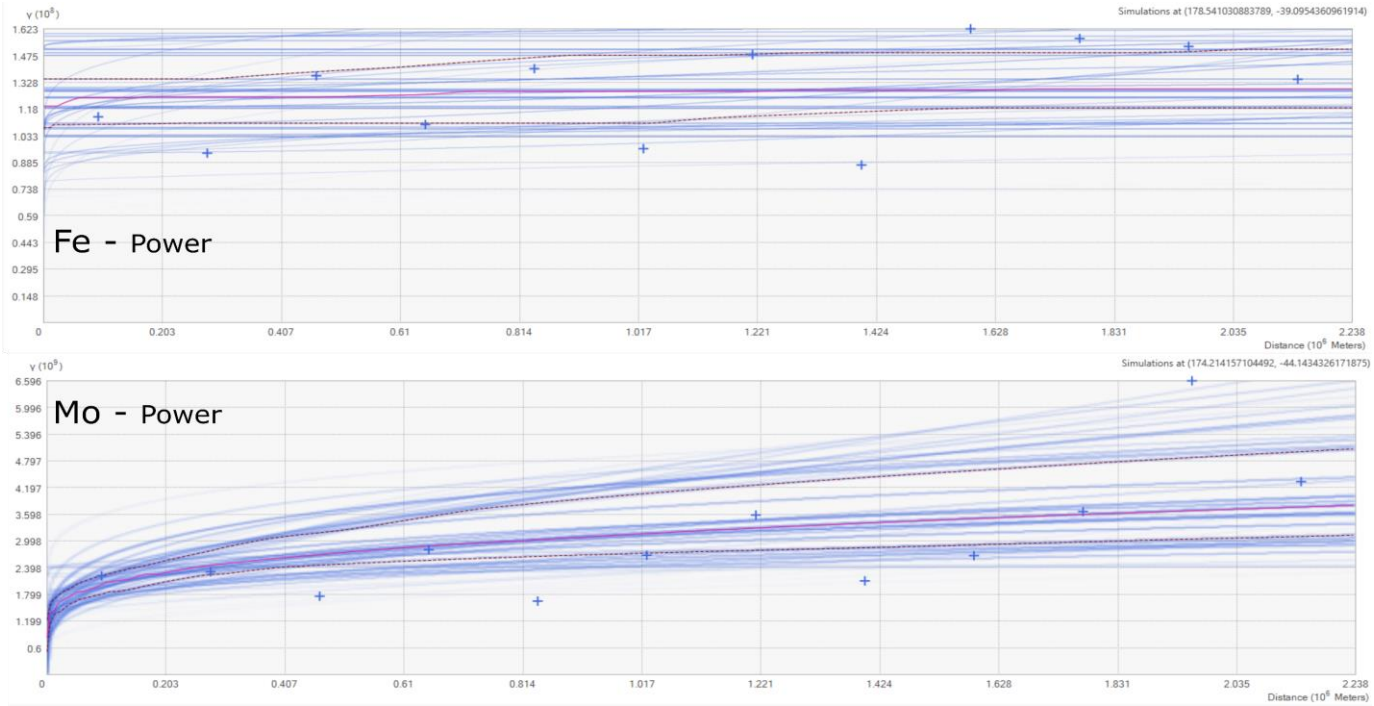

Figure 4.2g. Semivariograms for Fe and Mo. X-axis = distance in meters the centre of the sampling area, Y-axis = calculated semivariance. Both Fe and Mo data were not transformed, as all available transformations within the EBK function failed to improve the distribution. Light blue lines = semivariograms. High-density regions (more blue lines) = more semivariograms passing through the region. Blue crosses = empirical semi-variances. The red line = the median of the distribution. The dotted red = the 25th and 75th percentiles of the distribution.

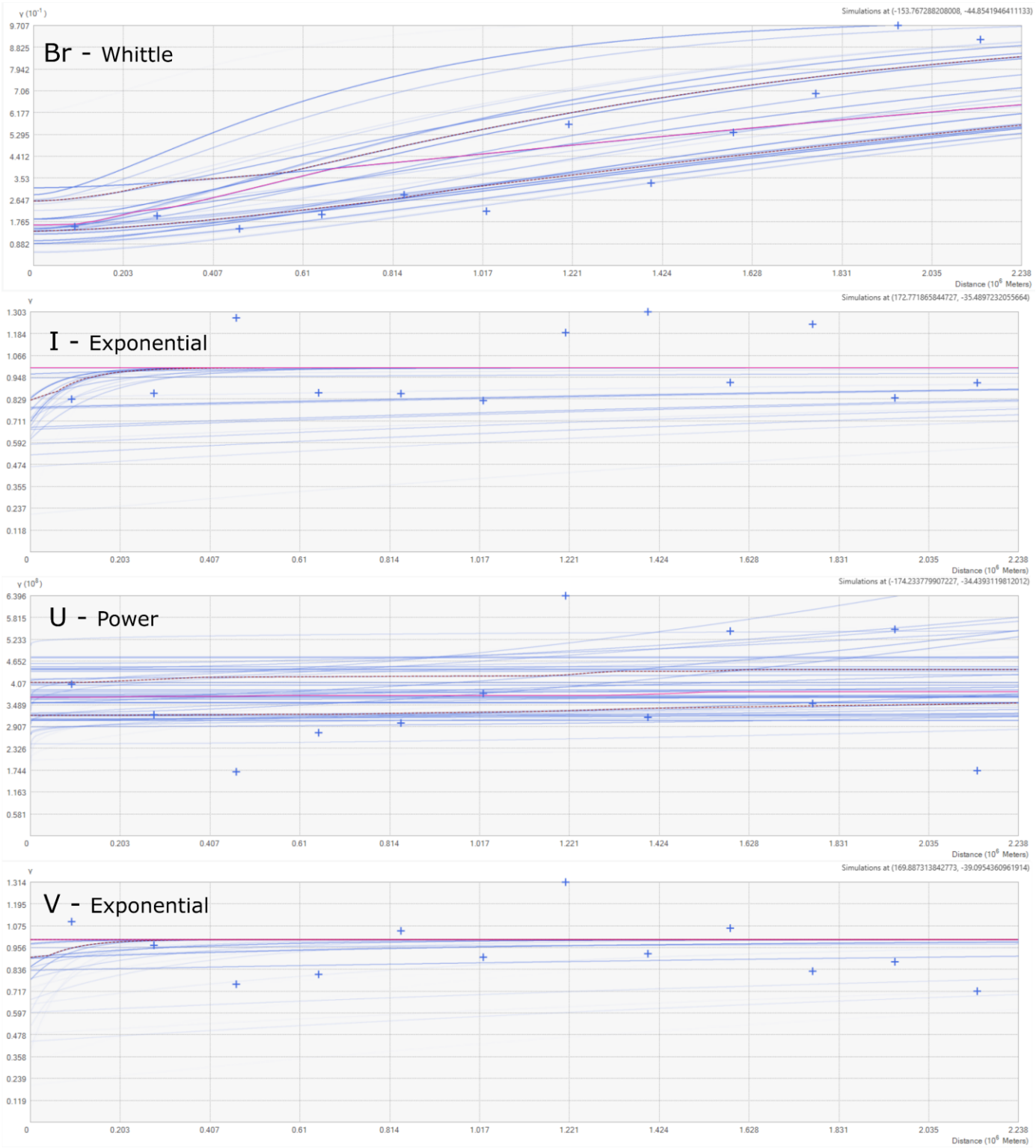

Figure 4.2h. Semivariograms for conservative-type distributed elements. X-axis = distance in meters from the centre of the sampling area, Y-axis = calculated semivariance. V and I data have been transformed using the empirical transformation offered by the EBK function. Likewise, Br was logarithmically transformed using the available logarithmic transformation in the EBK function. U data were not transformed as all available transformations failed to improve the data distribution. Light blue lines = semivariograms. High-density regions (more blue lines) = more semivariograms passing through the region. Blue crosses = empirical semi-variances. The red line = the median of the distribution. The dotted red = the 25th and 75th percentiles of the distribution.

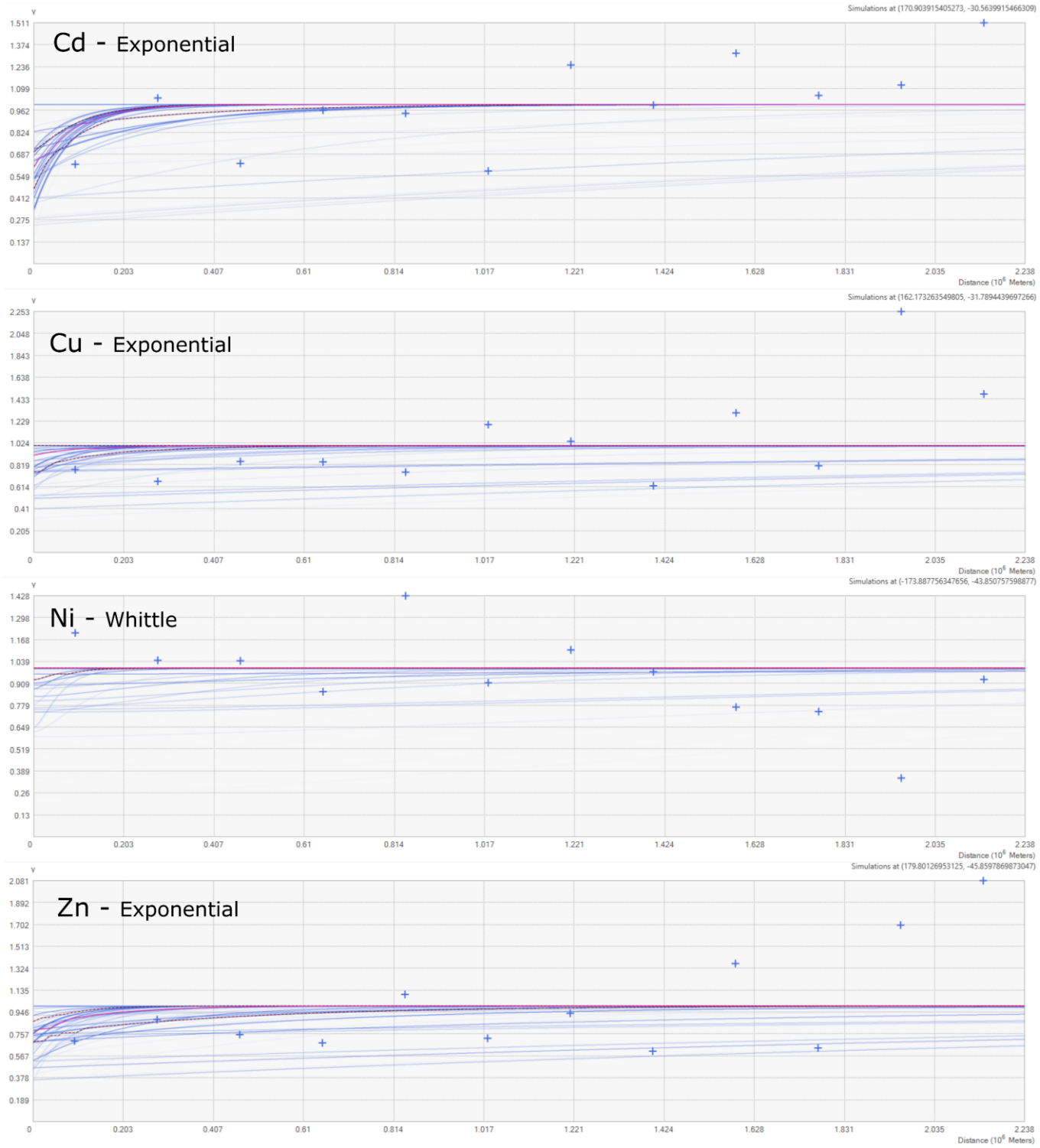

Figure 4.2i. Semivariograms for nutrient-type distributed elements. X-axis = distance in meters from the centre of the sampling area, Y-axis = calculated semivariance. Cd and Cu data have been transformed using the empirical transformation offered by the EBK function. Zn was logarithmically transformed using the available logarithmic transformation in the EBK function. Ni data was not transformed as all available transformations failed to improve the data distribution. Light blue lines = semivariograms. High-density regions (more blue lines) = more semivariograms passing through the region. Blue crosses = empirical semi-variances. The red line = the median of the distribution. The dotted red = the 25th and 75th percentiles of the distribution.

Prediction Variability

The prediction error statistics (Root Mean Square Error [RMSE] predicted & measured Standard Error [SE]) for the EBK model are presented in Table 4.2k. Interpretation of the EBK output prediction error statistics was carried out based on interpretations presented in Magesh et al. (2017).

Prediction vs measured error statistics reveal similar root mean square predictions and average standard errors for most elements, suggesting the variability of the predicted values is low. Additionally, the deviation of the standardised RMS values from 1.00 is small, not exceeding ±15% for any element. Therefore, the variability of predicted values is within acceptable bounds (of ±15%) for all elements.

Element	*n*	*RMS Prediction*	*RMS Standardised*	*Avg. Standard Error*
Br	32	5924082	1.11	5135894
I	32	6049	0.97	6258
Mo	32	45669	0.96	48385
U	32	20208	0.99	20160
V	32	24603	0.91	26780
Zn	32	72006	0.97	75312
Cd	32	83992	0.87	97692
Ni	32	9158	0.99	9268
Cu	32	6150	0.92	6672
Fe	32	12891	1.08	11642

Table 4.2k. Table of prediction error statistics for elements used in EBK function. RMS = root mean square. RMS prediction refers to root mean square error of prediction for each element (ppb). Average standard error refers to the standard error (SE) of the measured values for each element (ppb). Standardised RMS refers to the ratio of RMS to SE.

4.2.3.2.3 Measured – Predicted Regression Models

The regression models (Figures 4.2j & 4.2k) performed poorly for most elements, plotting with near-vertical regression lines for some (Ni, I and V), and (seemingly) randomly for others (Cu). Elements Mo, Cd, I and Fe are among the better performing models, with regression lines somewhat agreeing with the measured-predicted data spread, as indicated by data points plotting close to the regression line in blue. Unfortunately, the geostatistical toolbox used to retrieve the map statistics did not provide an in-depth statistical analysis. As such, r-square and p-values were not available to quantitatively assess the quality of the prediction. Therefore, the quality of each map is assessed qualitatively via visual analysis of the plotted regression lines in relation to the spread of the data. Here, elements such as Mo perform the best, whereas Cu and V perform the worst.

The low variability of predicted values likely owes to poorly autocorrelated elements and a resultant poor regression model, as indicated by near-vertical regression lines (I, V & Cu - Figures 4.2j & 4.2k) alongside relatively flat-lying semivariograms (Figures 4.2i & 4.2h). For example, elements I, V and Cu produce predicted values that plot in the same tick increment of the x-axis (Figures 4.2j & 4.2k), implying the predicted concentrations are constant across most coral samples, reducing the predicted variability significantly. Considering the semivariograms for the same elements also exclude multiple empirical semi-variances and are poorly autocorrelated, it is likely these elements have no spatial relationship between black coral colonies, or the data is too sparsely distributed to discern any spatial relationship. Their map outputs have therefore been excluded from the results.

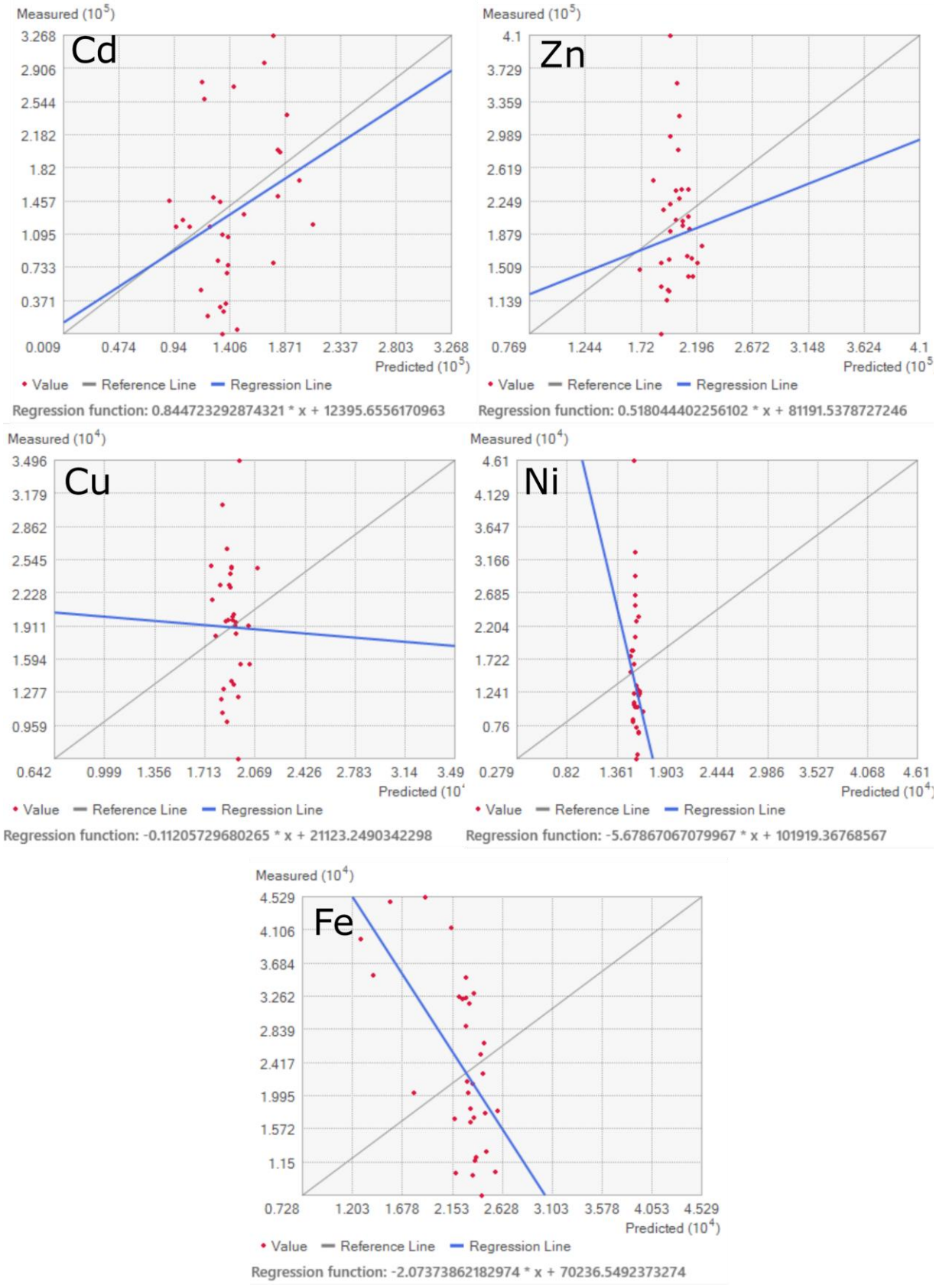

Figure 4.2j. Plots showing predicted (x) vs measured (y) elemental concentrations (ppb) derived from the EBK function.

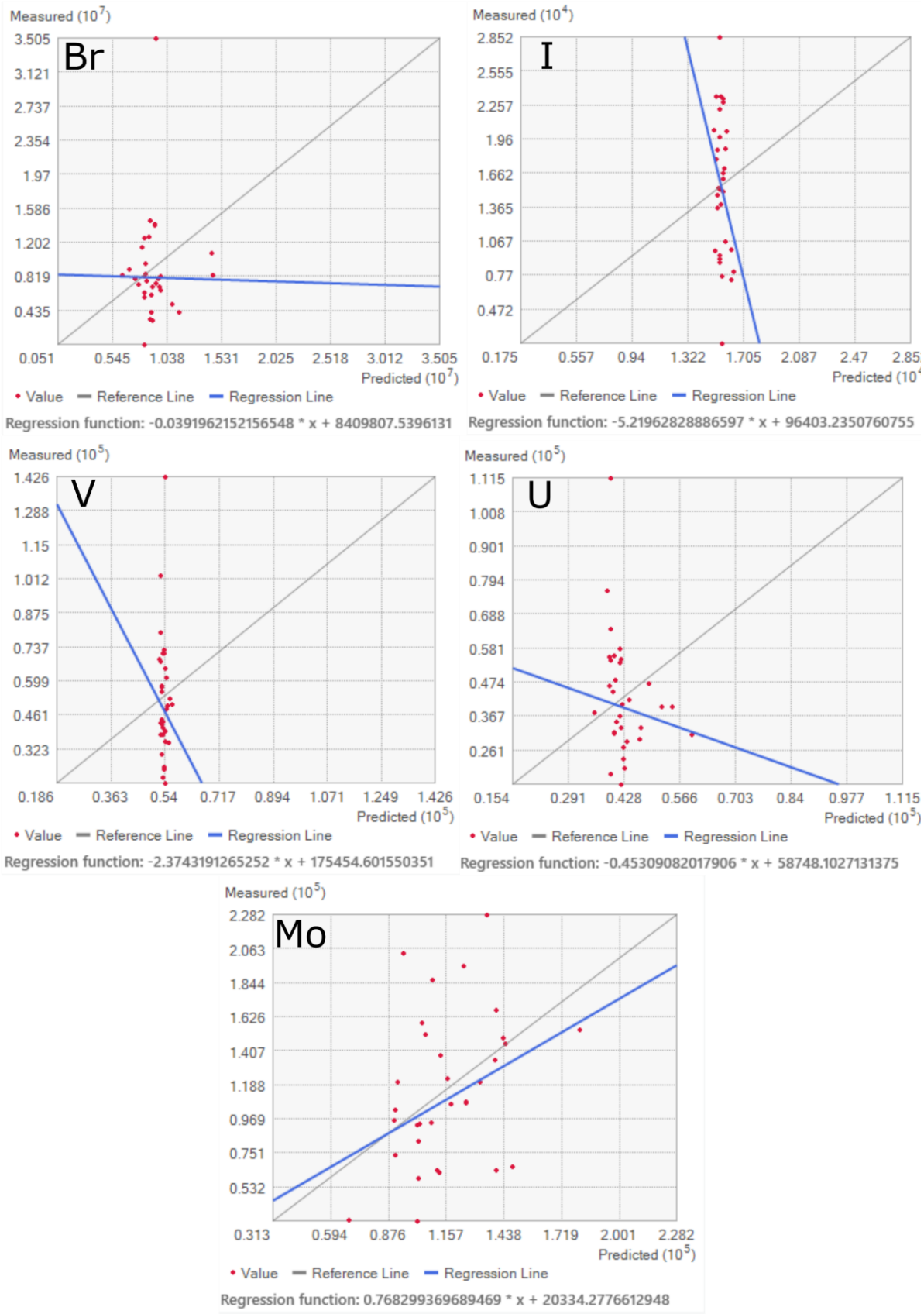

Figure 4.2k. Plots showing predicted (x) vs measured (y) elemental concentrations (ppb) derived from the EBK function.

4.2.3.2.4 Nutrient / Scavenged Type Distributed Trace Elements

Nutrient-type and scavenged-type EBK maps are presented in Figure 4.2l. If nutrient-type elements are reflecting surface ocean chemistry, their spatial distributions should approximately match the location of the major oceanographic fronts and related regions of heightened productivity.

Cadmium and Zn are expected have similar oceanic distributions due to their similar biochemical functions in most primary producers (see Section 2.5.3) and previous evidence from Sinclair (unpup 2018) (see Figure 2.5c). However, there is no evidence on the EBK maps to support this, with Cd and Zn producing no spatial trends. Because of this, it is thought that the lack of spatial relationships on the EBK maps are representative of, or affected by, processes additional to changes in productivity, the location of oceanographic fronts and coastal proximity.

Cadmium

Cadmium concentrations vary by ~45% between highest and lowest predicted values, with the lowest concentrations being recorded north of the BoP, around the Hikurangi Margin and coast proximal Chatham Rise. The largest Cd concentrations are recorded in the BoP, Cape Reinga, to the west of the North Island and to both the far south and far east. The Cd distribution forms no distinct spatial trend in relation to the location of major oceanographic fronts, coastal proximity, or productivity gradients.

Zinc

Zinc concentrations vary by only 23% between highest and lowest predicted values, with concentrations remaining fairly constant around most of NZ. Zinc concentrations decrease slightly moving north and are greatest across coast-distal Chatham Rise and Bay of Plenty. The interpolated Zn distribution shows no spatial trend in relation with NZ's regional oceanography, coastal proximity or productivity gradients.

Iron

Iron concentrations vary by 62% between highest and lowest predicted values, with concentrations increasing to the north and south, and decreasing to the east. The elevated predicted Fe concentrations in the northern samples are within agreement with the expected distribution of micronutrients with respect to the location of regional

oceanographic fronts. The behaviour of Fe to the south, however, disagrees with expected micronutrient behaviour, with the highly productive sub-Antarctic waters around Stewart Island showing an unexpected increase in Fe concentration.

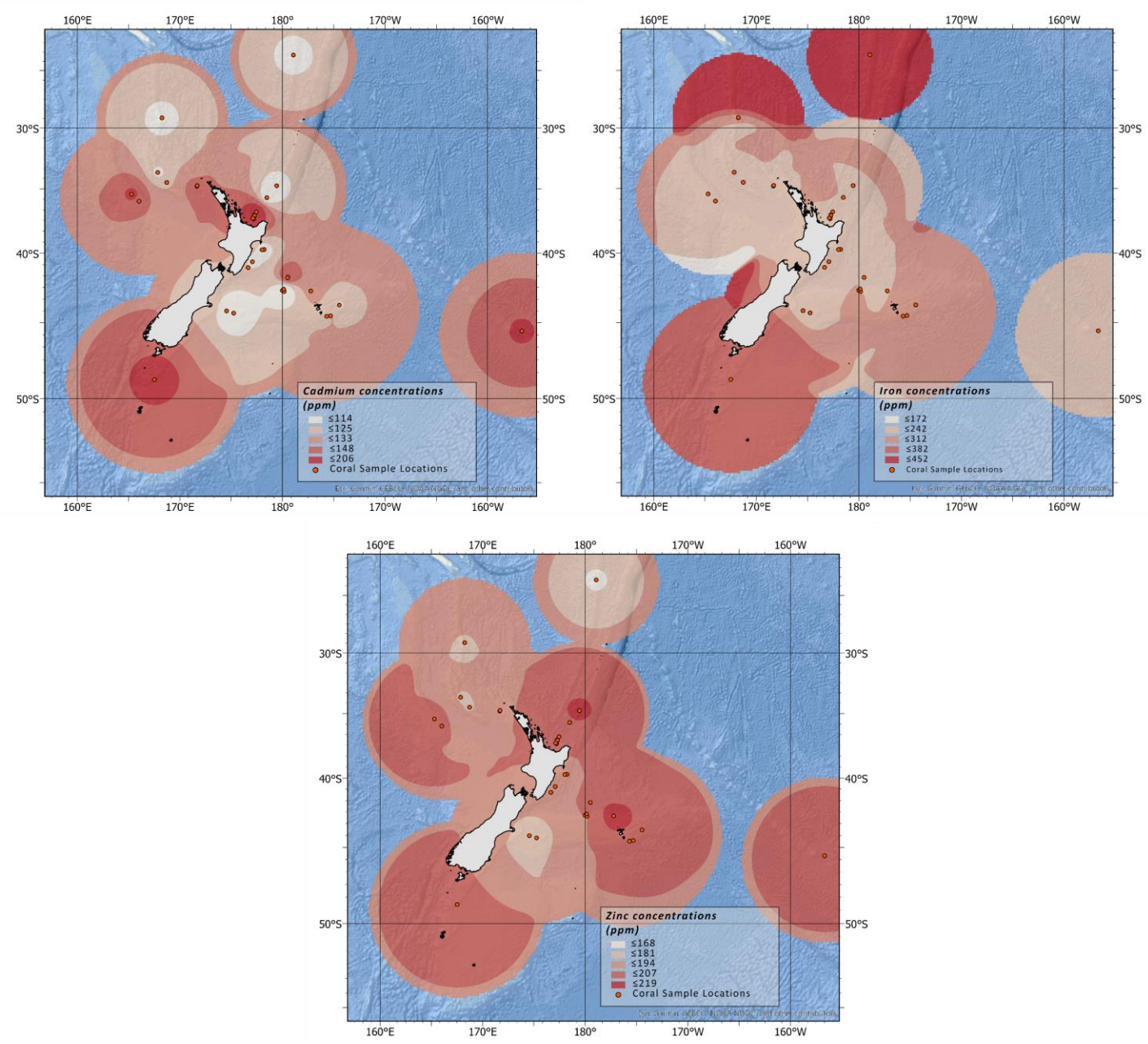

Figure 4.2l. EBK interpolated elemental surfaces for nutrient-type distributed elements Cd, Zn & Fe. Cd data have been empirically transformed and use an exponential semivariogram type. Zn data have been logarithmically transformed and use an exponential semivariogram. Fe data were not transformed and use a power-type semivariogram.

4.2.3.2.5 Conservative Type Distributed Elements

Conservative-type elemental maps are presented in Figure 4.2m. If conservative type elements are reflecting surface ocean or ambient seawater chemistry, the variation in concentration between coral samples should be minimal, matching their generally homogeneous distributions throughout the world's oceans.

The surface maps for the conservative type elements reveal similar distributions for U and Br but not Mo. All elemental maps show a distinct 'tongue' of enrichment coming from the West of the North Island. The variation in all mapped conservative elements is larger than expected for most dissolved conservative elements in seawater. This suggests processes additional to those controlling their concentrations in seawater are affecting their measured concentrations in the skeletons of black corals.

Bromine

Predicted bromine concentrations vary by ~75% between largest and smallest predicted values, with concentrations decreasing to the north and increasing to the south and west. Interpolated concentrations remain relatively constant over the Chatham Rise and to the far east, producing a weak spatial gradient consistent with a slight increase in salinity at depth moving south (see Table 2.2a).

Uranium

Predicted uranium concentrations vary by ~61% between highest and lowest values, with concentrations increasing to the south and west, and decreasing to the far east. Uranium concentrations remain constant over the Chatham Rise and in the northernmost waters. Overall, the uranium EBK map shows a weak spatial gradient consistent with a slight increase in salinity at depth moving south across the STF (see Table 2.2a).

Molybdenum

Predicted molybdenum concentrations vary by 78% between the smallest and largest values, much greater than the total variation between specimens of 45% (Table 4.1a). Molybdenum concentrations increase to the west, decrease to the north and south and remain constant moving to the far east. Overall, the molybdenum EBK map shows no spatial gradient in relation to salinity or regional oceanography.

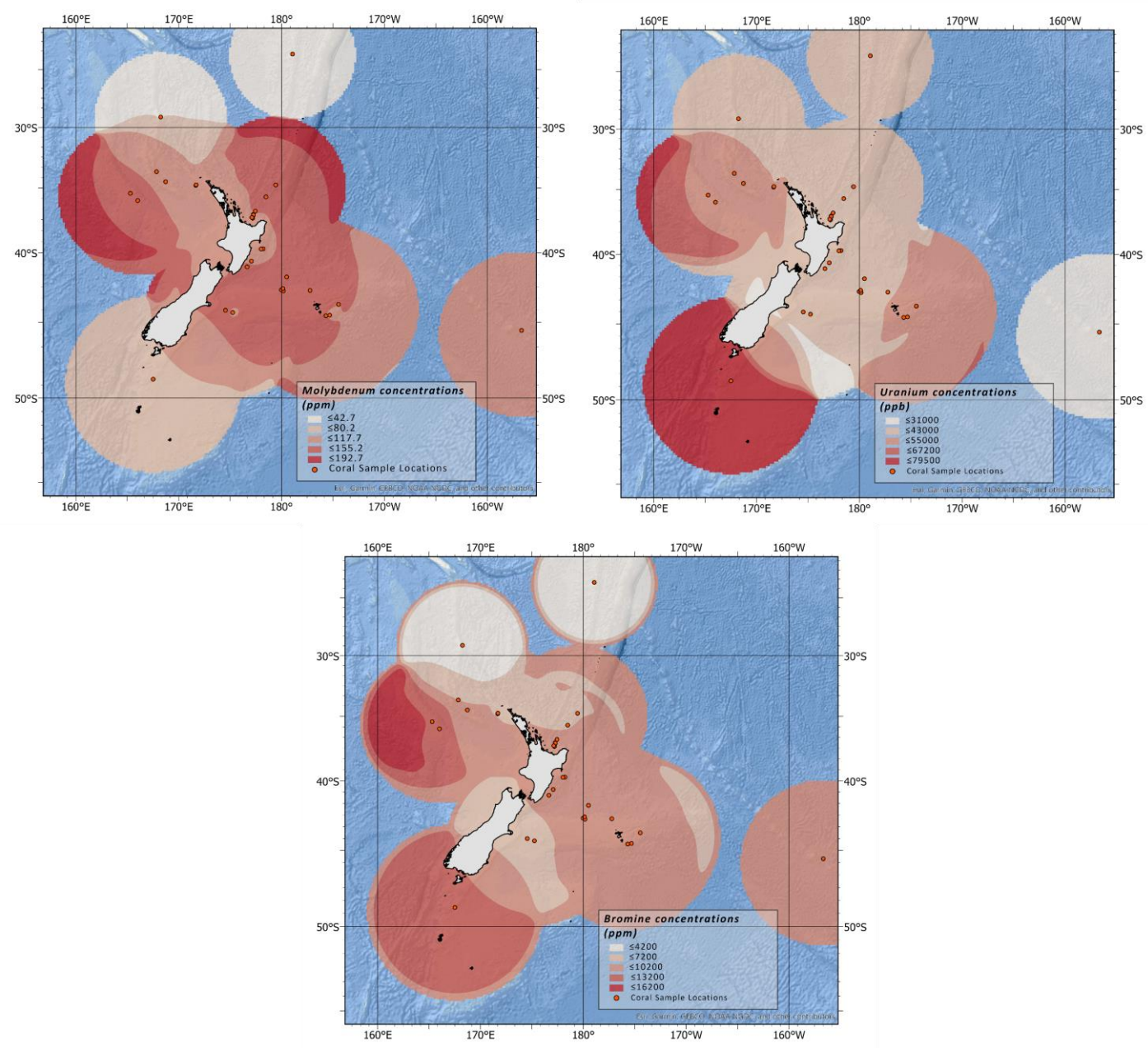

Figure 4.2m. EBK interpolated elemental surfaces for conservative-type distributed elements U, V and Br. V data have been empirically transformed and use an exponential semivariogram type. Br has been logarithmically transformed and uses a whittle semivariogram. U has not been transformed as no available transformations were able to normalise the data beyond its original spread. U implements a power semivariogram.

4.2.7 Hierarchical Linear Regression

The previous environmental tests gauge the effect of each individual environmental variable on elemental concentrations. However, they do not account for the collective effect of multiple environmental variables on the coral TE content. For example, it is clear from the depth tests (Section 4.2.1), that collection depth can individually explain up to 40% of the variation in some elements; however, the test does not account for the effects of additional environmental (and intrinsic) variables such as distance from the coast and surface productivity. These additional variables may explain more variation in TE content than just depth alone and are therefore important to consider.

Here, results are presented from hierarchical linear regressions (HLR) testing whether or not the environmental variables (depth, distance from coast and chlorophyll-a) and coral genera can collectively explain a statistically significant amount of variance in trace element concentrations. Results are presented in Table 4.2l & 4.2m.

Element	*Predictors*	*p value (ANOVA)*	*DoF*	*F statistic*	*r square*	*Δr square*	*Statistically Significant r square*
sqrt Cd	Genus	0.34	2 & 39	2.63	0.119	-	no
	Genus + Depth	1.00	3 & 38	0.005	0.119	0.0002	no
	Genus + Depth + Coastal Prx	1.00	4 & 37	0.44	0.130	0.011	no
	Genus + Depth + Coastal Prx + ChlA	1.00	5 & 36	0.18	0.134	0.004	no
log Zn	Genus	0.01	2 & 39	7.85	0.287	-	yes
	Genus + Depth	1.00	3 & 38	0.31	0.292	0.005	no
	Genus + Depth + Coastal Prx	0.55	4 & 37	1.84	0.324	0.03	no
	Genus + Depth + Coastal Prx + ChlA	1.00	5 & 36	0.00	0.324	0	no
log Ni	Genus	0.59	2 & 39	2.00	0.093	-	no
	Genus + Depth	1.00	3 & 38	0.26	0.100	0.006	no
	Genus + Depth + Coastal Prx	1.00	4 & 37	0.41	0.110	0.01	no
	Genus + Depth + Coastal Prx + ChlA	1.00	5 & 36	0.12	0.113	0.003	no
Log Cu	Genus	0.02	2 & 39	6.22	0.242	-	yes
	Genus + Depth	0.07	3 & 38	5.37	0.342	0.10	no
	Genus + Depth + Coastal Prx	0.48	4 & 37	1.43	0.367	0.03	no
	Genus + Depth + Coastal Prx + ChlA	0.62	5 & 36	0.26	0.371	0.004	no
sqrt Fe	Genus	0.35	2 & 39	2.60	0.118	-	no
	Genus + Depth	1.00	3 & 38	0.54	0.130	0.01	no
	Genus + Depth + Coastal Prx	1.00	4 & 37	0.03	0.131	0.0008	no
	Genus + Depth + Coastal Prx + ChlA	1.00	5 & 36	0.45	0.142	0.01	no

Table 4.2l. Table presenting results from hierarchical linear regressions comparing the relative contribution to changes in nutrient-type elemental concentrations from each environmental variable. P < 0.05, F > 5 = a statistically significant change in r-square for the added predictor. n = 40.

Data have been cleaned to remove all replicates, *A. fiordensis* corals and contaminated specimens (n=40). *Antipathes* corals were included to test for the effects of coral taxonomy between *Antipathes* and *Leiopathes* corals.

Prior to running the HLR, the relevant statistical assumptions were tested. The samples size (n=40) was deemed adequate given the four predictor variables chosen to be included (Hair et al., 2014). An analysis of correlations between predictor variables revealed that genus and depth are moderately correlated (r-square 0.65, $p << 0.05$, $f >> 5$). However, this was deemed acceptable as the variance inflation factor (VIF) for genus and depth is below five (Table 4.2n), indicating the degree of collinearity is unlikely to affect the analyses (based on recommendations from Becker et al. (2015)). Assumptions of data normality were satisfied via transforming the data using a logarithmic or square root transformation.

Element	*Predictors*	*p value (ANOVA)*	*DoF*	*F statistic*	*r square*	*Δr square*	*Statistically Significant r square*
sqrt Br	Genus	0.04	2 & 39	5.3	0.21	-	yes
	Genus + Depth	0.56	3 & 38	0.3	0.22	0.007	no
	Genus + Depth + Coastal Prx	0.42	4 & 37	2.0	0.26	0.039	no
	Genus + Depth + Coastal Prx + ChlA	0.42	5 & 36	2.3	0.30	0.044	no
I	Genus	0.87	2 & 39	0.6	0.03	-	no
	Genus + Depth	0.05	3 & 38	7.1	0.18	0.145	yes
	Genus + Depth + Coastal Prx	0.87	4 & 37	0.6	0.21	0.033	no
	Genus + Depth + Coastal Prx + ChlA	0.22	5 & 36	3.4	0.26	0.049	no
log V	Genus	0.44	2 & 39	2.3	0.11	-	no
	Genus + Depth	1.00	3 & 38	0.3	0.11	0.006	no
	Genus + Depth + Coastal Prx	1.00	4 & 37	0.4	0.12	0.009	no
	Genus + Depth + Coastal Prx + ChlA	1.00	5 & 36	0.1	0.13	0.003	no
log U	Genus	0.91	2 & 39	1.5	0.07	-	no
	Genus + Depth	1.00	3 & 38	0.1	0.08	0.003	no
	Genus + Depth + Coastal Prx	1.00	4 & 37	0.2	0.08	0.006	no
	Genus + Depth + Coastal Prx + ChlA	1.00	5 & 36	0.1	0.08	0.001	no
Mo	Genus	0.17	2 & 39	2.7	0.12	-	no
	Genus + Depth	0.003	3 & 38	14.0	0.35	0.23	yes
	Genus + Depth + Coastal Prx	0.91	4 & 37	0.01	0.35	0.00	no
	Genus + Depth + Coastal Prx + ChlA	0.17	5 & 36	3.9	0.41	0.06	no

Table 4.2m. Table presenting results from a hierarchical linear regression comparing the relative contribution to changes in conservative-type elemental concentrations from each environmental variable. P < 0.05, F > 5 = a statistically significant change in r-square for the added predictor.

Table 4.2l presents the results of the HLR on nutrient and scavenged-type distributed elements. While the addition of any variable increases the r-square value in almost all cases, the only statistically significant increase in r-square occurs with the initial inclusion of the genus predictor for Cu and Zn ($P < 0.05$, $F < 5$), where the genus predictor explains 24% and 29% of the variability in Cu and Zn concentrated, respectively.

Table 4.2m presents the results of a HLR on conservative-type distributed elements. The addition of any new variable improves the r-square in almost all cases; however, the only statistically significant increase in r-square occurs with the addition of the depth predictor for I and Mo and the genus predictor for Br ($p < 0.05$, $f > 5$). The depth predictor can explain an additional 14.5% and 23% variability in I and Mo, respectively. The genus predictor can explain an additional 21% of the variation in Br.

In almost all cases, the addition of a predictor fails to produce a statistically significant change in r-square, suggesting factors outside of depth, location, surface productivity, and distance from the coast are controlling the recorded variations in elements concentrated by black corals. While few of the predictors produce statistically significant changes in r-square, they may still collectively explain between 8% and 41% of the variation in all trace elements.

Predictor	*VIF*	*DoF*
Genus	4.2	2
Depth	1.79	1
Coastal prox	1.98	1
ChlA	1.94	1

Table 4.2n. Table presenting calculated Variance inflation factors (VIF). The VIF determines the strength of correlation between independent variables. Values >5 indicates a minimal degree of (multi)collinearity between independent variables, see Becker et al. (2015). Calculated in R-studio.

4.3 Chemical Comparisons

4.3.1 Living Tissue vs Skeletal Chemistry

Here, the living tissue and skeletal composition for *Antipathes* and *Leiopathes* corals are compared using a skeleton - living tissue enrichment factor and plot (Table 4.3a, Figure 4.3a). The differences in concentration of trace elements between the coral skeleton and living tissue can provide us with clues regarding the functional roles (or lack thereof) of trace elements in black corals. When this behaviour is combined with the known behaviour of the various TEs in other marine organisms and a known origin for TEs in the black coral skeleton, this information can provide insight into the element's utilities in palaeoenvironmental reconstructions. The partitioning of TEs between the coral tissue and skeleton can be represented by a coral skeleton enrichment factor (K) where:

$$K_{Tissue} = \frac{TE\ Conc\ in\ Skeleton}{TE\ Conc\ in\ Tissue}$$

Where: KTiss < 1 = trace element enrichment in living tissue relative to coral skeleton, and K > 1 = trace element enrichment in coral skeleton relative to living tissue.

NB: a visual representation of the skeleton – tissue comparisons is presented in Figure 4.3a

	Mo	I	Br	U	Cd	V	Ni	Cu	Zn	Fe
KTiss	309	117	113	89.6	6.69	6.63	2.50	0.60	0.03	0.01

Table 4.3a. Table of enrichments factors (K) for trace elements between coral living tissue and skeleton. K < 1 = TE enriched in coral tissue relative to skeleton. K > 1 = TE enriched in coral skeleton relative to tissue. K ≈ 1 = TE enrichment is the same for coral tissue and skeleton. Data are representative of the coral skeletons (n=4) and their respective living tissue samples (n = 4). These include both Leiopathes and Antipathes corals and exclude A. fiordensis specimens.

Differences in TE concentrations between the living tissue and skeleton may result from a differing binding affinity for TEs between the organic material comprising living tissue vs skeleton of the coral. However, they may also arise due to differing biochemical utilities or toxicities of the TEs to the coral (Esslemont et al., 2000; Saha et al., 2016). Where trace elements are potentially useful or toxic to the organism, they may be

actively transferred through the tissue (into the skeleton) instead of being passively transferred (Esslemont et al., 2000; Komugabe, 2015a).

When an element is enriched in the tissue relative to the skeleton (i.e. KTiss < 1 – Cu, Fe, Zn) this may indicate that the element is biologically utilised and hence under metabolic control. On the other hand, elements enriched in the skeleton relative to the tissue (i.e. KTiss > 1 – Mo, U, Br, Cd, I, & V) may have little to no biological utility and thus are not under heavy metabolic control. In the latter case, these elements may be better suited to palaeo-reconstructive applications.

However, it is noted that elements enriched in the skeleton relative to the living tissue may be actively excluded from the living tissues via the release of metal-binding proteins (Deb and Fukushima, 1999; Phillips and Rainbow, 1989b) in response to their toxicity (Rainbow, 2002). In this case, the skeleton could be acting as some form of metabolic dump, storage or detoxification location for TEs supplied to the coral in large, toxic concentrations, such as Cd (Hwang et al., 2018; Rainbow, 2002).

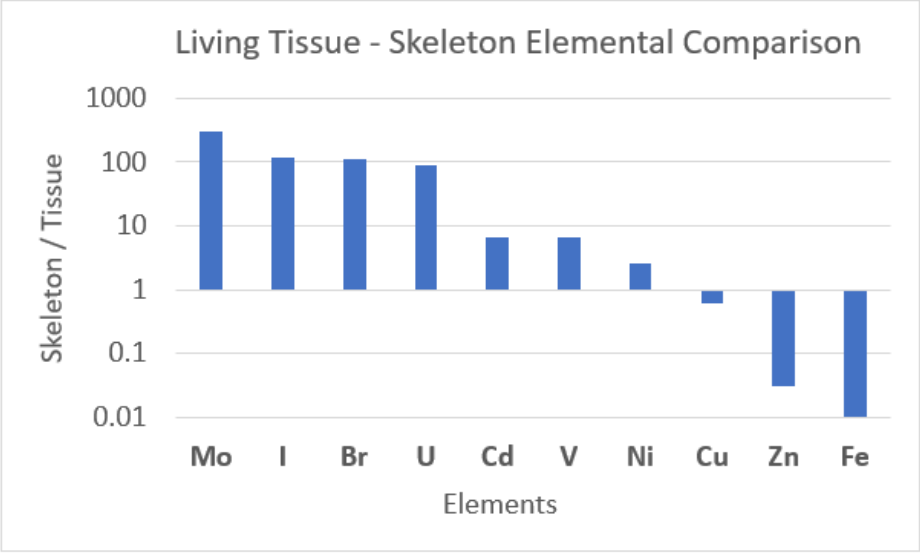

Figure 4.3a. Skeleton normalised, skeleton-tissue comparison. Elements plotting below 1 indicate enrichment in the living tissue relative to the skeleton. Elements plotting above 1 indicate enrichment in the skeleton relative to the living tissue. Data are representative of the coral skeletons (n=4) and their respective living tissue samples (n = 4). These include both Leiopathes and Antipathes corals and exclude A. fiordensis specimens.

4.3.2 Bi-Elemental Regression

Here, we present elements that show significant correlations between all coral samples, classified by the three defined regions: The Chatham Rise, The Bay of Plenty and Cape Reinga (Figure 4.3b). Regression models used clean data with all contaminants, replicates, *Antipathella fiordensis* corals and corals outside of the major regions removed (n =35). Not all the best-correlating elemental combinations are presented; see supplementary material for an exhaustive list of r-square values for all combinations.

Uranium and vanadium produce a remarkable correlation (avg. r-square = 0.98) in all regions. The correlation is within agreement to prior

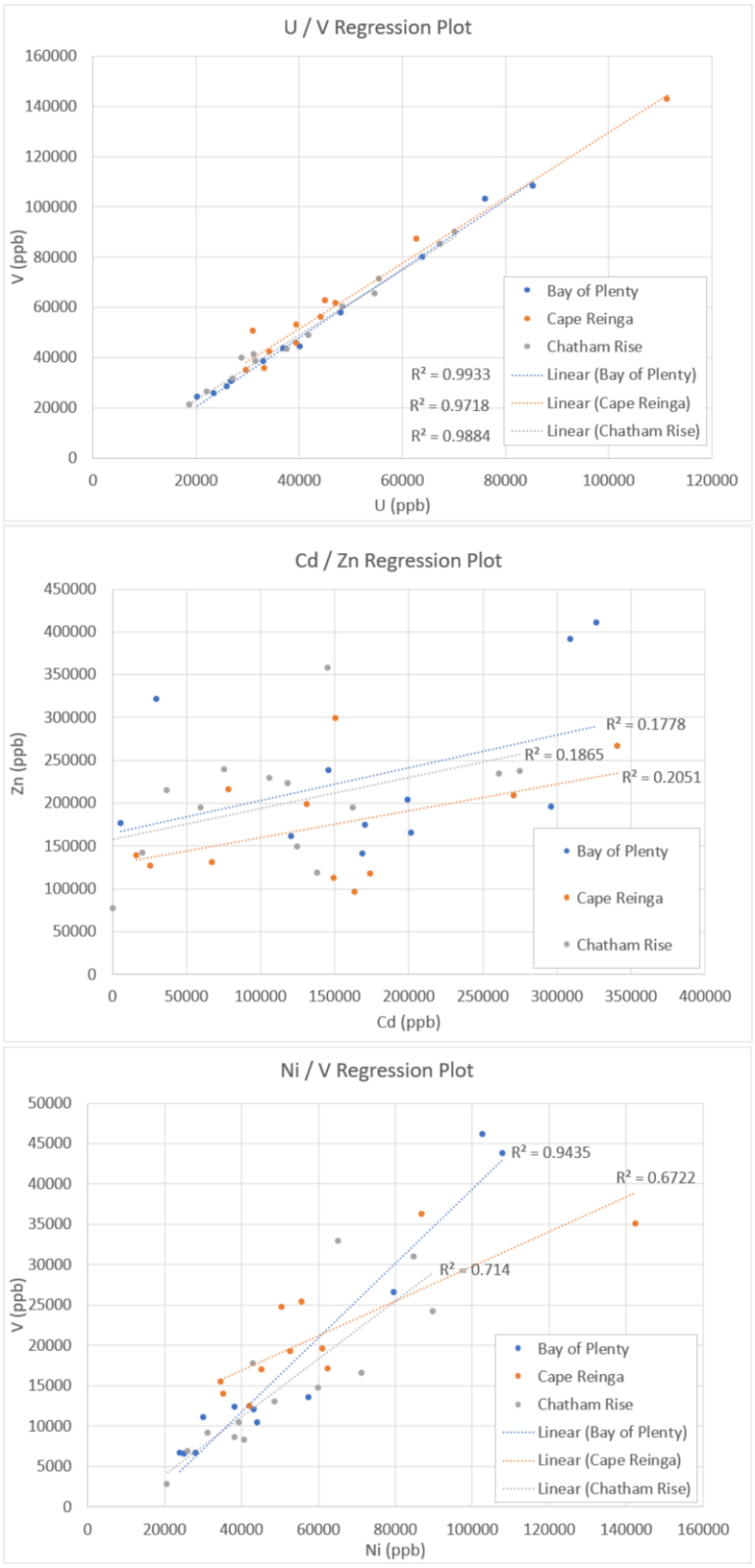

Figure 4.3b. Bi-elemental regression plots for U vs V, Cd vs Zn and Ni vs V. Units = ppb. Blue dots = BoP samples, orange dots = Cape Reinga samples and grey dots = Chatham Rise samples.

research from Komugabe (2015a), where U vs V r-square values were ~0.95.

Vanadium and nickel (and uranium and nickel) are similarly highly correlated (avg. r-square 0.8), however, not across all regions. For example, the V/Ni correlation decreases to 0.67 and 0.71 over Cape Reinga and the Chatham Rise and increases to 0.94 in the Bay of Plenty. This change in correlation between regions may describe changes to the corals physiological demand for these elements or their presence in the water column or a combination of the two.

Cadmium and zinc correlations are lower than expected based on comparisons to prior research from Komugabe (2015a) and D. Sinclair (2018 unpup) (see Figure 2.5c), correlating with an average r-square of 0.18 compared to 0.65 (Komugabe, 2015a). This correlation decreases slightly in the BoP and Chatham Rise but increases around Cape Reinga. Including all other coral samples (n=45) improves the r-square to 0.34. Cadmium and Zn are known to show similar vertical distribution throughout the world's oceans based on their similar fulfilment of biological roles in phytoplankton, so if corals were accumulating these elements directly from the surface ocean or ambient seawater, we would expect to see a high degree of correlation between them. As we do not, it is possible the corals may be selectively up taking/excluding these nutrient independent of their presence in the water column (possibly driven by a limited supply in one or more trace elements).

4.4 Measured Skeletal Trace Element Concentration Summary Table

Measured average concentrations for each analysed coral genus imply *Leiopathes* and *Antipathes* corals accumulate similar proportions of trace elements in their skeletons. *Leiopathes* corals do, however, accumulate slightly larger amounts of Cd, V, Ni, Zn, Mo, U and Cu than *Antipathes* corals. *Antipathella* genus corals accumulate the lowest proportions of almost all anlaysed trace elements, including U, I, Zn, Cu and Ni. The lower measured TE concentrations in the *Antipathella* corals likely reflects the unique fjordic habitat and its associated differences in TE chemistry to the open ocean.

Element	*Antipathella*	*Antipathes*	*Leiopathes*	*Uncertainty (±)*	*Element*	*Antipathella*	*Antipathes*	*Leiopathes*	*Uncertainty (±)*
Li	0.072	0.102	0.093	0.013	**Cr**	1.043	0.969	1.376	0.030
Y	0.027	0.044	0.065	0.002	**Mn**	2.503	1.545	1.393	0.070
Mo	68.40	71.58	112.1	1.810	**Co**	0.074	0.117	0.085	0.002
Pd	0.002	0.003	0.003	0.001	**Ni**	2.865	9.884	17.32	0.263
Cd	0.704	83.96	155.6	2.971	**Cu**	6.311	14.88	19.39	1.367
Sb	0.099	0.123	0.237	0.017	**Zn**	35.90	127.5	207.6	9.436
Ba	0.126	0.324	0.161	0.013	**As**	0.093	0.148	0.147	0.027
La	0.006	0.007	0.008	0.001	**Sr**	16.62	32.17	18.11	0.282
Ce	0.016	0.028	0.019	0.002	**I**	1.588	14.06	15.29	0.369
Pr	0.008	0.019	0.016	0.002	**U**	23.81	30.68	46.68	0.764
Nd	0.004	0.011	0.011	0.001	**Mg**	1382	2075	1801	60.71
W	0.985	2.293	2.119	0.026	**S**	1428	1722	1291	40.47
Hg	3.421	39.72	100.1	1.000	**Ca**	1817	3740	1828	111.3
Pb	0.198	0.564	0.196	0.013	**V**	25.76	33.14	59.31	1.163
B	100.6	55.77	73.60	1.985	**Fe**	23.16	34.47	22.91	1.599
Al	101.4	41.93	19.58	5.365	**Ge**	0.010	0.020	0.101	0.012
Si	107.7	136.3	107.9	21.74	**Se**	119.9	32.16	10.58	1.157
P	44.39	39.89	27.652	1.984	**Br**	9920	4642	9483	350.4
Ti	1.452	2.222	0.596	0.046					

Table 4.4a. Summary table for average measured trace element concentrations in black coral skeletons from New Zealand waters organised by coral genera. ***Units = ppm****. Leiopathes sample size = 37, Antipathes = 5, Antipathella = 5. Uncertainty represented by analytical RSD.*

Chapter 5 - Discussion

5.1 Introduction

Before we can use trace elements from black coral skeletons as environmental proxies, we first need to know where these trace metals are coming from (i.e. surface or ambient seawater) and how they are making it into the skeleton (passive or active uptake). Uptake pathways have not been extensively studied; however, Komugabe (2015a) posited four potential uptake pathways (see Section 2.1.5.2, Figure 2.1b). Trace metals may be sourced from either ambient dissolved seawater, particulate organic matter (POM) or both, and uptake may be either passive (abiotic) or active (under metabolic control).

POM is composed of phytoplankton remains that have adsorbed elements from the surface ocean (de la Rocha and Passow, 2014b; Schneider et al., 2003), so it can be assumed to reflect the elemental concentration of surface seawater. If corals source trace elements from POM, then their skeletons might likewise reflect surface seawater concentrations. Conversely, if corals source trace elements from the seawater in which they are growing (e.g. through passive diffusion), then their chemistry would reflect deep/intermediate seawater (herein referred to as “ambient” seawater).

Vertical TE distributions in seawater follow predictable patterns, with nutrient-like TE’s showing a distinct change in concentration between surface and intermediate (ambient) depths. Likewise, both conservative and nutrient-like elements show spatial (latitudinal and longitudinal) patterns at both surface and intermediate depths, in response to a range of environmental gradients (e.g. productivity, proximity to land, proximity to major ocean fronts, etc.). In this chapter, we attempt to deduce the source and uptake pathway of TE’s to black coral skeletons by exploring for these spatial and depth relationships in the coral data.

5.2 Recap: Primary Productivity and Regional Oceanography

5.2.1 Surface Ocean Waters

Four distinct features characterise the surface ocean around New Zealand (see Section 2.2.2 for details): Sub Antarctic Water (SAW), Sub Tropical Water (STW), the Tasman Front (TF) and the Sub Tropical Front (STF) (Figure 5.2a). STW represents the warm, salty, macronutrient depleted and micronutrient enriched waters of the subtropics, whereas SAW represents the colder, less saline, macronutrient enriched, and micronutrient depleted sub-polar waters (Chiswell et al., 2015; Roemmich and Cornuelle, 1992). The TF defines the northern extent of the Tasman Sea STW and the southern extent of the Pacific Ocean STW. The TF is generally characterised by warm, salty, and (macro)nutrient-depleted surface waters.

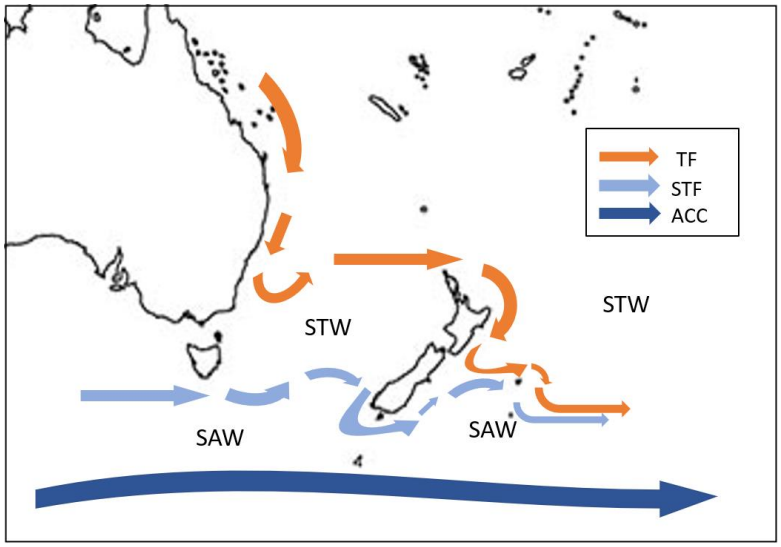

Figure 5.2a. Schematic (simplified) diagram of surface circulation around NZ adapted from (Chiswell et al., 2015). Dark blue arrow = Antarctic Circumpolar Current, blue arrows = Sub Tropical Front, orange arrows = Tasman Front. SAW = Sub Antarctic water, STW = Sub Tropical Water.

SAW and STW are separated by the STF (Chiswell et al., 2015). The STF defines a major gradient in surface temperature (~5˚C change), salinity (~0.5psu change) and sea water nutrient content (Chiswell et al., 2015; Orsi et al., 1995; Sutton and Roemmich, 2001).

Around the Chatham Rise and across NZ's submerged continental landmass, the STF and the southern SAW spill out across the Chatham Rise and mix with the northern TF & STW see Bostock et al. (2013); Chiswell et al. (2015). Here, ideal conditions are set up for phytoplankton growth, leading to the very high productivity seen in New Zealand waters (Murphy et al., 2001). South of the SAW, the surface flows of the ACC become Fe limited, leading to enhanced macro and micronutrient loads (Boyd et al., 1999; de Baar

et al., 1995; Orsi et al., 1995). Since the mixing waters have different trace element concentrations, this is also expected to be a region of strong TE gradients.

5.2.2 Intermediate Ocean Waters

Three water masses characterise the oceanography of intermediate (~30 – 1300m) waters around New Zealand: Antarctic Intermediate Water (AAIW), Sub Tropical Mode Water (STMW) and Sub Antarctic Mode Water (SAMW) (Chiswell et al., 2015; Hanawa and Talley, 2001; Tsubouchi et al., 2007) (Figure 5.2b). All intermediate waters contain higher concentrations of *nutrient* trace elements than their surficial counterparts (Figures 4.2c, 4.2d & 4.2e), and we anticipate that the micronutrient trace metal content will be highest beneath highly productive regions such as below the STF.

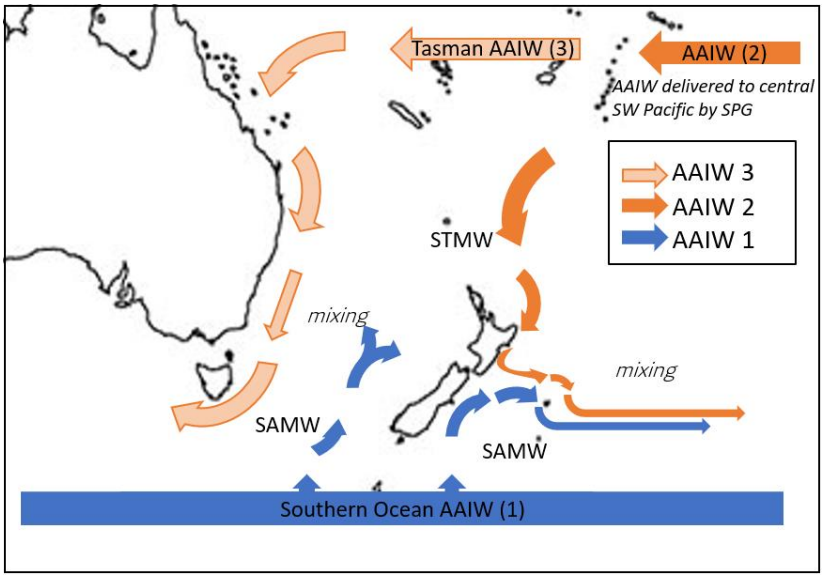

Figure 5.2b. Schematic diagram of intermediate circulation in the NZ region adapted from (Chiswell et al., 2015). SO AAIW (1) – intermediate water formed along the STF (Cold, low salinity), Tasman AAIW (3) – formed in the semi closed Tasman gyre (warmer, high salinity, expected increased micronutrient load), AAIW (2) – main AAIW created in SE Pacific and delivered to Central SW Pacific by south Pacific gyre (v. low nutrients, v. low salinity). See Bostock et al. (2013); (Sutton and Bowen, 2014) for further AAIW subtype classification details. SAMW – Sub Antarctic Mode Waters, STMW – Sub Tropical Mode Waters

Much like their surficial counterparts, STMW is warmer and saltier than the southern SAMW (Hanawa and Talley, 2001; McCartney, 1979; Roemmich and Cornuelle, 1992). Underlying these mode waters are the AAIW, which may be split into three subtypes in our study region (Bostock et al., 2013): the Southern Ocean AAIW (AAIW 1), the Tasman Sea AAIW (AAIW 3) and the South-eastern Pacific AAIW (AAIW 2) (Figure 5.2d). The northern TSAAIW and STMW are expected to have slightly higher salinities and micronutrient contents than the southern SOAAIW and SAMW due to the increased

micronutrient supply to the ocean off the coast of Australia (Schlitzer, 2018). AAIW entering from the Southern Ocean may contain similar amounts of micronutrients to the TSAAIW due to Fe limitation resulting in a surplus of these elements in surface/intermediate waters. AAIW 2 is expected to have a very low salinity and nutrient load (Bostock et al., 2013).

5.2.3 Deep Ocean Waters

None of the coral specimens used in this study grew below 1500m. Their TE chemistry is therefore unlikely to reflect deep ocean processes. The deepest specimens, however (~1450m), may sample the upper reaches of deep-water masses such as the Pacific Deep Water (PDW) and Upper Circumpolar Deep Water (UCDW) (Figure 5.2c). These waters are characterised by a salinity gradient that increases moving south towards Antarctica – the opposite to surface and intermediate waters (see Table 1.2a).

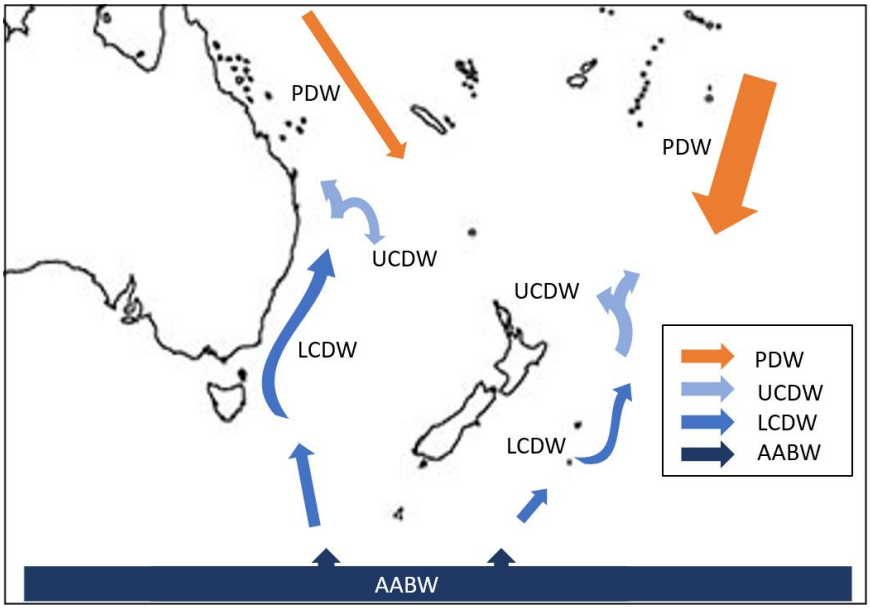

Figure 5.2c. Schematic diagram of deep-water circulation around the SW Pacific. PDW – Pacific Deep Water, UCDW – Upper Circumpolar Deep Water, LCDW – Lower Circumpolar Deep Water and AABW – Antarctic Base Water. Circumpolar Deep Water (CDW) = LCDW + UCDW. Adapted from Chiswell et al. (2015).

PDW is the dominant deep water mass north of the Chatham Rise, and the CDW to the south, both at ~1500m+ water depth (Chiswell et al., 2015; Mantyla and Reid, 1983). Both UCDW and PDW have relatively similar physical characteristics; however, PDW is characterised by slightly lower salinities and warmer temperatures (Chiswell et al., 2015; Mantyla and Reid, 1983; Whitworth III et al., 1999). All deep water masses are expected to have slightly lower micronutrient loads than the overlying intermediate waters due to the deep ocean forming a major sink for many micronutrients (Bruland et al., 2013). The

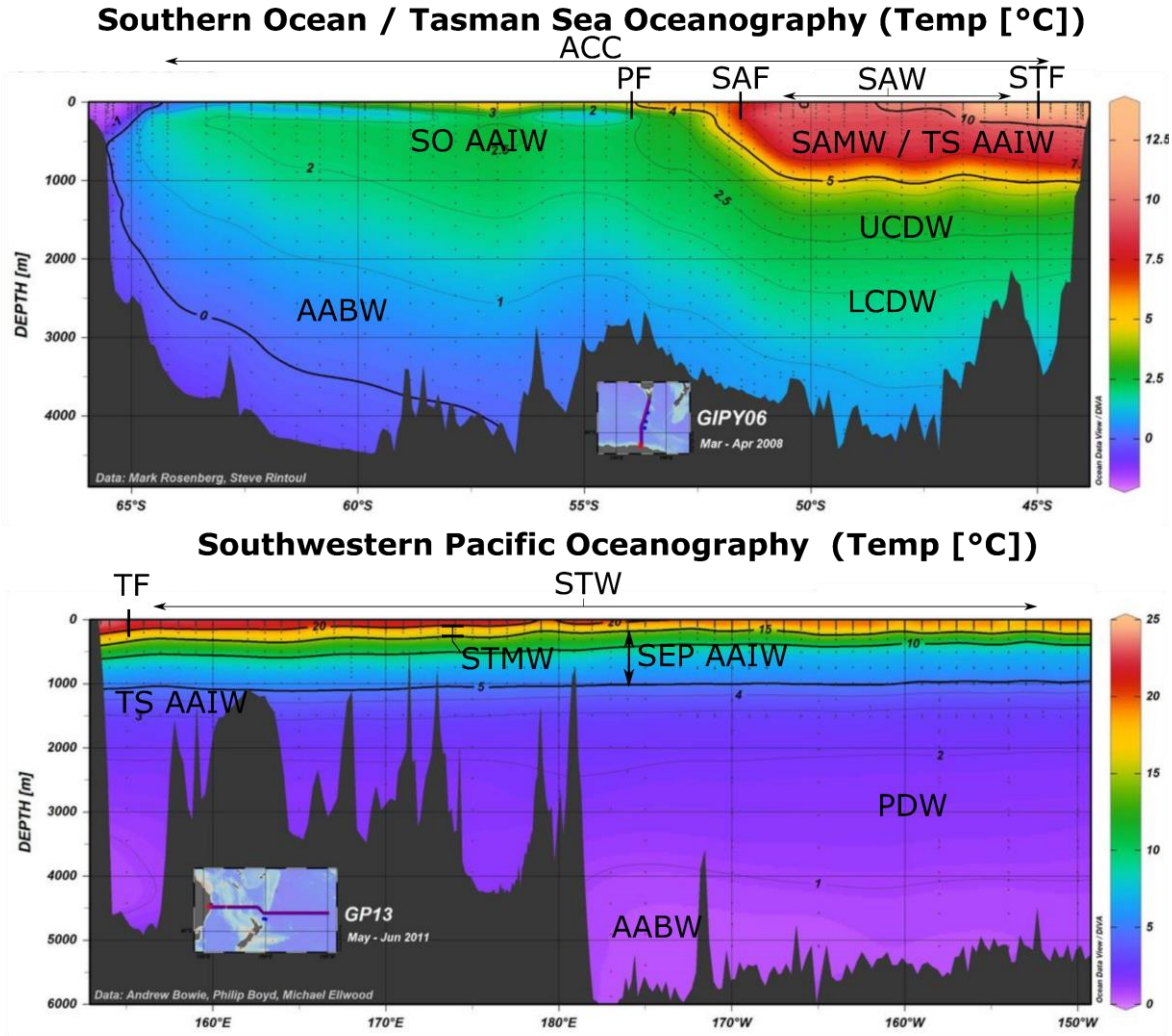

Figure 5.2d. Annotated water temperature vertical profiles showing vertical relationships between various water masses in the study region. Transect GIPY06 is representative of subtropical, subpolar and polar circulations/fronts to the SW of NZ. Transect GP13 is representative of subtropical circulations/fronts to the north of NZ. ACC – Antarctic Circumpolar Current, PF – Polar Front, SAW – Sub Antarctic Water, STF – Sub Tropical Front, SAMW – Sub Antarctic Mode Water, SEP AAIW / AAIW2 – SE Pacific Antarctic Intermediate Water, TS AAIW – Tasman Sea AAIW, SO AAIW- Southern Ocean AAIW, UCDW – Upper Circumpolar Deep Water, LCDW – Lower Circumpolar Deep Water, PDW – Pacific Deep Water and AABW – Antarctic Base Water.

complex bathymetry of the NZ region may enhance the variability in deep sea/sea floor micronutrient concentrations, with hydrothermal vents forming significant sources (and sinks) for some elements (Fe, Cu and Mn) (German et al., 1991; Middag et al., 2011), and Fe-Mn nodule formation/sub-oxic sediments forming a significant sink for many elements (U, V, Mo) (Emerson and Huested, 1991; Ho et al., 2018).

5.3 Recap: Trace Element Behavior – Spatial and Depth Patterns

5.3.1 Nutrient Elements

The distributions and concentrations of trace elements in the ocean are generally controlled by: 1) (terrestrial) sources and (deep ocean) sinks, 2) general circulation, 3) water mixing, and 4) biogeochemical cycling (Bruland et al., 2013). Trace metals are predominantly delivered to the ocean by rivers, wind-blown dust and/or hydrothermal input near mid-ocean ridges (see Table 2.5b, Section 2.5.4). Trace metals are removed via settling at the seafloor alongside passive and active uptake by marine organisms.

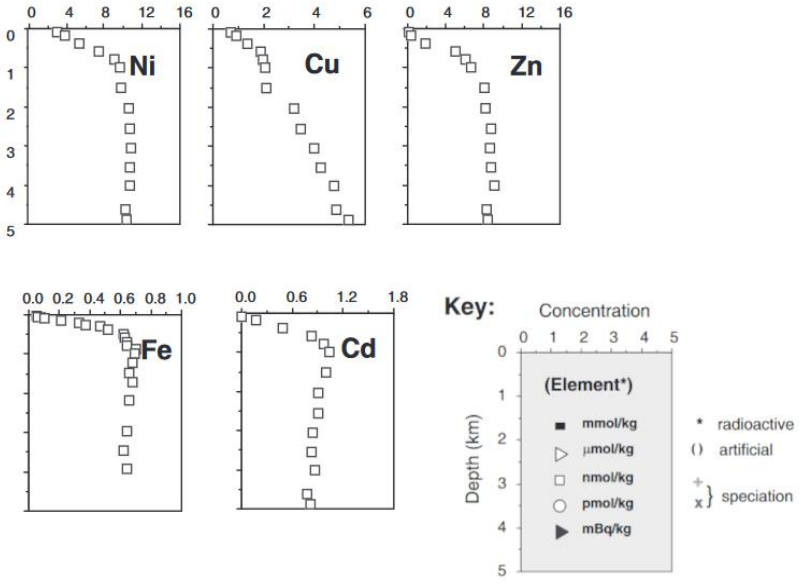

Figure 5.3a. Nutrient-type distributed elements. Figures adapted from Sarmiento (2013). Distributions are schematic representations and may vary between ocean basins. NB: Fe is included as a nutrient type element despite hybrid behaviour in the South Pacific, see Boyd et al. (1999); Raimundo et al. (2013).

The distributions of nutrient-type trace elements are predominantly controlled by major biogeochemical cycles: taken up by planktonic organisms at the surface and re-mineralised at intermediate depths (Bruland et al., 2014). This results in surface water depletion, enrichment at intermediate depths (~1000m) and a steady decrease approaching great depths (>~1500m) (Figure 5.3a). Ultimately, this results in a strong

difference between surface and intermediate waters. Most micronutrient trace metals (e.g. Cd, Zn, Cu, Fe and Ni) display similar vertical profiles (Figure 5.3a). Copper, however, can show slightly less regeneration at intermediate depths than other micronutrient metals. However, this does not affect its surface or deep-water expression. Iron can also display a hybrid profile depending on the proximity to terrestrial sources. For example, close to dust sources, Fe can exhibit a scavenged distribution (see Section 2.5.3) with a surface maximum and decrease with depth. Conversely, far from atmospheric sources (specifically high nitrogen low chlorophyll regions such as the Southern Ocean (Boyd et al., 1999)), Fe exhibits a nutrient profile almost identical to the other nutrient trace metals (Moore et al., 2001).

5.3.2 Conservative Elements

The distributions and concentrations of conservative elements throughout the world's oceans are predominantly driven by sources/sinks and ocean circulation (Bruland et al., 2013; Sarmiento, 2013), with only a minor contribution from biological productivity. These elements are generally weakly reactive, have long residence times (over 100 kyr) and maintain a constant ratio to salinity (Bruland et al., 2013). They may be involved in biogeochemical cycles; however, these processes are thought to have a weak effect on their overall ocean distribution. Therefore, conservative elements are characterised by homogeneous distributions across all depths of the world ocean (Figure 5.3b).

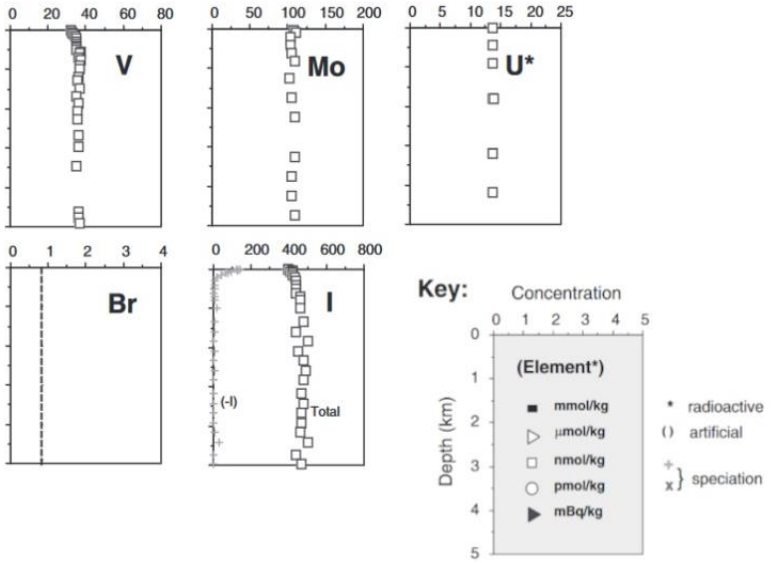

Figure 5.3b. Conservative-type distributed elements. Figure adapted from Sarmiento (2013). Distributions are schematic representations and may vary between ocean basins.

Elements V, I and Mo may display slight depletion at the surface waters of productive regions due to uptake by phytoplankton (Figure 5.3b); however, this depletion is weak compared to the surface depletion exhibited by nutrient trace elements (Bruland et al., 2014). These conservative elements (V, I and Mo) may also be elevated (relative to deep waters) close to terrestrial sources (Dellwig et al., 2007; Wang and Wilhelmy, 2009).

5.4 Interpretation of Results

This section presents a summary of interpretations, reviewing the outcomes of each environmental test and what the results potentially tell us about the source of trace elements in the black coral skeleton.

5.4.1 Empirical Bayesian Kriging Maps

EBK maps, and their associated statistics, reveal whether there are any consistent spatial relationships/gradients in the distribution of skeletal trace elements around NZ. The presence of a spatial relationship would indicate that environmental parameters are influencing skeletal TE concentrations. Since surface waters have higher spatial gradients than mid-depth waters, the presence of a strong spatial gradient may also suggest a surface-water origin for the skeletal trace elements (although spatial gradients in TEs also exist at depth). Conversely, the lack of any consistent spatial relationship in skeletal TEs may indicate:

1) Corals do not record environmental parameters (or endogenous variability is too high).

2) Local effects have a larger influence on TEs than any environmental gradient; this may include depth-related effects.

3) The distribution of coral samples is too sparse/suboptimal to resolve a gradient.

or

4) There is no strong environmental gradient.

5.4.2 Inter-Basin Comparisons

There are two GEOTRACES transects that intersect New Zealand's waters: GP13, which passes through the Southwestern Pacific Basin, and GIPY06, which passes through the Tasman Basin (see inset maps of Figures 4.2c, 4.2d & 4.2e). These transects (and associated data) allows us to compare the dissolved concentrations with the coral skeletal concentrations between the two basins (Table 5.4a). These binary comparisons,

in turn, allow us to determine if the skeletal trace elements behave consistently with surface or intermediate dissolved concentrations. If the proportional change of a TE in the coral skeleton matches the proportional change in dissolved concentration, then this might indicate that skeletal trace elements are sourced from that water mass. Therefore, the question here is: *Do coral TE data change proportional to dissolved TEs between the Pacific and the Tasman Sea basins?*

Source: Schlitzer 2018 - eGEOTRACES
Location: 155°E - 170°W (Pacific), 43°S - 50°S (Tasman Sea)

Element	*Depth (m)*	*Units*	*W. Pacific Known Concentrations*	*Tasman Sea Known Concentrations*	*Units*	*W. Pacific Measured Concentrations*	*Tasman Sea Measured Concentrations*
Cd	0	ppt	11.2	11.2	ppm	60.8	122
	1000	ppt	67.4	67.5	-	-	-
	2000	ppt	89.9	89.9	-	-	-
Cu	0	ppt	31.8	31.8	ppb	22500	19800
	1000	ppt	63.6	63.6	-	-	-
	2000	ppt	191	127	-	-	-
Fe	0	ppt	11.2	5.58	ppb	28200	18550
	1000	ppt	41.9	22.3	-	-	-
	2000	ppt	36.3	41.9	-	-	-
Ni	0	ppt	117	176	ppb	11200	17300
	1000	ppt	323	367	-	-	-
	2000	ppt	440	411	-	-	-
Zn	0	ppt	65.4	164	ppm	245	163
	1000	ppt	196	245	-	-	-
	2000	ppt	425	441	-	-	-

Table 5.4a. Table presenting comparisons between measured coral and known dissolved trace element concentrations between the Tasman Sea and Southwestern Pacific. "Known" trace element data was extracted from the northern and western portions of the GEOTRACES transects GIPY06 and GP13, respectively. Measured trace element data presents averages of 5 coral samples closest to transect GIPY06 and 4 samples closest to transect GP13.

If yes, then tentative evidence is provided supporting the source of that element being the water mass, although this could always be coincidental. However, if the coral trace element varies significantly less than the variation between basins (or opposite in sign), this strongly rules out the element coming from that water mass. Alternatively, if the change in the coral is significantly more than the change in the seawater, then it could simply be that other local or endogenous processes have a strong influence on coral TE composition ('overwriting' any effect of water mass concentration), meaning that we cannot draw any firm conclusions from the data.

5.4.3 Proximity to the Sub Tropical Front

The STF represents a region of major change in water chemistry and productivity, which is expected to be reflected in the TE content of the seawater and potentially the

coral (see Section 5.2 & 4.2.4 for further info). Therefore, as we move towards the STF (from the North), we should expect to see a distinct change in the nutrient (and micronutrient) content of surface waters, exhibited by the coral TE data as either positive or negative relationships with STF proximity. For example, dissolved Ni data (Figure 4.2c) displays a distinct increase in concentration approaching the STF and dissolved Fe data (Figure 4.2e) show a distinct decrease in concentration approaching the front. If corals are recording the overlying waters' TE chemistry, we would expect to see these gradients.

If coral TEs show a statistically significant *negative* relationship with distance from the STF, this would be consistent with the TEs being derived from a surface source, where high productivity along/within the STF has depleted TEs (e.g. see Figures 4.2c, 4.2d & 4.2e, Section 4.2.4). This effect would be expected to be strongest for nutrient trace elements.

If coral TEs show a statistically significant *positive* relationship with STF proximity, this suggests that other processes have a stronger influence on TE composition that 'overwrite' any oceanographic gradient effect. Exception: Fe from surface water environments is expected to show a positive increase across/approaching the front (based on observations in Figure 4.2e, Section 4.2.4). Cadmium may also show a positive relationship; however, this trend may be partially obscured by the data gap from 34˚S - 42˚S in Figures 4.2c, 4.2d & 4.2e.

If a TE does not show any relationship with proximity to the STF then it may provide evidence in support of deep-water (ambient) origin for the TEs (based on the minimal change seen in intermediate waters approaching the STF, see Figures 4.2c, 4.2d & 4.2e, Section 4.2.4). However, it may also imply that any gradients across the STF are weak, local/endogenous effects generate too much scatter in the data to resolve any gradient, or additional effects, such as metabolic processes, are obscuring any trace element-STF relationship.

5.4.4 Surface Productivity

Surface productivity (as indicated by Chl-a concentration) is expected to influence trace elements at both surface and intermediate depths. In the former case, trace elements (particularly micronutrient metals) are removed from the surface waters. In

the latter case, trace elements are regenerated at depth as the exported organic matter breaks down (see Section 4.2.3).

A *positive* relationship between coral TE content and Chl-a might indicate that we are seeing an intermediate-depth origin for skeletal TEs. Conversely, a *negative* relationship would imply a surface origin for biologically utilised TEs. However, the latter scenario is predicated on several assumptions: Firstly, that phytoplankton tissues take up TEs in proportion to their dissolved concentrations in the surface water. Secondly, that TE concentrations in the coral skeleton are proportional to the concentration of the element in the organic matter consumed by the coral (as opposed to – for example – the total flux of the trace element from the surface ocean).

No relationship between TE content and Chl-a would suggest that the corals are not responding to overlying productivity. Alternatively, it may be that productivity does affect TEs, but the effect is masked by other processes that are local to each coral. Lastly, it is possible that a relationship exists but cannot be resolved because the distribution of corals in this study is not optimal for testing correlation with Chl-a.

5.4.5 Magnitude of Trace Element Variability in Coral vs Seawater

At the most basic level, we can compare the amplitude of trace element variation in seawater with the amplitude of variation across coral skeletons (Table 5.4b). In the absence of any other data for comparison, this may allow us to rule out seawater as a source of the variations seen in the coral.

These comparisons were carried out by comparing the total (Tier 4) skeletal variability for all conservative TEs to the known variability of the respective elements in seawater from supporting literature (as presented in Table 5.4b).

If the total variation in skeletal TE content varies by a significantly greater percentage than the reported natural variability in seawater, then we can conclude that other processes (e.g. local or endogenous processes) have a significant impact on the coral composition and that any environmentally-driven variation may be heavily obscured.

If the total variation in skeletal TE content varies by a percentage similar to (or less than) the reported natural variability in the seawater, then evidence is provided supporting corals sampling elements in proportion to their presence in seawater. However, it is noted that this may also be coincidental.

Element	*Sources*	*Units*	*Natural variability*	*Avg. Known Concentration*	*Avg. Measured Coral Conc.*	*Total Skeletal Varibaility*
U	(Andersen et al, 2010; Chen et al, 1986)	ppb	5%	3.3	3868±760	46%
V	(Huang et al, 2015)	ppb	22%	1.8 - 2.3	46230±1160	51%
Mo	(Collier, 1985; Tuit, 2003)	ppb	31%	9.0 - 13.0	91830±1810	45%
Br	(Eggencamp, 2014)	ppm	0.10%	65	7062±350	57%
I tot	(Huang et al, 2005)	ppt	41%	45 - 76	14700000±370000	40%

Table 5.4b. Table presenting comparisons between natural variability and measured total black coral variability of conservative-type elements. Average measured concentrations column includes both Antipathes and Leiopathes corals. Uncertainty represented by analytical RSD. Presented total variability is as calculated in Section 4.2.5. 'I tot' refers to total iodine concentration as opposed to its dissolved iodide (I-) species.

5.4.6 Depth Effects

Since some trace elements (notably the micronutrient metals) have a significant depth variation in the ocean (see vertical profiles Figure 5.3a), the presence of a relationship between skeletal TE concentrations and the depth of the colony may indicate whether corals are incorporating trace elements from their ambient water mass (as opposed to surface water). Thus, if skeletal TEs are correlated with depth, this supports ambient seawater as the source of the elements. However, this relationship is somewhat confounded by taxonomy, as different coral genera do display a depth preference (Tracey and Hjorvarsdottir, 2019; Tracey et al., 2014).

If no correlation between coral TEs and depth is seen (for elements known to have a depth variation), then this potentially rules out an ambient seawater origin for those elements. However, this would tell us little about the source of elements that do not have a significant depth variation (e.g. the conservative elements)

5.4.7 Living Tissue – Skeleton Comparison

Comparing the TE content of coral tissue with coral skeleton can provide insights into an element's behaviour and biological utility. For example, a high tissue concentration might imply that the element has a biological utility and is therefore under metabolic control. This would suggest that the element is unlikely to provide a reliable environmental reconstruction. These skeleton-tissue TE comparisons may be defined by

KTiss (the skeleton-tissue enrichment factor), where $K_{Tiss} < 1$ indicates trace element enrichment in living tissue relative to coral skeleton, and $K_{Tiss} > 1$ indicates trace element enrichment in coral skeleton relative to living tissue.

Suppose a TE is enriched in the tissue relative to the coral skeleton (i.e. (KTissue < 1, see Section 4.3.1.1), then it suggests some metabolic utility for that TE. On the other hand, if TE is enriched in the skeleton relative to the tissue (i.e. KTissue > 1, See section 4.3.1.1), it suggests the coral may be actively excluding the element from its tissue (but not from the skeleton). The latter scenario might imply that the skeleton is passively taking up trace element from the ambient water (which may mean that the skeletal composition could be used to reconstruct the local water). However, it is also possible that the relative enrichment in the skeleton represents some kind of metabolic 'dump' for metals unwanted metals, or those supplied in large, toxic, concentrations (Phillips and Rainbow, 1989a; Rainbow, 2002).

In both cases, however, a relative enrichment or depletion of the trace element in the skeleton may arise because the material comprising the skeleton has a different intrinsic binding affinity for that element than the material in the tissue (Rainbow, 2002; Saha et al., 2016).

5.4.8 Coral Skeleton TE Enrichments Relative to POM

The enrichment of skeletal TE's over their food – POM – can potentially resolve whether trace elements are soured via ingested organics. This enrichment is defined by K_{POM} (see Komugabe (2015b)), which represents the following equation:

$$K_{POM} = \frac{TE\ Conc\ \ in\ Coral}{TE\ Conc\ in\ POM}$$

KPOM values were extracted from Komugabe (2015b) and are summarised in Table 5.4c.

Given that skeletal organics and tissues have distinctly different organic compositions, with presumably different binding sites for metals, it would be highly coincidental to find a K_{POM} close to one if the skeleton was absorbing elements from the water. Therefore, if we do find a K_{POM} close to one, this might indicate that skeletal trace element concentrations are limited by supply and sourced from POM.

If the K_{POM} is >> 1 (e.g. enriched by 1,000,000 times), it would be hard to justify a POM source for that element. Carbon is a major element in organic material, and TEs are typically orders of magnitude less concentrated. This would mean for the skeleton to have sourced TEs *solely* from POM, then for every atom of the TE transferred from food to skeleton, many millions of C atoms must have 'passed through' the coral's system but not been used for building the skeleton. Although this is possible (e.g. if the organism metabolically 'dumps' TEs into the skeleton that are present/supplied in large, toxic concentrations as part of the process of excluding it from tissue), it is more likely that the TE was passively concentrated when skeletal organic material absorbed it from an ambient water source.

5.4.9 Taxonomic Comparisons

If coral taxon has a strong influence on average trace element concentration in the skeleton, then this will confound any environmental studies that do not control for coral genus and may thus compromise the use of black corals in palaeoenvironmental reconstructions. The presence of a relationship between trace elements and coral genera may be driven by: variations in growth between genera, variations in metal tolerance between genera, variations in feeding characteristics between genera or different skeletal compositions with intrinsically different metal-binding characteristics.

The absence of any relationship between trace elements and coral genera may indicate that the method of retrieval/incorporation and/or supply of TEs are the same for all coral genera, or that taxonomic effects are minor in relation to other 'local' factors (such as individual physiology or microenvironmental effects).

Test/Question	Nutrient						Conservative				
	Cu	Zn	Cd	Fe	Ni	Mo	V	U	Br	I
Do EBK stats indicate a spatial relationship?	(not tested)						(not tested)	weak		(not tested)
Do coral TE data change in the same way that dissolved TEs change between the Pacific and Tasman Sea basins?	deep			surface + int	surface	(not tested)	(not tested)	(not tested)	(not tested)	(not tested)
Do data show a correlation with distance from the STF?									weak -ve gradient	
Do data show a correlation with Chl-A?										weak -ve gradient
Do coral TE data vary by a % that is similar to (or less than) reported natural variability in the Ocean?	(not tested)	(not tested)	(not tested)	(not tested)	(not tested)	same	> than	> than	> than	same
Are coral TE data correlated with depth in the ocean?	moderate +ve gradient					strong +ve gradient			weak +ve gradient	
Do trace elements vary systematically with taxonomy?			strong							strong
Enrichment factor (KTiss): TE conce in coral / TE conc in coral tissue	1	1	10^3	10^-1	10^1	10^3	10^1	10^2	10^1	10^3
Enrichment factor (KPOM): TE conc in coral / TE conc in POM	10^5	(not tested)	10^6	10^3	10^4	10^7	10^5	10^6	(not tested)	(not tested)

Table 5.4c. Summary table of results used to inform water column origin and uptake pathways for trace elements into black coral skeletons.
Yellow box = Yes
White box = No
Red box = Yes (with a strong relationship)

5.5 Nutrient-type Trace Element Interpretations

This section explores the possible source(s) and palaeoceanographic utility of the *nutrient-type* trace metals in black coral skeletons based on the results presented in Chapter 4 and the general interpretations presented in Section 5.4 and in Table 5.4c. Section 5.6 explores the *conservative* trace metals.

5.5.1 Copper

The presence of a positive relationship between coral Cu concentrations and depth suggests that corals may be sourcing copper from the ambient water. This accords with the lack of a relationship with STF proximity and the large KPOM enrichment factor (10^5). However, the lack of a relationship between surface productivity and Cu concentration, the presence of a taxonomic effect, and a moderate inter-colony variability (27% RSD) all indicate that additional, possibly biological, processes may obscure any environmental signal. The skeleton-tissue enrichment factor (KTissue < 1 indicating that coral's tissues are more enriched than the skeleton) implies that the living tissue of black corals contains different functional groups with a higher binding affinity for Cu, or that Cu is actively concentrated in the tissues of black corals. The latter would suggest that Cu may have some specific biological function.

Copper is known to have a role in iron + oxygen acquisition as well as protein synthesis (Annett et al., 2008; Maldonado et al., 2006), so it is plausible that the corals are actively extracting Cu from seawater. This process may be partially responsible for the lack of any relationship between Cu and surface productivity, as the uptake of Cu may be dictated by a physiological demand as opposed to the concentration of Cu in the water column. We tentatively conclude that Cu is actively taken up by black corals and therefore is unlikely to be directly related to the seawater concentration, thereby serving little utility in palaeoenvironmental reconstructions. However, additional research into black coral biomineralisation and trace metal uptake pathways would be required to rule out copper's utility in palaeoenvironmental reconstructions definitively.

5.5.2 Zinc

Skeletal zinc does not show any spatial relationship with depth, surface productivity or proximity to STF or the coast. Likewise, there is no consistent relationship between

skeletal Zn and ocean basins. This makes it impossible to determine whether coral Zn derives from an ambient or surface ocean source. A moderate intrinsic variability between individuals (34% T3 RSD) and a strong taxonomic effect suggest that there are unknown intrinsic processes that have a larger influence on Zn composition than environmental drivers.

Like copper, corals have a higher Zn concentration in their tissue than in their skeleton (KTissue < 1), suggesting that Zn may be utilised for some biological purpose. As with Cu, this may explain the lack of any relationship to the environmental drivers and is consistent with Zn having a known role in carbon acquisition in many other marine organisms (Coleman, 1998; Morel et al., 1994; Sinoir et al., 2012). We, therefore, suggest that skeletal Zn is strongly influenced by the coral's biology and may serve little utility in palaeoenvironmental reconstruction.

5.5.3 Cadmium

As with Zn, Cd shows no consistent spatial relationships (including depth), meaning we cannot determine if it derives from an ambient or surface seawater source. A strong taxonomic effect and specimen-to-specimen variability (47% T3 RSD) suggest that coral biology significantly influences skeletal Cd. Unlike Zn, however, Cd is strongly enriched in the skeleton (or excluded from the tissue), displaying a large tissue enrichment factor (KTissue >> 1). The skeleton is also strongly enriched over the coral's food (KPOM is over 10^6). This provides tentative evidence that the skeleton may be passively absorbing Cd from an ambient seawater source.

However, Cd is also likely being actively excluded from the tissue as it is widely reported to be toxic to many marine organisms, especially in high concentrations (Engel and Fowler, 1979; Okocha and Adedeji, 2011; Wahyu et al., 2020). Therefore, it is possible that the skeleton also serves as a 'metabolic dump' for Cd that is sourced from the coral's food and environment.

Ultimately, there is insufficient evidence supporting any seawater origin or uptake pathway for Cd in black corals skeletons. The utility of skeletal Cd in palaeoenvironmental reconstructions, therefore, remains unknown.

5.5.4 Iron

There is tentative evidence supporting a surface water origin for skeletal Fe in the form of a consistent Fe behavior between the two basins and EBK statistics supporting a spatial relationship. A lack of Fe correlation with depth rules out the possibility that we are seeing a deep-water signal, and a lack of Fe enrichment in POM (KPOM ~ 10^3) implies that we are not seeing a concentration of Fe in the skeleton due to absorption from ambient water. However, a surface water origin for coral Fe is complicated by the lack of any relationship with surface productivity or proximity to the STF or coast, any of which might have been expected to impart a surface ocean gradient in Fe concentrations.

Subtle environmental signals may be masked by intrinsic variation between individuals (inter-colony RSD is 31%), and the enrichment of Fe in the corals tissues over the skeleton suggests a possible metabolic control on Fe uptake. Indeed, Fe is a biolimiting micronutrient in many parts of the ocean (Boyd and Ellwood, 2010; Tagliabue et al., 2017) and has a role in respiration and growth of many marine organisms (Butler, 1998; Morel and Price, 2003; Sunda, 2012). At this stage, the palaeoenvironmental utility of Fe is unknown, although the hints at a systematic surface variation warrant further investigation.

5.5.5 Nickel

A strong taxonomic effect and large specimen-to-specimen variability (47% T3 RSD) suggest that coral biology or unknown intrinsic processes significantly influence skeletal Ni concentrations. These processes are likely responsible for the lack of any spatial relationship in skeletal Ni (including depth, surface productivity or proximity to STF or the coast), making it difficult to deduce any seawater source. There is, however, a similar, possibly coincidental, inter-basin change to surface water concentrations that may provide tentative evidence for a surface water Ni origin.

The large tissue and POM enrichment factors (KPOM over 10^4) suggest Ni is passively absorbed to the skeleton (or actively excluded from the tissue) from an ambient seawater source. However, considering Ni can be toxic to many marine organisms and is a major anthropogenic contaminant (Blewett and Leonard, 2017; DeForest and Schlekat, 2013), the skeleton may also serve as a metabolic dump for Ni.

We conclude that Ni may yet offer some utility in palaeoenvironmental reconstructions; however, there is insufficient evidence in support of any seawater origin, and more data is required.

5.6 Conservative-type Trace Elements Interpretations

Here we examine evidence for the origin and possible utility of the conservative-type trace metals in black coral skeletons, based on the observations reported in Chapter 4 and general interpretations presented in Section 5.4 and in Table 5.4c.

5.6.1 Molybdenum

Molybdenum displays moderate specimen-to-specimen variability (~24% T3 RSD) and a strong relationship with depth and taxonomy. This suggests that unknown processes, possibly coral biology, exert considerable control on the Mo concentrated in black coral skeletons. Despite this, skeletal Mo concentrations show a similar magnitude of variability to Mo in dissolved seawater (45% T4 RSD vs 34% variation in seawater, see Figure 5.4b), offering tentative support for the possibility that Mo may be incorporating in proportion to its presence in seawater. It is noted, however, that this could easily be coincidental.

The significant enrichment of Mo in the skeleton relative to both POM (KPOM 10^7) and tissue support the idea that Mo is passively adsorbed onto the coral skeleton from an ambient source. However, the lack of any meaningful spatial relationship in skeletal Mo concentrations makes it difficult to discern any additional evidence for a seawater origin. The absence of a relationship with STF proximity or surface productivity may support an ambient seawater source, but considering Mo is only weakly biologically active (Collier, 1985), it is possible its seawater concentrations simply are not affected by any environmental gradient. These hints at a possible seawater origin for Mo merit some follow up study.

5.6.2 Vanadium

Skeletal V concentrations show no spatial relationships or any similarity in variation to seawater, again, making it difficult to discern a seawater origin. Moderate inter-colony variability (33% T3 RSD) and a strong taxonomic effect suggest additional processes, possibly biological, have a larger influence on V concentrations than any of the tested

environmental variables. This likely confounds the utility of V as a palaeoenvironmental proxy; however, skeletal V concentrations may simply be insensitive to any of the tested environmental variables. In either case, additional data is required before V can offer any utility in palaeoenvironmental reconstructions.

Vanadium is preferentially concentrated in the coral skeleton as indicated by a large tissue enrichment factor and evidence in support of compositional zoning throughout skeleton layers (see Komugabe (2015a) EMPA maps). The large POM enrichment factor (KPOM 10^5) may provide tentative evidence supporting an ambient seawater origin; however, more data is required to deduce any seawater source with confidence.

5.6.3 Uranium

Tentative evidence is provided in support of an ambient seawater origin for U in the form of a weak spatial relationship on the EBK map and a lack of any spatial relationship with surface productivity or distance from the coast and STF. However, there is a possibility that U is not responding to these environmental relationships due to its conservative nature and/or biological process overriding any such relationship. This is supported by moderate variability within (and between) specimens and a total skeletal variation (46% T4 RSD) much greater than the natural variability of U in seawater (~5% see Chen et al. (1986) (Table 5.4b)). This ultimately makes it difficult to deduce *any* water column source for U in black corals and may confound its utility in palaeoenvironmental reconstructions.

Elemental biplots for U vs V produce a strong correlation (r-square – 0.98), supported by a similarly strong correlation found by Komugabe (2015a). This correlation appears to be driven by just one parameter because this relationship holds within single specimens, between multiple specimens, and across multiple ocean basins. Although not shown, this relationship also exists *within* a single coral (as seen in laser-ablation data presented by Komugabe and collected by another student attached to this project).

We speculate that this correlation may be driven by a changing concentration within the coral skeleton of a single organic phase (or functional group) with a high binding affinity for both U and V. This implies that the two elements show identical behaviour with respect to the source, uptake, and utilisation of the elements by black corals. Therefore, like vanadium, the large skeleton-tissue enrichment factor (KTiss > 1) may

provide evidence in support of the preferential concentration of U in the skeletons of black corals. Additionally, a large POM enrichment factor (KPOM 10^6) may provide tentative evidence in support of an ambient seawater origin; however, more data is required to deduce any seawater source with confidence.

5.6.4 Bromine

Bromine shows the highest concentrations of any analysed element in black coral skeletons, comprising up to 1wt% of the black coral skeleton on average. Bromine is also known to be selectively accumulated by black corals, with Br forming a structural role in the skeletal organics (see Nowak et al. (2009) and Komugabe (2015a)). Coral Br concentrations are therefore likely to be under heavy metabolic control and may offer little utility in any environmental reconstruction. This is supported by strong evidence suggesting intrinsic (biological), processes significantly impact skeletal Br concentrations as indicated by a total skeletal variability (57% T4 RSD) greater than seawater (0.1% see Eggenkamp (2014)) (Table 5.4b), strong evidence for a taxonomic relationship and moderate specimen to specimen (33% T3 RSD) variability. This is also supported by a large skeleton-tissue enrichment factor (KTiss >> 1) and a lack of any spatial relationship (aside from an insignificant negative relationship with STF proximity).

5.6.5 Iodine

Iodine is a known structural component in the glue regions between skeletal layers in black corals where it has been observed to concentrate at a weight-per cent level (Komugabe, 2015a; Nowak et al., 2009). Iodine from these glue regions likely serves little utility in environmental reconstructions due to metabolic control. However, the role of iodine in the skeletal layers (which were exclusively sampled in this study) is less well known and thus, it may yet offer some utility in environmental reconstructions.

The weak negative gradient with surface productivity combined with a lack of any relationship between iodine concentrations and depth provide tentative evidence suggestive of a surface water origin. This is potentially contradicted by a lack of any relationship with STF and coastal proximity, which may be interpreted as evidence *against* a surface seawater origin for biologically active elements. However, it is possible that skeletal I concentrations are insensitive to any oceanographic or coastal-distance gradient, or there simply are no gradients in I concentrations.

The skeleton-tissue enrichment factor (KTissue >1) provides evidence in support of either the active exclusion of iodine from coral tissue or an enhanced binding affinity for iodine in the skeleton relative to the living tissue. Both implications may provide evidence in support of an ambient seawater origin for iodine.

The evidence in support of a water column origin for iodine in black corals is therefore conflicting. The similarity in variability between coral samples and within natural seawater suggests iodine may offer some utility in environmental reconstructions (possibly as a palaeo-nutrient tracer). However, it is also possible that this is coincidental. More data is required to confidently deduce any seawater origin or biological utilisation of this element in the skeletal layers of the black corals.

5.7 Summary

In summary, there is insufficient evidence supporting any seawater origin or uptake pathway for most of the elements analysed in the black coral skeletons. In almost all cases, any relationship with an environmental variable that might provide us with an insight to the seawater origin for a TE is obscured by a large intrinsic variability within and between coral colonies. Despite this, tentative evidence remains supporting an ambient seawater origin for Mo, Cu, U and Br, and a surface seawater origin for Fe and possibly I.

Unfortunately, Fe, Br, Zn and Cu likely serve no utility in palaeoenvironmental reconstructions due to evidence suggesting their uptake is under metabolic control. All other elements (I, U, V, Mo, Ni, and Cd) require additional data and further research to deduce any seawater origin or uptake pathway with confidence.

Chapter 6 - Conclusion

6.1 Project Summary

The main objective for this research was to study the distribution of trace elements in black corals from around New Zealand to determine whether corals are systematically incorporating elements in proportion to their distribution in the surface ocean. Addressing this required us to address the following secondary questions:

- Where do black corals source their trace elements from, i.e. ambient or surface seawater?
- How do black corals uptake trace metals, i.e. are the uptake pathways passive (abiotic)? Or active (under metabolic control)?

Before we could address these questions, however, it was necessary to develop an analytical protocol for the precise determination of trace metals in the organic skeletons of black corals. This method is presented in Chapter 3 and summarized in Section 6.2.1. Additional tests interested in TE variability within and between corals colonies were also carried out to deduce any underlying endogenous/intrinsic (vital or biological) effects that might influence TE concentrations.

Having successfully developed an analytical method and measured TE concentrations in a suite of black corals, we addressed the research questions by testing for relationships between coral TE concentrations and several environmental variables (see Section 4.2). This included generating elemental maps which were also tested for any significant spatial relationships that might be broadly correlated with other environmental variables such as regional oceanography and changes in salinity. Additional clues to uptake pathways were obtained by analysis of the enrichment, relative to skeleton, of TEs in black coral tissues (this project) and particulate organic material (from Komugabe (2015a)). Environmental correlations were compared to colony-to-colony variability to evaluate any underlying endogenous/intrinsic (vital or biological) effects that might influence TE concentrations.

6.2 Key Outcomes

The key outcomes of this project are presented below:

6.2.1 Chapter 3 – Key Outcomes: Methodology

- The successful development of an analytical protocol for measuring trace elements in the skeletons and living tissues of three genera of black corals (*Antipathella, Antipathes* and *Leiopathes*) using solution ICP-MS. This has allowed for:
    - The accurate (± 8.5% average RSD) quantification of Li, Cd, B, P, Ti, Cr, Mn, Fe, Ni, Cu, Zn, U, Si and As in black coral skeletons using a matrix-matched black coral standard calibrated by Standard Additions.
    - The semi-quantitative (± 13% average RSD) measurement of Y, Mo, Pd, Sb, Ba, La, Ce, Pr, Nd, W, Pb, Al, Co, Sr, Mg, S, Ca, V, Ge, and Br in black coral skeletons using a river water standard.
    - Measurement of *relative* levels of I, Hg and Se (±15% average RSD).

  Additional methodology notes and findings

  - All TE measurements are highly reproducible, producing an average RSDs of ~15%, ranging from >1-36%.
  - Most TE measurements are well above the limits of detection except for Li, Pd, La, Nd and Al.
  - Calibration error for elements calibrated to the non-matrix matched SLRS-5 standard is estimated to be 30-40%.
  - It is noted that the contamination of the procedural blanks poses a considerable uncertainty source for elements Li, Pd, Pb, Al, Si, Ti, Ba, La, Ce, Pr, Nd, Cr, Co, and Hg. The presumed source for this contamination was from gold weighing-boats that went through the digestion protocol. Fortunately, the ten elements of most interest were largely unaffected by this contamination, and we suggest that contamination may be avoided in future studies by using purer-gold or alternative weighing strategies.

6.2.2 Chapter 4 – Key Outcomes: Results

- Black corals concentrate trace elements in their skeletons in large proportions (at up to 10^8 times their concentrations in seawater).

  - This may suggest that the corals are incapable of recording subtle changes to seawater chemistry.
  - This is consistent with similarly large concentrations reported in Hitt, unpup (2020), Komugabe (2015a), Raimundo et al. (2013) and Williams and Grottoli (2011).
  - Order of elements from highest to lowest measured avg. concentrations: Br>Zn>Cd>Mo>V>U>Fe>Cu>Ni>I
  - It is noted that trace elements Zn, Cd, Mo, V, Cu and Ni can be bio-magnified in some aquatic food-chains, specifically in organisms at lower tropic levels (Ikemoto et al., 2008; Szynkowska et al., 2018). This process may partially explain some of the large, measured concentrations for these elements in the black coral skeleton.
- The discovery of a naturally high amount of (intrinsic) variability in trace element content both within (intra-colony) and between (inter-colony) coral colonies (avg. intra-colony RSD 28%, avg. inter-colony RSD 35%). Up to 47% of all variation in TE content can be attributed to intrinsic effects.
  - The intra-colony variabilities are consistent with those reported in Hitt, unpup (2020), Komugabe (2015a) and Williams and Grottoli (2011).
- The discovery of a statistically significant taxonomic relationship between coral genera and concentrations of some TE's, including Cd, Zn, Ni, Cu, V, I, Mo and Br.
  - This relationship does not hold to a species level within the *Leiopathes* sample pool.
  - This is in agreement with suggestions from Williams and Grottoli (2011).
  - Coral taxonomy can explain up to 80% of the variability in the TE content between all coral samples.
- The HLR results indicate the combined effects of coral genus, coastal proximity, depth and chl-a describe a statistically insignificant amount of variation in each TE except for I and Mo. This implies factors additional to coastal proximity, depth, chl-a and coral genus are affecting coral TE concentrations. Up to 21% and 41% of variation in I and Mo may be explained by a combination of coastal proximity, chl-a, depth and genus in the HLR analyses, respectively.

6.2.3 Chapter 5 - Key Outcomes: Discussion

- Attempts to find relationships between TEs and possible environmental drivers were largely inconclusive due to high levels of intrinsic variability.
- The identification of tentative water column origins for Cu, Mo & Br (ambient seawater) and Fe (surface seawater), implying black corals can uptake TEs from both ambient seawater (their growth medium) and POM (their food source).
- The tentative identification of:
    - An active uptake pathway for Cu, Zn and Fe into the coral tissue
    - Confirmation of an active uptake pathway for Br directly into the coral skeleton
    - A passive uptake pathway for U, V, Mo, and I.
    - A passive uptake pathway for Cd and Ni with weak evidence suggesting the skeleton is some form of 'metabolic dump' for these elements.

6.3 Overall Conclusions

The results from the presented research are inconclusive, with only tentative evidence found in support of any seawater origin and uptake pathway for TEs in the black coral skeletons. In almost all cases for all TE's, the variability arising from intrinsic effects is similar to or greater than the variability attributable to any of the environmental variables. This makes it impossible to *accurately* discern any relationship with an environmental variable that might provide us with an insight into the origin and/or mechanism of uptake for a TE. Despite this, tentative evidence supporting a passive uptake pathway and ambient seawater origin for Mo and U suggests these elements may yet show promise as palaeo-redox tracers in black corals. Conversely, tentative evidence supporting active uptake pathways for Br, Cu, Zn and Fe suggests these elements are unlikely to offer any utility in palaeo-reconstructions as they may be under metabolic control. However, it is important to note that there is still insufficient evidence to rule these elements out in palaeo-reconstructive applications. All other elements require additional data before we can rule out the potential for their use.

While matters are left open regarding the utility of TEs as palaeo-proxies, we have successfully developed a (micro) analytical protocol for the matrix-matched analysis of

TEs in black coral skeletons. Future researchers may use this protocol to further the study into TEs in black coral skeletons.

6.4 Future Directions & Recommendations

Because black coral skeletons are composed of organic material, the uptake of trace metals into the skeleton may not be determined solely by physiochemical interactions with seawater. Instead, the incorporation mechanism(s) for TEs is/are likely controlled by either dietary requirements or physiochemical interactions with seawater, or both.

Although the presented research endeavoured to deduce such incorporation mechanisms, any relationship with an environmental variable that might provide us with an insight into the surface (food/dietary), or ambient (or both) seawater origin was often complicated/obscured by the large intrinsic variability both between and within corals. Therefore, this intrinsic variability needs to be controlled to confidently deduce any environmental relationships or water column origin for TEs in the coral and ultimately for the TE's concentrated in the skeletons to serve any utility in palaeoenvironmental reconstructions.

This variability in TE concentrations between coral colonies could be better understood with a larger specimen sample pool focused over a single region with known TE concentrations in both ambient seawater and POM. Here, ideally only corals of a similar age, size and genus would be analysed, ideally ensuring the sampled skeletal layers are concurrent with each other. This may allow us to constrain the processes driving the variation in TE content between coral colonies from a similar location and provide a more detailed insight into the origin of TE's in the black coral skeleton.

It is also important to note that the trace elements, especially when derived from an organic biological medium, are convoluted proxy sources to begin with. This is because their utility in environmental reconstructions (specifically for black corals) depends on the following codependent assumptions:

1. That trace metals in the tissues of phytoplankton are proportional to the concentration in the surface waters.

and

2. That the TE content of POM is proportional to the concentrations in phytoplankton tissues.

and

3. That the trace element composition of the coral skeleton is proportional to the trace element composition of the corals' food.

and

4. That the coral's dominant food source is POM.

Thus, there are multiple steps during a single elements journey from seawater to the coral skeleton where these assumptions could break down, confounding any trace elements utility as a palaeoenvironmental proxy. It is because of this, the only way trace elements in black coral skeletons may offer any *real* unequivocal utility in environmental reconstruction is if we have precise data pertaining to the biogeochemical cycles of trace elements in seawater and observational data (i.e. in situ or cultured laboratory studies) on the mechanisms of incorporation (and biological utility) for various TEs into the black coral skeleton.

While such data may not be easy to obtain, the global biogeochemist community is currently growing with the advent of the GEOTRACES programme and associated high precision ship-side microanalytical techniques. As such, it is only a matter of time before data pertaining to the biogeochemical cycles of trace elements around New Zealand (and many other less-covered regions of the world's oceans) are gathered and released. This data would be immensely useful in constraining the behaviour of TE's in seawater, and therefore the relationships between coral TE content and the environmental variables.

Moreover, the deep-sea coral research community is also growing, so it is plausible for cultured laboratory studies looking into skeletogenesis and associated TE uptake to be carried out by researchers in the future. A culture-based study would be ideal in furthering our understanding of the skeletogenesis, biomineralisation, TE utilisation and TE uptake pathways of black corals. Here, multiple corals could be grown in a controlled environment where responses to a changing growth medium could be monitored, providing an insight into the dietary requirements and interactions of the black coral skeleton with ambient seawater (the growth medium). A major challenge with this, however, would be the extremely slow skeletal growth rates (um/yr) of black coral

skeletons, meaning any laboratory-based culture study would require years of preparation and observation. Such large timescales could prove impractical.

Chapter 7 - References

Achterberg, E.P. and Van Den Berg, C.M. (1997) Chemical speciation of chromium and nickel in the western Mediterranean. Deep Sea Research Part II: Topical Studies in Oceanography 44, 693-720.

Adkins, J.F., Boyle, E.A., Curry, W. and Lutringer, A. (2003) Stable isotopes in deep-sea corals and a new mechanism for “vital effects”. Geochimica et Cosmochimica Acta 67, 1129-1143.

Andersen, M.B., Stirling, C.H., Zimmermann, B. and Halliday, A.N. (2010) Precise determination of the open ocean 234 U/ 238 U composition. Geochemistry, Geophysics, Geosystems 11, n/a-n/a.

Anderson, O., Tracey, D., Bostock, H., Williams, M. and Clark, M. (2014) Refined habitat suitability modelling for protected coral species in the New Zealand EEZ. NIWA Client Report prepared for Department of Conservation. WLG2014-69.

Annett, A.L., Lapi, S., Ruth, T.J. and Maldonado, M.T. (2008) The effects of Cu and Fe availability on the growth and Cu:C ratios of marine diatoms. Limnology and Oceanography 53, 2451-2461.

Arrigo, K.R., Robinson, D.H., Worthen, D.L., Dunbar, R.B., DiTullio, G.R., VanWoert, M. and Lizotte, M.P. (1999) Phytoplankton Community Structure and the Drawdown of Nutrients and CO₂ in the Southern Ocean. Science 283, 365-367.

Auscavitch, S.R., Deere, M.C., Keller, A.G., Rotjan, R.D., Shank, T.M. and Cordes, E.E. (2020) Oceanographic drivers of deep-sea coral species distribution and community assembly on seamounts, islands, atolls, and reefs within the Phoenix Islands Protected Area. Frontiers in Marine Science 7, 42.

Baars, O., Abouchami, W., Galer, S.J.G., Boye, M. and Croot, P.L. (2014) Dissolved cadmium in the Southern Ocean: Distribution, speciation, and relation to phosphate. Limnology and Oceanography 59, 385-399.

Barceloux, D.G. and Barceloux, D. (1999) Vanadium. Journal of Toxicology: Clinical Toxicology 37, 265-278.

Barnola, J.-M., Raynaud, D., Korotkevich, Y.S. and Lorius, C. (1987) Vostok ice core provides 160,000-year record of atmospheric CO2. Nature 329, 408-414.

Becker, J.-M., Ringle, C.M., Sarstedt, M. and Völckner, F. (2015) How collinearity affects mixture regression results. Marketing Letters 26, 643-659.

Behrenfeld, M.J., Randerson, J.T., McClain, C.R., Feldman, G.C., Los, S.O., Tucker, C.J., Falkowski, P.G., Field, C.B., Frouin, R. and Esaias, W.E. (2001) Biospheric primary production during an ENSO transition. Science 291, 2594-2597.

Belkin, I.M. and Gordon, A.L. (1996) Southern Ocean fronts from the Greenwich meridian to Tasmania. Journal of Geophysical Research: Oceans 101, 3675-3696.

Bennett, W.W. and Canfield, D.E. (2020) Redox-sensitive trace metals as paleoredox proxies: A review and analysis of data from modern sediments. Earth-Science Reviews 204, 103175.

Bermin, J., Vance, D., Archer, C. and Statham, P.J. (2006) The determination of the isotopic composition of Cu and Zn in seawater. Chemical Geology 226, 280-297.

Bertucci, A., Moya, A., Tambutté, S., Allemand, D., Supuran, C.T. and Zoccola, D. (2013) Carbonic anhydrases in anthozoan corals—A review. Bioorganic & medicinal chemistry 21, 1437-1450.

Biscéré, T., Ferrier-Pagès, C., Grover, R., Gilbert, A., Rottier, C., Wright, A., Payri, C. and Houlbrèque, F. (2018) Enhancement of coral calcification via the interplay of nickel and urease. Aquatic Toxicology 200, 247-256.

Biscéré, T., Lorrain, A., Rodolfo-Metalpa, R., Gilbert, A., Wright, A., Devissi, C., Peignon, C., Farman, R., Duvieilbourg, E., Payri, C. and Houlbrèque, F. (2017) Nickel and ocean warming affect scleractinian coral growth. Marine Pollution Bulletin 120, 250-258.

Blanchard, J.L., Jennings, S., Holmes, R., Harle, J., Merino, G., Allen, J.I., Holt, J., Dulvy, N.K. and Barange, M. (2012) Potential consequences of climate change for primary production and fish production in large marine ecosystems. Philosophical Transactions of the Royal Society B: Biological Sciences 367, 2979-2989.

Blewett, T.A. and Leonard, E.M. (2017) Mechanisms of nickel toxicity to fish and invertebrates in marine and estuarine waters. Environmental Pollution 223, 311-322.

Bostock, H.C., Hayward, B.W., Neil, H.L., Sabaa, A.T. and Scott, G.H. (2015) Changes in the position of the Subtropical Front south of New Zealand since the last glacial period. Paleoceanography 30, 824-844.

Bostock, H.C., Sutton, P.J., Williams, M.J. and Opdyke, B.N. (2013) Reviewing the circulation and mixing of Antarctic Intermediate Water in the South Pacific using

evidence from geochemical tracers and Argo float trajectories. Deep Sea Research Part I: Oceanographic Research Papers 73, 84-98.

Bostock, H.F.-R., Grace (2019) Chapter 5. Geological and Oceanographic Setting, in: Tracey, D.H., Freya (Ed.), The state of knowledge of deep-sea corals in the New Zealand region. NIWA, New Zealand, pp. 29-36.

Bowie, A.R., Lannuzel, D., Remenyi, T.A., Wagener, T., Lam, P.J., Boyd, P.W., Guieu, C., Townsend, A.T. and Trull, T.W. (2009) Biogeochemical iron budgets of the Southern Ocean south of Australia: Decoupling of iron and nutrient cycles in the subantarctic zone by the summertime supply. Global Biogeochemical Cycles 23.

Boyd, P., LaRoche, J., Gall, M., Frew, R. and McKay, R.M.L. (1999) Role of iron, light, and silicate in controlling algal biomass in subantarctic waters SE of New Zealand. Journal of Geophysical Research: Oceans 104, 13395-13408.

Boyd, P.W. (2015) Toward quantifying the response of the oceans' biological pump to climate change. Frontiers in Marine Science 2, 77.

Boyd, P.W. and Ellwood, M.J. (2010) The biogeochemical cycle of iron in the ocean. Nature Geoscience 3, 675-682.

Boyle, E.A. (1992) Cadmium and delta13C Paleochemical Ocean Distributions During the Stage 2 Glacial Maximum. Annual Review of Earth and Planetary Sciences 20, 245-287.

Boyle, E.A., Sclater, F. and Edmond, J.M. (1976) On the marine geochemistry of cadmium. Nature 263, 42.

Bruland, K.W. (1989) Complexation of zinc by natural organic ligands in the central North Pacific. Limnology and Oceanography 34, 269-285.

Bruland, K.W. (1992) Complexation of cadmium by natural organic ligands in the central North Pacific. Limnology and Oceanography 37, 1008-1017.

Bruland, K.W., Donat, J.R. and Hutchins, D.A. (1991) Interactive Influences of Bioactive Trace Metals on Biological Production in Oceanic Waters. Limnology and Oceanography 36, 1555-1577.

Bruland, K.W., Middag, R. and Lohan, M.C. (2013) Controls of Trace Metals in Seawater. Elsevier Inc.

Bruland, K.W., Middag, R. and Lohan, M.C. (2014) 8.2 - Controls of Trace Metals in Seawater, in: Holland, H.D., Turekian, K.K. (Eds.), Treatise on Geochemistry (Second Edition). Elsevier, Oxford, pp. 19-51.

Brüske, A., Weyer, S., Zhao, M.-Y., Planavsky, N., Wegwerth, A., Neubert, N., Dellwig, O., Lau, K. and Lyons, T. (2020) Correlated molybdenum and uranium isotope signatures in modern anoxic sediments: implications for their use as paleo-redox proxy. Geochimica et Cosmochimica Acta 270, 449-474.

Butler, A. (1998) Acquisition and utilization of transition metal ions by marine organisms. Science 281, 207-209.

Butler, A. and Carter-franklin, J.N. (2004) The role of vanadium bromoperoxidase in the biosynthesis of halogenated marine natural products. Natural Product Reports 21, 180-188.

Cairns, S.D. (2007) Deep-water corals: an overview with special reference to diversity and distribution of deep-water scleractinian corals. Bulletin of marine Science 81, 311-322.

Carlier, A., Le Guilloux, E., Olu, K., Sarrazin, J., Mastrototaro, F., Taviani, M. and Clavier, J. (2009) Trophic relationships in a deep Mediterranean cold-water coral bank (Santa Maria di Leuca, Ionian Sea). Marine Ecology Progress Series 397, 125-137.

Cempel, M. and Nikel, G. (2006) Nickel: A Review of Its Sources and Environmental Toxicology. Polish Journal of Environmental Studies 15, 375-382.

Ceriani, S.A., Roth, J.D., Sasso, C.R., McClellan, C.M., James, M.C., Haas, H.L., Smolowitz, R.J., Evans, D.R., Addison, D.S. and Bagley, D.A. (2014) Modeling and mapping isotopic patterns in the Northwest Atlantic derived from loggerhead sea turtles. Ecosphere 5, 1-24.

Chen, J., Edwards, R.L. and Wasserburg, G.J. (1986) 238U, 234U and232Th in seawater. Earth and Planetary Science Letters 80, 241-251.

Chiswell, S.M., Bostock, H.C., Sutton, P.J.H. and Williams, M.J.M. (2015) Physical oceanography of the deep seas around New Zealand: a review. New Zealand Journal of Marine and Freshwater Research 49, 286-317.

Chiswell, S.M. and Sutton, P.J. (2020) Relationships between long-term ocean warming, marine heat waves and primary production in the New Zealand region. New Zealand Journal of Marine and Freshwater Research, 1-22.

Coleman, J.E. (1998) Zinc enzymes. Current Opinion in Chemical Biology 2, 222-234.

Collier, R.W. (1985) Molybdenum in the Northeast Pacific Ocean 1. Limnology and Oceanography 30, 1351-1354.

Corrège, T. (2006) Sea surface temperature and salinity reconstruction from coral geochemical tracers. Palaeogeography, Palaeoclimatology, Palaeoecology 232, 408-428.
Cui, X., Bianchi, T.S., Savage, C. and Smith, R.W. (2016) Organic carbon burial in fjords: Terrestrial versus marine inputs. Earth and Planetary Science Letters 451, 41-50.
Cullen, J.T. (2001) The biogeochemistry of cadmium and iron in the ocean: Uptake by marine phytoplankton. Rutgers The State University of New Jersey - New Brunswick, Ann Arbor, p. 151.
de Baar, H.J.W., de Jong, J.T.M., Bakker, D.C.E., Löscher, B.M., Veth, C., Bathmann, U. and Smetacek, V. (1995) Importance of iron for plankton blooms and carbon dioxide drawdown in the Southern Ocean. Nature 373, 412-415.
De La Rocha, C. and Passow, U. (2014a) 8.4–The Biological Pump. Treatise on Geochemistry (2nd edn.), edited by: Turekian, HDHK, Elsevier, Oxford.
de la Rocha, C. and Passow, U. (2014b) The biological pump. Elsevier Science.
Deb, S. and Fukushima, T. (1999) Metals in aquatic ecosystems: mechanisms of uptake, accumulation and release-Ecotoxicological perspectives. International Journal of Environmental Studies 56, 385-417.
DeForest, D.K. and Schlekat, C.E. (2013) Species sensitivity distribution evaluation for chronic nickel toxicity to marine organisms. Integrated environmental assessment and management 9, 580-589.
Dellwig, O., Beck, M., Lemke, A., Lunau, M., Kolditz, K., Schnetger, B. and Brumsack, H.-J. (2007) Non-conservative behaviour of molybdenum in coastal waters: Coupling geochemical, biological, and sedimentological processes. Geochimica et Cosmochimica Acta 71, 2745-2761.
Dembitsky, V. (2002) Bromo- and Iodo-Containing Alkaloids from Marine Microorganisms and Sponges. Russian Journal of Bioorganic Chemistry 28, 170-182.
DeVries, T., Primeau, F. and Deutsch, C. (2012) The sequestration efficiency of the biological pump. Geophysical Research Letters 39.
Donat, J.R., Lao, K.A. and Bruland, K.W. (1994) Speciation of dissolved copper and nickel in South San Francisco Bay: a multi-method approach. Analytica Chimica Acta 284, 547-571.
Dupont, C.L., Barbeau, K. and Palenik, B. (2008) Ni Uptake and Limitation in Marine Synechococcus Strains. Applied and Environmental Microbiology 74, 23-31.

Eggenkamp, H. (2014) The Geochemistry of Stable Chlorine and Bromine Isotopes, 1st ed. 2014. ed. Springer Berlin Heidelberg, Berlin, Heidelberg.

Ehrlich, H. (2019) Marine Biological Materials of Invertebrate Origin, 1st ed. 2019. ed. Springer International Publishing, Cham.

Elderfield, H. and Truesdale, V.W. (1980) On the biophilic nature of iodine in seawater. Earth and Planetary Science Letters 50, 105-114.

Emerson, S.R. and Huested, S.S. (1991) Ocean anoxia and the concentrations of molybdenum and vanadium in seawater. Marine Chemistry 34, 177-196.

Engel, D.W. and Fowler, B.A. (1979) Factors influencing cadmium accumulation and its toxicity to marine organisms. Environmental health perspectives 28, 81-88.

England, M.H. (1992) On the formation of Antarctic Intermediate and Bottom Water in Ocean general circulation models. Journal of Physical Oceanography 22, 918-926.

Environment, M.f.t. (2019) Climate change is affecting marine ecosystems, taonga species, and us. 1.

Esslemont, G., Harriott, V. and McConchie, D. (2000) Variability of trace-metal concentrations within and between colonies of Pocillopora damicornis. Marine Pollution Bulletin 40, 637-642.

Falkowski, P.G. and Raven, J.A. (2013) Aquatic photosynthesis. Princeton University Press.

Falkowski, P.G. and Woodhead, A.D. (2013) Primary productivity and biogeochemical cycles in the sea. Springer Science & Business Media.

Fallon, S.J., McCulloch, M.T., van Woesik, R. and Sinclair, D.J. (1999) Corals at their latitudinal limits: laser ablation trace element systematics in Porites from Shirigai Bay, Japan. Earth and Planetary Science Letters 172, 221-238.

Field, A., Miles, J. and Field, Z. (2012) Discovering Statistics Using R SAGE Publications Ltd.

Friedland, K.D., Stock, C., Drinkwater, K.F., Link, J.S., Leaf, R.T., Shank, B.V., Rose, J.M., Pilskaln, C.H. and Fogarty, M.J. (2012) Pathways between Primary Production and Fisheries Yields of Large Marine Ecosystems. PLOS ONE 7, e28945.

Fuge, R. and Johnson, C.C. (1986) The geochemistry of iodine—a review. Environmental geochemistry and health 8, 31-54.

German, C., Campbell, A. and Edmond, J. (1991) Hydrothermal scavenging at the Mid-Atlantic Ridge: modification of trace element dissolved fluxes. Earth and Planetary Science Letters 107, 101-114.

Glass, J. and Dupont, C. (2017) Oceanic nickel biogeochemistry and the evolution of nickel use, The Biological Chemistry of Nickel. Royal Society of Chemistry Cambridge, UK, pp. 12-26.

Gledhill, M. and Buck, K.N. (2012) The organic complexation of iron in the marine environment: a review. Frontiers in microbiology 3, 69.

Goldberg, W. (1976) Comparative study of the chemistry and structure of gorgonian and antipatharian coral skeletons. Marine Biology 35, 253-267.

Goldberg, W.M., Hopkins, T.L., Holl, S.M., Schaefer, J., Kramer, K.J., Morgan, T.D. and Kim, K. (1994) Chemical composition of the sclerotized black coral skeleton (Coelenterata: Antipatharia): a comparison of two species. Comparative Biochemistry and Physiology Part B: Comparative Biochemistry 107, 633-643.

Goldberg, W.M. and Taylor, G.T. (1989) Cellular structure and ultrastructure of the black coral Antipathes aperta: 1. Organization of the tentacular epidermis and nervous system. Journal of morphology 202, 239-253.

Gothmann, A.M., Higgins, J.A., Adkins, J.F., Broecker, W., Farley, K.A., McKeon, R., Stolarski, J., Planavsky, N., Wang, X. and Bender, M.L. (2019) A Cenozoic record of seawater uranium in fossil corals. Geochimica et Cosmochimica Acta 250, 173-190.

Grange, K.R. (1990) Antipathes fiordensis, a new species of black coral (Coelenterata: Antipatharia) from New Zealand. New Zealand Journal of Zoology 17, 279-282.

Gribov, A. and Krivoruchko, K. (2020) Empirical Bayesian kriging implementation and usage. Science of the Total Environment 722, 137290.

Grinbaum, B. and Freiberg, M. (2000) Bromine. Kirk-Othmer Encyclopedia of Chemical Technology, 1-28.

Gruber, N., Gloor, M., Mikaloff Fletcher, S.E., Doney, S.C., Dutkiewicz, S., Follows, M.J., Gerber, M., Jacobson, A.R., Joos, F. and Lindsay, K. (2009) Oceanic sources, sinks, and transport of atmospheric CO2. Global biogeochemical cycles 23.

Guilderson, T.P., McCarthy, M.D., Dunbar, R.B., Englebrecht, A. and Roark, E.B. (2013) Late Holocene variations in Pacific surface circulation and biogeochemistry inferred from proteinaceous deep-sea corals. Biogeosciences 10, 6019-6028.

Hair, J.F., Black, W.C., Babin, B.J., Anderson, R. and Tatham, R. (2014) Multivariate data analysis (new international edition). Harlow: Pearson Education.

Hamilton, L. (2006) Structure of the subtropical front in the Tasman Sea. Deep Sea Research Part I: Oceanographic Research Papers 53, 1989-2009.

Hanawa, K. and Talley, L.D. (2001) Mode waters. International Geophysics Series 77, 373-386.

Harriott, V. (1999) Coral growth in subtropical eastern Australia. Coral Reefs 18, 281-291.

Hartin, C.A., Fine, R.A., Kamenkovich, I. and Sloyan, B.M. (2014) Comparison of Subantarctic Mode Water and Antarctic Intermediate Water formation rates in the South Pacific between NCAR-CCSM4 and observations. Geophysical Research Letters 41, 519-526.

Heath, R.A. (1985) A review of the physical oceanography of the seas around New Zealand — 1982. New Zealand Journal of Marine and Freshwater Research 19, 79-124.

Heezen, B.C., Ewing, M. and Menzies, R.J. (1955) The influence of submarine turbidity currents on abyssal productivity. Oikos 6, 170-182.

Herraiz-Borreguero, L. and Rintoul, S.R. (2011) Regional circulation and its impact on upper ocean variability south of Tasmania. Deep Sea Research Part II: Topical Studies in Oceanography 58, 2071-2081.

Hill, K., Rintoul, S., Ridgway, K. and Oke, P. (2011) Decadal changes in the South Pacific western boundary current system revealed in observations and ocean state estimates. Journal of Geophysical Research: Oceans 116.

Hitt, N.T., Sinclair, D.J., Fallon, S.J., Neil, H.L., Tracey, D.M., Komugabe-Dixson, A. and Marriott, P. (2020) Growth and longevity of New Zealand black corals. Deep Sea Research Part I: Oceanographic Research Papers 162, 103298.

Ho, P., Lee, J.-M., Heller, M.I., Lam, P.J. and Shiller, A.M. (2018) The distribution of dissolved and particulate Mo and V along the US GEOTRACES East Pacific Zonal Transect (GP16): The roles of oxides and biogenic particles in their distributions in the oxygen deficient zone and the hydrothermal plume. Marine Chemistry 201, 242-255.

Holm, S. (1979) A simple sequentially rejective multiple test procedure. Scandinavian journal of statistics, 65-70.

Horner, T.J., Lee, R.B.Y., Henderson, G.M. and Rickaby, R.E.M. (2013) Nonspecific uptake and homeostasis drive the oceanic cadmium cycle. Proceedings of the National Academy of Sciences of the United States of America 110, 2500.

Howe, J.A., Austin, W.E., Forwick, M., Paetzel, M., Harland, R. and Cage, A.G. (2010) Fjord systems and archives: a review. Geological Society, London, Special Publications 344, 5-15.

Huang, J.-H., Huang, F., Evans, L. and Glasauer, S. (2015) Vanadium: Global (bio) geochemistry. Chemical Geology 417, 68-89.

Hwang, J.-S., Dahms, H.-U., Huang, K.L., Huang, M.-Y., Liu, X.-J., Khim, J.S. and Wong, C.K. (2018) Bioaccumulation of trace metals in octocorals depends on age and tissue compartmentalization. PloS one 13, e0196222.

Ikemoto, T., Tu, N.P.C., Okuda, N., Iwata, A., Omori, K., Tanabe, S., Tuyen, B.C. and Takeuchi, I. (2008) Biomagnification of trace elements in the aquatic food web in the Mekong Delta, South Vietnam using stable carbon and nitrogen isotope analysis. Archives of environmental contamination and toxicology 54, 504-515.

Johnson, K.S., Gordon, R.M. and Coale, K.H. (1997) What controls dissolved iron concentrations in the world ocean? Marine chemistry 57, 137-161.

Juárez-de la Rosa, B., Ardisson, P.-L., Azamar-Barrios, J., Quintana, P. and Alvarado-Gil, J. (2007) Optical, thermal, and structural characterization of the sclerotized skeleton of two antipatharian coral species. Materials Science and Engineering: C 27, 880-885.

Kabata-Pendias, A. and Mukherjee, A.B. (2007) Trace elements from soil to human. Springer Science & Business Media.

Keppler, F., Eiden, R., Niedan, V., Pracht, J. and Schöler, H.F. (2000) Halocarbons produced by natural oxidation processes during degradation of organic matter. Nature 403, 298.

Klinkhammer, G. and Palmer, M. (1991) Uranium in the oceans: where it goes and why. Geochimica et Cosmochimica Acta 55, 1799-1806.

Komugabe, A.F. (2015a) Mid-to late-holocene environmental changes in the Southwest Pacific : records from deep-sea Black Corals, in: Komugabe, A.F. (Ed.).

Komugabe, A.F. (2015b) Mid-to late-holocene environmental changes in the Southwest Pacific: records from deep-sea Black Corals.

Komugabe, A.F., Fallon, S.J., Thresher, R.E. and Eggins, S.M. (2014) Modern Tasman Sea surface reservoir ages from deep-sea black corals. Deep-Sea Research Part II 99, 207-212.

Krivoruchko, K. (2012) Empirical bayesian kriging. ESRI: Redlands, CA. California: USA. Available online at: http://www. esri. com/news/arcuser ….

Krivoruchko, K. and Gribov, A. (2014) Pragmatic Bayesian kriging for non-stationary and moderately non-Gaussian data, Mathematics of Planet Earth. Springer, pp. 61-64.

La Barre, S., Potin, P., Leblanc, C. and Delage, L. (2010) The halogenated metabolism of brown algae (Phaeophyta), its biological importance and its environmental significance. Marine drugs 8, 988-1010.

La Fontaine, S., Quinn, J.M., Nakamoto, S.S., Page, M.D., Gohre, V., Moseley, J.L., Kropat, J. and Merchant, S. (2002) Copper-Dependent Iron Assimilation Pathway in the Model Photosynthetic Eukaryote Chlamydomonas reinhardtii. Eukaryotic Cell 1, 736.

Lai, X., Norisuye, K., Mikata, M., Minami, T., Bowie, A.R. and Sohrin, Y. (2008) Spatial and temporal distribution of Fe, Ni, Cu and Pb along 140°E in the Southern Ocean during austral summer 2001/02. Marine Chemistry 111, 171-183.

Lane, T.W. (2000) A Biological Function for Cadmium in Marine Diatoms. Proceedings of the National Academy of Sciences of the United States of America 97, 4627-4631.

Law, C.S., Rickard, G.J., Mikaloff-Fletcher, S.E., Pinkerton, M.H., Behrens, E., Chiswell, S.M. and Currie, K. (2018) Climate change projections for the surface ocean around New Zealand. New Zealand Journal of Marine and Freshwater Research 52, 309-335.

Leri, A.C., Hakala, J.A., Marcus, M.A., Lanzirotti, A., Reddy, C.M. and Myneni, S.C.B. (2010) Natural organobromine in marine sediments: New evidence of biogeochemical Br cycling. Global Biogeochemical Cycles 24.

Lewis, J.B. (1978) Feeding mechanisms in black corals (Antipatharia). Journal of Zoology 186, 393-396.

Little, S.H., Vance, D., Siddall, M. and Gasson, E. (2013) A modeling assessment of the role of reversible scavenging in controlling oceanic dissolved Cu and Zn distributions. Global Biogeochemical Cycles 27, 780-791.

Lough, J. and Barnes, D. (2000) Environmental controls on growth of the massive coral Porites. Journal of experimental marine biology and ecology 245, 225-243.

Lovley, D.R. and Phillips, E.J. (1992) Reduction of uranium by Desulfovibrio desulfuricans. Applied and Environmental Microbiology 58, 850-856.

Lyalkova, N. and Yurkova, N. (1992) Role of microorganisms in vanadium concentration and dispersion. Geomicrobiology Journal 10, 15-26.

Magesh, N.S., Chandrasekar, N. and Elango, L. (2017) Trace element concentrations in the groundwater of the Tamiraparani river basin, South India: Insights from human health risk and multivariate statistical techniques. Chemosphere 185, 468-479.

Maldonado, M.T., Allen, A.E., Chong, J.S., Lin, K., Leus, D., Karpenko, N. and Harris, S.L. (2006) Copper-dependent iron transport in coastal and oceanic diatoms. Limnology and Oceanography 51, 1729-1743.

Mantyla, A.W. and Reid, J.L. (1983) Abyssal characteristics of the World Ocean waters. Deep Sea Research Part A. Oceanographic Research Papers 30, 805-833.

Marchitto, T.M. and Broecker, W.S. (2006) Deep water mass geometry in the glacial Atlantic Ocean: A review of constraints from the paleonutrient proxy Cd/Ca. Geochemistry, Geophysics, Geosystems 7.

Markich, S.J. (2002) Uranium speciation and bioavailability in aquatic systems: an overview. TheScientificWorldJOURNAL 2, 707-729.

Marriott, P., Tracey, D.M., Bostock, H., Hitt, N. and Fallon, S. (2020) Ageing deep-sea black coral Bathypathes patula.

Martin, J.H. and Fitzwater, S.E. (1988) Iron deficiency limits phytoplankton growth in the north-east Pacific subarctic. Nature 331, 341-343.

Martin, J.H., Fitzwater, S.E. and Gordon, R.M. (1990) Iron deficiency limits phytoplankton growth in Antarctic waters. Global Biogeochemical Cycles 4, 5-12.

McCartney, M. (1979) Subantarctic mode water. Woods Hole Oceanographic Institution Contribution 3773, 103-119.

Middag, R., de Baar, H.J.W., Laan, P. and Klunder, M.B. (2011) Fluvial and hydrothermal input of manganese into the Arctic Ocean. Geochimica et Cosmochimica Acta 75, 2393-2408.

Mikaloff Fletcher, S., Gruber, N., Jacobson, A.R., Doney, S., Dutkiewicz, S., Gerber, M., Follows, M., Joos, F., Lindsay, K. and Menemenlis, D. (2006) Inverse estimates of anthropogenic CO2 uptake, transport, and storage by the ocean. Global biogeochemical cycles 20.

Miller, M.W. and Hay, M.E. (1998) Effects of fish predation and seaweed competition on the survival and growth of corals. Oecologia 113, 231-238.

Mitchell, J.S., Mackay, K.A., Neil, H.L., Mackay, E.J., Pallentin, A. and P., N. (2012) Undersea New Zealand, 1:5,000,000, Miscellaneous Series NIWA, New Zealand.

Moffett, J.W. and Brand, L.E. (1996) Production of strong, extracellular Cu chelators by marine cyanobacteria in response to Cu stress. Limnology and Oceanography 41, 388-395.

Moffett, J.W. and Dupont, C. (2007) Cu complexation by organic ligands in the sub-arctic NW Pacific and Bering Sea. Deep-Sea Research Part I 54, 586-595.

Molodtsova, T. (2011) A new species of Leiopathes (Anthozoa: Antipatharia) from the Great Meteor seamount (North Atlantic). Zootaxa 3138, 52-64.

Moore, J.K., Doney, S.C., Glover, D.M. and Fung, I.Y. (2001) Iron cycling and nutrient-limitation patterns in surface waters of the World Ocean. Deep Sea Research Part II: Topical Studies in Oceanography 49, 463-507.

Moore, J.K., Doney, S.C. and Lindsay, K. (2004) Upper ocean ecosystem dynamics and iron cycling in a global three-dimensional model. Global Biogeochemical Cycles 18.

Moreda-Pineiro, A., Romaris-Hortas, V. and Bermejo-Barrera, P. (2011) A review on iodine speciation for environmental, biological and nutrition fields. Journal of Analytical Atomic Spectrometry 26, 2107-2152.

Morel, F.M. (2008) The co-evolution of phytoplankton and trace element cycles in the oceans. Geobiology 6, 318-324.

Morel, F.M. (2013) The oceanic cadmium cycle: Biological mistake or utilization? Proceedings of the National Academy of Sciences 110, E1877-E1877.

Morel, F.M., Hudson, R.J. and Price, N.M. (1991) Limitation of productivity by trace metals in the sea. Limnology and Oceanography 36, 1742-1755.

Morel, F.M.M. and Price, N.M. (2003) The Biogeochemical Cycles of Trace Metals in the Oceans. Science 300, 944-947.

Morel, F.M.M., Reinfelder, J.R., Roberts, S.B., Chamberlain, C.P., Lee, J.G. and Yee, D. (1994) Zinc and carbon co-limitation of marine phytoplankton. Nature 369, 740.

Morford, J.L. and Emerson, S. (1999) The geochemistry of redox sensitive trace metals in sediments. Geochimica et Cosmochimica Acta 63, 1735-1750.

Morris, M., Stanton, B. and Neil, H. (2001) Subantarctic oceanography around New Zealand: preliminary results from an ongoing survey. New Zealand Journal of Marine and Freshwater Research 35, 499-519.

Mountjoy, J.J., Howarth, J.D., Orpin, A.R., Barnes, P.M., Bowden, D.A., Rowden, A.A., Schimel, A.C., Holden, C., Horgan, H.J. and Nodder, S.D. (2018) Earthquakes drive large-scale submarine canyon development and sediment supply to deep-ocean basins. Science advances 4, eaar3748.

Murphy, R., Pinkerton, M., Richardson, K., Bradford-Grieve, J. and Boyd, P. (2001) Phytoplankton distributions around New Zealand derived from SeaWiFS remotely-sensed ocean colour data. New Zealand Journal of marine and freshwater research 35, 343-362.

Nodder, S.D. and Boyd, P.W. (2001) What grows up must fall down: the potential impact of climate change on plankton and carbon export. Water & Atmosphere 9.

Nodder, S.D., Chiswell, S.M. and Northcote, L.C. (2016) Annual cycles of deep-ocean biogeochemical export fluxes in subtropical and subantarctic waters, southwest Pacific Ocean. Journal of Geophysical Research: Oceans 121, 2405-2424.

Nowak, D., Florek, M., Nowak, J., Kwiatek, W., Lekki, J., Chevallier, P., Hacura, A., Wrzalik, R., Ben-Nissan, B., Van Grieken, R. and Kuczumow, A. (2009) Morphology and the chemical make-up of the inorganic components of black corals. Materials Science & Engineering C 29, 1029-1038.

Obata, H., Shitashima, K., Isshiki, K. and Nakayama, E. (2008) Iron, manganese and aluminum in upper waters of the western South Pacific Ocean and its adjacent seas. Journal of oceanography 64, 233-245.

Okocha, R. and Adedeji, O. (2011) Overview of cadmium toxicity in fish. Journal of Applied Sciences Research 7, 1195-1207.

Opresko, D.M., Tracey, D. and Mackay, E. (2014) Antipatharia (Black Corals) for the New Zealand Region: A field guide of commonly sampled New Zealand black corals including illustrations highlighting technical terms and black coral morphology. Ministry for Primary Industries.

Orsi, A.H., Whitworth III, T. and Nowlin Jr, W.D. (1995) On the meridional extent and fronts of the Antarctic Circumpolar Current. Deep Sea Research Part I: Oceanographic Research Papers 42, 641-673.

Passow, U. and Carlson, C.A. (2012) The biological pump in a high CO2 world. Marine Ecology Progress Series 470, 249-271.

Pauly, D. and Christensen, V. (1995) Primary production required to sustain global fisheries. Nature 374, 255-257.

Petit, J.-R., Jouzel, J., Raynaud, D., Barkov, N.I., Barnola, J.-M., Basile, I., Bender, M., Chappellaz, J., Davis, M. and Delaygue, G. (1999) Climate and atmospheric history of the past 420,000 years from the Vostok ice core, Antarctica. Nature 399, 429.

Phillips, D.J. and Rainbow, P.S. (1989a) Strategies of trace metal sequestration in aquatic organisms. Marine Environmental Research 28, 207-210.

Phillips, D.J.H. and Rainbow, P.S. (1989b) Strategies of trace metal sequestration in aquatic organisms. Marine Environmental Research 28, 207-210.

Prouty, N., Roark, E., Buster, N. and Ross, S.W. (2011) Growth rate and age distribution of deep-sea black corals in the Gulf of Mexico. Marine Ecology Progress Series 423, 101-115.

Raimundo, J., Vale, C., Caetano, M., Anes, B., Carreiro-Silva, M., Martins, I., Matos, V.d. and Porteiro, F.M. (2013) Element concentrations in cold-water gorgonians and black coral from Azores region. Deep-Sea Research Part II 98, 129-136.

Rainbow, P.S. (2002) Trace metal concentrations in aquatic invertebrates: why and so what? Environmental pollution 120, 497-507.

Redfield, A.C. (1958) THE BIOLOGICAL CONTROL OF CHEMICAL FACTORS IN THE ENVIRONMENT. American Scientist 46, 230A-221.

Reinhard, C.T., Planavsky, N.J., Gill, B.C., Ozaki, K., Robbins, L.J., Lyons, T.W., Fischer, W.W., Wang, C., Cole, D.B. and Konhauser, K.O. (2017) Evolution of the global phosphorus cycle. Nature 541, 386.

Remsen, C.C. (1971) THE DISTRIBUTION OF UREA IN COASTAL AND OCEANIC WATERS 1. Limnology and Oceanography 16, 732-740.

Richon, C. and Tagliabue, A. (2019) Insights Into the Major Processes Driving the Global Distribution of Copper in the Ocean From a Global Model. Global Biogeochemical Cycles 33, 1594-1610.

Ridgway, K. and Godfrey, J. (1997) Seasonal cycle of the East Australian current. Journal of Geophysical Research: Oceans 102, 22921-22936.

Roark, B.E., Guilderson, T.P., Dunbar, R.B., Fallon, S.J. and Mucciarone, D.A. (2009a) Extreme longevity in proteinaceous deep-sea corals. Proceedings of the National Academy of Sciences 106, 5204-5208.

Roark, B.E., Guilderson, T.P., Dunbar, R.B., Fallon, S.J., Mucciarone, D.A. and Boyle, E.A. (2009b) Extreme Longevity in Proteinaceous Deep-Sea Corals. Proceedings of the National Academy of Sciences of the United States of America 106, 5204-5208.

Roark, E.B., Guilderson, T.P., Dunbar, R., B. and Ingram, B.L. (2006) Radiocarbon-based ages and growth rates of Hawaiian deep-sea corals. Marine Ecology Progress Series 327, 1-14.

Roark, E.B., Guilderson, T.P., Flood-Page, S., Dunbar, R.B., Ingram, B.L., Fallon, S.J. and McCulloch, M. (2005) Radiocarbon-based ages and growth rates of bamboo corals from the Gulf of Alaska. Geophysical Research Letters 32, n/a-n/a.

Robinson, L.F., Adkins, J.F., Frank, N., Gagnon, A.C., Prouty, N.G., Brendan Roark, E. and de Flierdt, T.v. (2014) The geochemistry of deep-sea coral skeletons: A review of vital effects and applications for palaeoceanography. Deep Sea Research Part II: Topical Studies in Oceanography 99, 184-198.

Roemmich, D. and Cornuelle, B. (1992) The subtropical mode waters of the South Pacific Ocean. Journal of physical oceanography 22, 1178-1187.

Rosenthal, Y., Boyle, E.A. and Labeyrie, L. (1997) Last Glacial Maximum paleochemistry and deepwater circulation in the Southern Ocean: Evidence from foraminiferal cadmium. Paleoceanography 12, 787-796.

Rue, E.L. and Bruland, K.W. (1995) Complexation of iron (III) by natural organic ligands in the Central North Pacific as determined by a new competitive ligand equilibration/adsorptive cathodic stripping voltammetric method. Marine chemistry 50, 117-138.

Saha, N., Webb, G.E. and Zhao, J.-X. (2016) Coral skeletal geochemistry as a monitor of inshore water quality. Science of the Total Environment 566, 652-684.

Saito, M. and Goepfert, T. (2008) Zinc-cobalt colimitation of Phaeocystis antarctica. Limnology and Oceanography 53, 266-275.

Sander, R., Keene, W., Pszenny, A., Arimoto, R., Ayers, G., Baboukas, E., Cainey, J., Crutzen, P., Duce, R. and Hönninger, G. (2003) Inorganic bromine in the marine boundary layer: a critical review. Atmospheric Chemistry and Physics 3, 1301-1336.

Sarmiento, J.L.G., Nicholas (2013) Ocean biogeochemical dynamics. Princeton university press.

Schiff, J., Batista, F., Sherwood, O., Guilderson, T., Hill, T., Ravelo, A., McMahon, K. and McCarthy, M. (2014a) Compound specific amino acid 13C patterns in a deep-sea proteinaceous coral: implications for reconstructing detailed 13C records of exported primary production. Lawrence Livermore National Lab.(LLNL), Livermore, CA (United States).

Schiff, J.T., Batista, F.C., Sherwood, O.A., Guilderson, T.P., Hill, T.M., Ravelo, A.C., McMahon, K.W. and McCarthy, M.D. (2014b) Compound specific amino acid δ13C patterns in a deep-sea proteinaceous coral: Implications for reconstructing detailed δ13C records of exported primary production. Marine Chemistry 166, 82-91.

Schlesinger, W.H. and Bernhardt, E.S. (2013) Biogeochemistry: an analysis of global change. Academic press.

Schlitzer, R. (2018) eGEOTRACES - Electronic Atlas of GEOTRACES Sections and Animated 3D Scenes. GEOTRACES, Alfred Wegener Institute for Polar and Marine Research, Bremerhaven, Germany.

Schmiedl, G. and Mackensen, A. (1997) Late Quaternary paleoproductivity and deep water circulation in the eastern South Atlantic Ocean: Evidence from benthic foraminifera. Palaeogeography, Palaeoclimatology, Palaeoecology 130, 43-80.

Schneider, B., Schlitzer, R., Fischer, G. and Nöthig, E.M. (2003) Depth-dependent elemental compositions of particulate organic matter (POM) in the ocean. Global Biogeochemical Cycles 17.

Shen, G.T. (1986) Lead and cadmium geochemistry of corals: reconstruction of historic perturbations in the upper ocean. Massachusetts Institute of Technology.

Shen, G.T. and Sanford, C.L. (1990) Trace Element Indicators of Climate Variability in Reef-Building Corals, in: Glynn, P.W. (Ed.), Elsevier Oceanography Series. Elsevier, pp. 255-283.

Sherwood, O., A. , Heikoop, J., M. , Scott, D., B. , Risk, M., J. , Guilderson, T.P. and McKinney, R., A. (2005) Stable isotopic composition of deep-sea gorgonian corals Primnoa spp.: a new archive of surface processes. Marine Ecology Progress Series 301, 135-148.

Sherwood, O.A. and Edinger, E.N. (2009) Ages and growth rates of some deep-sea gorgonian and antipatharian corals of Newfoundland and Labrador. Canadian Journal of Fisheries and Aquatic Sciences 66, 142-152.

Sherwood, O.A., Guilderson, T.P., Batista, F.C., Schiff, J.T. and McCarthy, M.D. (2013) Increasing subtropical North Pacific Ocean nitrogen fixation since the Little Ice Age. Nature 505, 78.

Sherwood, O.A., Lehmann, M.F., Schubert, C.J., Scott, D.B., McCarthy, M.D. and Boyle, E.A. (2011) Nutrient regime shift in the western North Atlantic indicated by compound-specific δ ¹⁵ N of deep-sea gorgonian corals. Proceedings of the National Academy of Sciences of the United States of America 108, 1011-1015.

Siebert, C., Nägler, T.F., von Blanckenburg, F. and Kramers, J.D. (2003) Molybdenum isotope records as a potential new proxy for paleoceanography. Earth and Planetary Science Letters 211, 159-171.

Sinoir, M., Butler, E.C.V., Bowie, A.R., Mongin, M., Nesterenko, P.N. and Hassler, C.S. (2012) Zinc marine biogeochemistry in seawater: a review. Marine and Freshwater Research 63, 644-657.

Smetacek, V., Klaas, C., Strass, V.H., Assmy, P., Montresor, M., Cisewski, B., Savoye, N., Webb, A., d'Ovidio, F., Arrieta, J.M., Bathmann, U., Bellerby, R., Berg, G.M., Croot, P., Gonzalez, S., Henjes, J., Herndl, G.J., Hoffmann, L.J., Leach, H., Losch, M., Mills, M.M., Neill, C., Peeken, I., Röttgers, R., Sachs, O., Sauter, E., Schmidt, M.M., Schwarz, J., Terbrüggen, A. and Wolf-Gladrow, D. (2012) Deep carbon export from a Southern Ocean iron-fertilized diatom bloom. Nature 487, 313-319.

Stanton, B. (1979) The Tasman Front. New Zealand Journal of Marine and Freshwater Research 13, 201-214.

Stats, N. (2019) Primary productivity.

Sunda, W. (2012) Feedback Interactions between Trace Metal Nutrients and Phytoplankton in the Ocean. Frontiers in Microbiology 3.

Sunda, W.G. and Huntsman, S.A. (2000) Effect of Zn, Mn, and Fe on Cd Accumulation in Phytoplankton: Implications for Oceanic Cd Cycling. Limnology and Oceanography 45, 1501-1516.

Sutton, P. (2001) Detailed structure of the Subtropical Front over Chatham Rise, east of New Zealand. Journal of Geophysical Research: Oceans 106, 31045-31056.

Sutton, P.J. and Bowen, M. (2014) Flows in the Tasman front south of Norfolk island. Journal of Geophysical Research: Oceans 119, 3041-3053.

Sutton, P.J. and Roemmich, D. (2001) Ocean temperature climate off north-east New Zealand. New Zealand Journal of Marine and Freshwater Research 35, 553-565.

Szynkowska, M.I., Pawlaczyk, A. and Maćkiewicz, E. (2018) Bioaccumulation and biomagnification of trace elements in the environment. Recent Advances in Trace Elements 251.

Tagliabue, A., Bowie, A.R., Boyd, P.W., Buck, K.N., Johnson, K.S. and Saito, M.A. (2017) The integral role of iron in ocean biogeochemistry. Nature 543, 51-59.

Talley, L.D. (2003) Shallow, intermediate, and deep overturning components of the global heat budget. Journal of Physical oceanography 33, 530-560.

Talley, L.D. (2008) Freshwater transport estimates and the global overturning circulation: Shallow, deep and throughflow components. Progress in Oceanography 78, 257-303.

Tessin, A., Chappaz, A., Hendy, I. and Sheldon, N. (2019) Molybdenum speciation as a paleo-redox proxy: A case study from Late Cretaceous Western Interior Seaway black shales. Geology 47, 59-62.

Thornton, D.C.O. (2012) Primary production in the ocean. Advances in Photosynthesis–Fundamental Aspects, edited by: Najafpour, MM, InTech, Rijeka, Croatia, 563-588.

Tracey, D. and Hjorvarsdottir, F. (2019) The state of knowledge of deep-sea corals in the New Zealand region. NIWA Science and Technology Series number 84, 140.

Tracey, D., Mackay, E., Cairns, S.D., Optesko, D., Alderslade, P., Sanchez, J. and Williams, G. (2014) Coral Identification Guide.

Tsubouchi, T., Suga, T. and Hanawa, K. (2007) Three types of South Pacific Subtropical Mode Waters: Their relation to the large-scale circulation of the South Pacific subtropical gyre and their temporal variability. Journal of physical oceanography 37, 2478-2490.

Tsuchiya, M. and Talley, L.D. (1996) Water-property distributions along an eastern Pacific hydrographic section at 135W. Journal of Marine Research 54, 541-564.

Tsuchiya, M. and Talley, L.D. (1998) A Pacific hydrographic section at 88°W: Water-property distribution. Journal of Geophysical Research: Oceans 103, 12899-12918.

Tsunogai, S. (1971) Iodine in the deep water of the ocean, Deep Sea Research and Oceanographic Abstracts. Elsevier, pp. 913-919.

Tsunogai, S. and Henmi, T. (1971) Iodine in the surface water of the ocean. Journal of the Oceanographical Society of Japan 27, 67-72.

Tuit, C.B. (2003) The marine biogeochemistry of molybdenum. MASSACHUSETTS INST OF TECH CAMBRIDGE.

Twining, B.S., Baines, S.B., Vogt, S. and Nelson, D.M. (2012) Role of diatoms in nickel biogeochemistry in the ocean. Global Biogeochemical Cycles 26.

Wadley, M.R., Stevens, D.P., Jickells, T.D., Hughes, C., Chance, R., Hepach, H., Tinel, L. and Carpenter, L.J. (2020) A global model for iodine speciation in the upper ocean. Global Biogeochemical Cycles 34, e2019GB006467.

Wagner, D., Luck, D.G. and Toonen, R.J. (2012) Chapter Two - The Biology and Ecology of Black Corals (Cnidaria: Anthozoa: Hexacorallia: Antipatharia), in: Lesser, M. (Ed.), Advances in Marine Biology. Academic Press, pp. 67-132.

Wahyu, D., Hindarti, D. and Permana, R. (2020) Cadmium toxicity towards marine diatom Thalassiosira sp. and its alteration on chlorophyll-a and carotenoid content. World News of Natural Sciences 31, 48-57.

Wang, D. and Wilhelmy, S.A.S. (2009) Vanadium speciation and cycling in coastal waters. Marine Chemistry 117, 52-58.

Warner, G. (1981) Species descriptions and ecological observations of black corals (Antipatharia) from Trinidad. Bulletin of Marine Science 31, 147-163.

Whitworth III, T., Warren, B., Nowlin Jr, W., Rutz, S., Pillsbury, R. and Moore, M. (1999) On the deep western-boundary current in the Southwest Pacific Basin. Progress in Oceanography 43, 1-54.

Williams, B. (2020) Proteinaceous corals as proxy archives of paleo-environmental change. Earth-Science Reviews, 103326.

Williams, B. and Grottoli, A.G. (2011) Solution and laser ablation inductively coupled plasma–mass spectrometry measurements of Br, I, Pb, Mn, Cd, Zn, and B in the organic skeleton of soft corals and black corals. Geochemistry, Geophysics, Geosystems 12.

Williams, B., Risk, M.J., Ross, S.W. and Sulak, K.J. (2006) Deep-water antipatharians: Proxies of environmental change. Geology 34, 773-776.

Wong, G.T., Brewer, P.G. and Spencer, D.W. (1976) The distribution of particulate iodine in the Atlantic Ocean. Earth and Planetary Science Letters 32, 441-450.

Wu, J., Boyle, E., Sunda, W. and Wen, L.-S. (2001) Soluble and colloidal iron in the oligotrophic North Atlantic and North Pacific. Science 293, 847-849.

Yeghicheyan, D., Bossy, C., Bouhnik Le Coz, M., Douchet, C., Granier, G., Heimburger, A., Lacan, F., Lanzanova, A., Rousseau, T.C. and Seidel, J.L. (2013) A compilation of silicon, rare earth element and twenty-one other trace element concentrations in the natural river water reference material SLRS-5 (NRC-CNRC). Geostandards and Geoanalytical Research 37, 449-467.

Zhang, X., Sigman, D.M., Morel, F.M. and Kraepiel, A.M. (2014) Nitrogen isotope fractionation by alternative nitrogenases and past ocean anoxia. Proceedings of the National Academy of Sciences 111, 4782-4787.

Zhao, Y., Vance, D., Abouchami, W. and de Baar, H.J.W. (2014) Biogeochemical cycling of zinc and its isotopes in the Southern Ocean. Geochimica et Cosmochimica Acta 125, 653-672.

Ziegler, M., Jilbert, T., de Lange, G.J., Lourens, L.J. and Reichart, G.-J. (2008) Bromine counts from XRF scanning as an estimate of the marine organic carbon content of sediment cores. Geochemistry, Geophysics, Geosystems 9.

Chapter 8 - Appendix

NIWA Cat ID No.	Coral Genus / Species	Trip/Station No.	No. of samples taken
47881	Leiopathes secunda	trip2626/207	1
64334	Leiopathes secunda	TAN1007/9	13
35104	Leiopathes	Trip2467/5	2
72786	Leiopathes	TAN1104/110	2
16406	Keratoisis	Z9777	2
35003	Leiopathes	TAN0413/175	1
15908	Leiopathes	Z9799	9
17106	Antipathes fiordensis	station 0824	1
17102	Antipathes	station 0799	1
91479	Antipathes	TAN0905/116	1
65560	Leiopathes sp.	TRIP2807/207	1
47887	Leiopathes	TRIP2704/1	1
42810	Leiopathes acanthophora	TRIP2626/176	3
24183	Leiopathes acanthophora	Z9806	1
47880	Leiopathes acanthophora	TRIP2626/207	3
24178	Leiopathes secunda	Z9844	1
24153	Leiopathes	TAN0413/21	1
42826	Leiopathes	TRIP2650/32	1
17107	Antipatharia	O824	3
15131	Antipatharia	Z8370	2
28400	Leiopathes	Z11101	1
76702	Leiopathes	TAN1003/169	1
24209	Leiopathes	Z9801	1
34996	Leiopathes	TAN709/118	2
19901	Antipathella fiordensis	O799	1
19903	Antipathella fiordensis	S0541D	1

NIWA Cat ID No.	Coral Genus / Species	Trip/Station No.	No. of samples taken
19983	Antipathella fiordensis	O803	1
17108	Antipathella fiordensis	O799	2
24186	Leiopathes bullosa	Z11101	1
24185	Leiopathes bullosa	Z11101	1
47420	Leiopathes	Z10068	1
24204	Leiopathes secunda	Z9805	1
24199	Leiopathes	Z9225	1
24205	Leiopathes		1
25100	Leiopathes acanthophora	TAN0604/133	1
65593	Leiopathes bullosa	TRIP2914/32	1
65561	Leiopathes secunda	TRIP2884/130	1
14786	Leiopathes	Z10874	1
47996	Leiopathes seunda	n/a	15
19749	Leiopathes	Z9320	1
47422	Leiopathes acanthophora	TRIP2714/123	1
19747	Leiopathes	J0676	1
19754	Leiopathes	Z9225	1
47426	Leiopathes secunda	n/a	1
47913	Leiopathes	TRIP2714/123	1
76750	Leiopatthes sp.	TAN1003/19	1
47885	Leiopathes	TRIP2232/7	1
60378	Leiopathes	TRIP2595/53	1
19750	Leipathes	Z9224	1
72765	Leiopathes bullosa	TAN1104/109	1
41158	Leiopathes bullosa	Z10060	1
80784	Antipathes	??	4

Appendix 1. List of sampled coral specimens and corresponding NIWA catalogue number + number of samples taken.

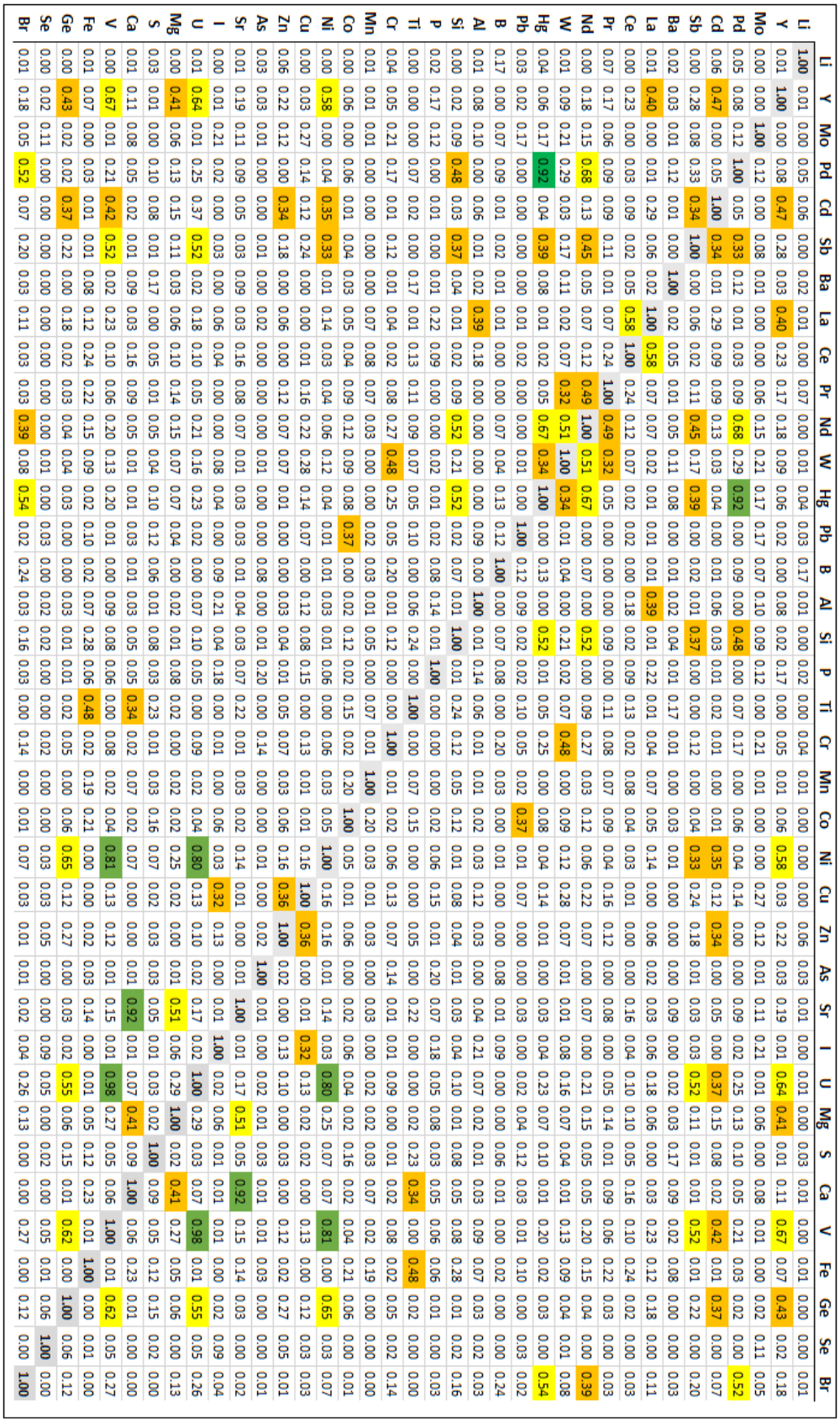

Appendix 2. Exhaustive list of r-square values from linear regressions between elemental pairs. Yellow – r-square = 0.5 – 0.8, Orange – r-square = 0.3 – 0.49, Green – r-square = 0.8+, Blank – r-square = less than 0.3.